CJSJ

Columbia Junior Science Journal

2023-2024

Table of Contents

Administrative

Original Research

Review Articles

Dear Readers,

We are so excited to announce the publication of the ninth edition of the *Columbia Junior Science Journal*! As editors of this journal, we have always strived to spotlight outstanding research done by high school students, and this issue features a collection of impressive and novel work across various scientific disciplines.

We would like to take this opportunity to thank everyone who was involved in the publication of this edition: the members and executive board of the *Columbia Undergraduate Science Journal*, the wonderful student authors featured, their research mentors, their parents and peers, and anyone else who contributed. We would also like to congratulate all of the authors on their remarkable achievement and their dedication to scientific excellence amidst the uncertainty and tumult left in the wake of COVID-19.

We recognize how COVID-19 and other worldwide crises have fundamentally changed the landscape of scientific research, particularly regarding access to resources and laboratories necessary for hands-on research. Our goal this year was to curate a journal that spans a wide range of scientific topics and disciplines, but to also create a cohesive publication that is sensitive to many of the most pressing issues in the world today. With this in mind, we received an unprecedented number of submissions this year, and our editors painstakingly reviewed each and every submission, selecting only a small fraction to publish. We hope that you read this journal not as a set of disparate articles, but as a thoughtful analysis of many contemporary issues that involve the scientific community. From tackling textile waste pollution to detecting cryptojacking using machine learning, we continue to cover a wide range of topics in our journal. We cordially invite you to join us as we explore these topics and offer insights and solutions along the way.

Overall, it has been a great pleasure serving as the 2023-2024 Editors-in-Chief of the *Columbia Junior Science Journal*. We look forward to seeing and reading about all of your continued scientific endeavors for many years to come!

Sincerely,

Coco Huang and Jimmy Zhang
Editors-in-Chief
Columbia Junior Science Journal

Dear Readers,

We are proud to announce the publication of the 2023-2024 edition of the *Columbia Junior Science Journal*! This year's edition features high-quality research across a wide variety of scientific disciplines, including but not limited to biology, medicine, computer science, environmental science, psychology, and engineering. The quality of research and the scholarship of our authors is truly impressive, and including their work in our publication is both a privilege and an honor.

The COVID-19 pandemic has drastically altered the way we navigate and conduct scientific research, limiting opportunities for students around the world, especially at a time when scientific literacy and research is needed the most. So, it is inspiring to know that so many young scientists across the world are advocating for science through their research and authorship as we continue to recover from the pandemic.

In addition to advocating for scientific research, it is important to increase the accessibility of scientific resources to all communities, as science is a collective endeavor. Therefore, we hope to fulfill this aim by giving high school students a platform to contribute to our scientific understanding of nature. Our science events, conferences, and outreach efforts are a few additional ways we try to increase accessibility of scientific involvement to all. I am incredibly proud of our editorial team for leading the *Columbia Junior Science Journal* in this cause.

As the Presidents of the *Columbia Undergraduate Science Journal*, it was an honor to assist in reading, editing, and reviewing the submissions made to our journal. We are extremely grateful to our *Columbia Junior Science Journal* team and editorial board for their significant contributions to our scientific review process and doing an incredible job leading this publication. We are especially grateful to Coco Huang and Jimmy Zhang, Editors-in-Chief of the *Columbia Junior Science Journal*, whose phenomenal leadership made this publication a success. We would also like to thank the *Columbia Undergraduate Science Journal* Faculty Advisory Board, whose support ensures publication of the highest quality of scholarship. Congratulations to our authors, and thank you to our readers!

Sincerely,

Priya Ray and Kynnedy Simone Smith
Presidents, Chief Editorial Officers
Columbia Undergraduate Science Journal

Masthead

Editorial Board

Coco Huang.....CJSJ Co-Editor-in-Chief
Jimmy Zhang.....CJSJ Co-Editor-in-Chief
Kynnedy Simone Smith....Co-President, CUSJ Editor-in-Chief
Priya Ray.....Co-President
Adriana Delagarza.....Columbia Scientist Editor-in-Chief
Kayla Pham.....DEI Director
Madeline Douglas.....Comms Director
Samvat Jai Yadav.....Outreach Director

CJSJ Editors

Anita Raj.....CJSJ Associate Editor
Aruna Das.....CJSJ Associate Editor
Bhavya Bellannagari.....CJSJ Associate Editor
Christine Chow.....CJSJ Associate Editor
Erin White.....CJSJ Associate Editor
Frances Cohen.....CJSJ Associate Editor
Rohan Raghavan.....CJSJ Associate Editor
Shivani Patel.....CJSJ Associate Editor

Editors

Amanda Prashad.....CUSJ Associate Editor
Emily Kilroy.....CUSJ Associate Editor
Saachi Kuthari.....CUSJ Associate Editor
Tara Isabel Dee Lago.....CUSJ Associate Editor
Aroosha Irfan.....CUSJ Associate Editor
Ava Rotondo.....Columbia Scientist Associate Editor
Ceyda Topcu.....Columbia Scientist Associate Editor
Cindy Lu.....Columbia Scientist Associate Editor
Diana Sanchez.....Columbia Scientist Associate Editor
Harry Xiao.....Columbia Scientist Associate Editor
Jessica Wu.....Columbia Scientist Associate Editor
Kevin Rostram.....Columbia Scientist Associate Editor
Mariana Guerrero.....Columbia Scientist Associate Editor
Stephanie Nnaji.....Columbia Scientist Associate Editor
William Ostling.....Columbia Scientist Associate Editor
Ana Paiva.....Associate Editor
Emily Liu.....Associate Editor
Joanna Lin.....Associate Editor
Luanna Quinalha.....Associate Editor
Naia Marcelino.....Associate Editor
Rumeysa Camlica.....Associate Editor
Sebastian David-Mercado.....Associate Editor
Caitlin Ang.....Associate Editor
Erika Maria Gonzales.....Associate Editor
Lina Huang.....Associate Editor
Ashika Prakash.....Associate Editor
Michelle Mai.....Associate Editor
Giovanna Napoleone.....Associate Editor
Aileen Qi.....Associate Editor
Sumaiyah Rahman.....Associate Editor
Samantha Silva.....Associate Editor
Monica Wu.....Associate Editor
Krystell Santiago.....Associate Editor
Madeline Maldonado Gutierrez.....Associate Editor
Sarah Sherman.....Associate Editor
Tani Omoyeni.....Associate Editor
Hiya Jain.....Associate Editor

Faculty Advisory Board

Hugh Ducklow.....Primary Advisor, Professor of Earth & Environmental Sciences
Ivana Hughes.....Director of Frontiers of Science & Senior Lecturer in Discipline-Chemistry
Marko Jovanovic.....Assistant Professor of Biological Sciences
Laura Kaufman.....Professor of Chemistry
Patricia Lindemann.....Director of Undergraduate Studies & Lecturer in Discipline-Psychology
Kyle Mandli.....Professor of Applied Mathematics
Gerard Parkin.....Professor of Chemistry
Ron Prywes.....Professor of Biological Sciences
Rachel Rosen.....Associate Professor of Physics
Samuel Sternberg.....Assistant Professor of Biochemistry & Molecular Biophysics

Cryptojacking Detection: A Novel Two-Step Approach Integrating Machine Learning and DNS Monitoring

Anishka Vissamsetty[1]

***Abstract*— The rapid emergence of cryptocurrencies and blockchain technology has introduced not only innovative opportunities, but also cybersecurity challenges. One such threat is cryptojacking, in which cybercriminals exploit victims' computing power for unauthorized cryptocurrency mining. This study proposes a novel two-step approach for efficient cryptojacking detection: the first step employs machine learning to identify fluctuations in CPU and memory utilization, with a focus on accurate detection by considering network traffic in the second step. DNS logs are analyzed to identify new domains during CPU spikes, cross-referenced against a curated dataset. The proposed model achieved an accuracy of 89% using gradient-boosted decision trees on real-world data. This fusion of machine learning and network monitoring provides a potent defense against the growing menace of cryptojacking, with practical applications spanning corporate environments, cloud infrastructure, and personal devices.**

I. Introduction

In recent years, cryptocurrency has become popular as a new form of digital currency. Cryptocurrency is a virtual currency that uses a computer network to process transactions. Unlike traditional physical currencies, cryptocurrency does not rely on a central authority, such as a bank or government, to maintain it. Cryptocurrency relies on a ledger called blockchain to record a list of transactions. Blockchain utilizes cryptographic techniques, a practice of securing communication and protecting data.

Cryptocurrency mining is the process by which new cryptocurrency is created and transactions, or the transfer of cryptocurrency between two parties, are initiated. Transactions are first sent to a network of computers, or nodes, where they are checked for legitimacy. Only valid transactions are then grouped into blocks, forming the basis of the blockchain. Miners compete to solve complex mathematical puzzles in order to create the next block. This process of solving the puzzle is known as Proof of Work (POW) and requires significant computational power and resources. The first miner to successfully solve the puzzle adds their block to the blockchain, earning cryptocurrency rewards and transaction fees. The idea behind providing rewards is to incentivize miners to use their computational power and resources to maintain the cryptocurrency network [1].

The rapid proliferation of cryptocurrencies and blockchain technology has introduced innovative possibilities in the digital landscape. For example, it has created faster global transactions, automation, technological advancements, and investment opportunities.

With the advancements in blockchain, cybercriminals have devised a threat to digital security: cryptojacking. Cryptojacking is an attack where criminals infect a user's device with malware to run cryptocurrency software and generate money. For criminals, cryptojacking is a lucrative crime because they are able to generate a large amount of cryptocurrency. Cryptojacking can occur for anywhere between 10 minutes to months, depending on how long the attacks go unnoticed. [2] However, cryptojacking may lead to performance degradation, device damage, financial losses, and data breach risks for victims. In 2023, the total number of cryptojacking attacks in the United States was 215 million, a 340% increase from a year ago [3]. The number of cryptojacking incidents continues to increase with new advancements in technology such as increased GPU usage and availability of mining tools. Moreover, cryptojacking attacks can often go unnoticed for large periods of time since they operate covertly.

Case Study

A recent cryptojacking attack by Gui-vil, an Indonesian threat group, demonstrates the process of cryptojacking. In 2023, Gui-vil exploited AWS EC2 instances to facilitate illegal crypto-mining operations. The group was able to gain initial access to AWS servers by using publicly compromised credentials from vulnerable GitLab instances. They gained access keys which allowed them to enter the AWS environment. Using compromised credentials is one way to gain initial access, but other methods include phishing, supply chain attacks, or infecting websites.

The group performed internal reconnaissance to explore the AWS services and maintain presence. Gui-vil ran large instances in the victims' AWS organization that they used for crypto-mining, which cost tens of thousands of dollars daily. The group then attempted to evade detection by modifying logs and disabling monitoring or alerts [4].

Gui-vil's case study shows just one instance of illegal crypto-mining and its damaging effects.

Proposal

This study aims to propose a two-step approach that can efficiently and accurately detect cryptojacking and its associated evasion techniques to avoid detection. The first step is employing a machine learning model to identify fluctuations in victims' memory and CPU utilization rates. Statistical data analysis has shown that the CPU utilization rate of mining scripts ranged from 5% to 90%, and half of the attacks had rates less than 70% [5]. Therefore, CPU monitoring alone is inaccurate and may result in false positives because CPU usage can increase due to ordinary workload spikes. Thus, the second step involves network monitoring to collect Domain Name System (DNS) logs. DNS logging is used to verify if a cryptojacking attack is occurring. By recording all DNS connections, the logs can

[1]A.V. is with Notre Dame High School, 596 S Second St, San Jose, CA 95112 (corresponding author to email: anishka18v@gmail.com).

be checked to verify if there are any malicious domains within a network.

II. Methods

Data Collection and Processing

The data used in this study was obtained from NVIDIA's Anomalous Behavior Profiling dataset, which contains 80,241 logs of benign and malware workflows [6]. This dataset contains NVIDIA GPU and CPU metrics sampled at regular time intervals. There are 31 features, including timestamps, memory usage, power consumption, temperature, and clock frequencies. The labels were encoded into numerical values, with 0 representing an attack and 1 representing no attack or a benign state. The dataset was then standardized using the Standard Scaler, which uses the Z-score transformation on every input variable. The Z-formula calculates the number of standard deviations a data point is away from the mean value, providing a measure of its position within a distribution.

Machine Learning

The dataset was first split into training and test sets, with 80% used for training and 20% used for testing. Several supervised machine-learning models were then trained on the data. These models included logistic regression, a statistical model that calculates the probability of binary classification tasks; random forest classifier, an ensemble learning method that constructs multiple decision trees during training; and gradient-boosted decision trees, a model that uses boosting on trees to iteratively learn and minimize errors and variance [7]. Gradient-boosting is an algorithm in which the predictions of weak learners are combined to improve overall performance. These models were chosen because they are well-suited for classification tasks and have a range of complexities, from linear to ensemble methods.

DNS Logging Collection

When a crypto-mining operation is orchestrated, the miner initiates an outbound connection to the mining pool using specific protocols and network communication. A mining pool is a joint group of cryptocurrency miners who share their resources to maximize rewards. Mining pools have associated server addresses or domain names that miners use to connect their software.

The second step of this approach proposes to collect DNS logs originating from a machine, as shown in Figure 1. DNS logging reveals detailed data on DNS traffic, including domain name queries, timestamps, and other records. We continuously monitor and collect DNS logs, creating a time-series model for each machine.


```
,"query_timestamp":"2023-08-05T23:44:54Z","query_name":"google.com.","query_type":"A"}
,"query_timestamp":"2023-08-05T23:44:54Z","query_name":"google.com.","query_type":"AAAA"}
,"query_timestamp":"2023-08-06T00:56:07Z","query_name":"pool-phx.supportxmr.com.","query_type":"AAAA","query_class"}
,"query_timestamp":"2023-08-06T00:56:07Z","query_name":"pool.supportxmr.com.","query_type":"A"}
,"query_timestamp":"2023-08-06T00:56:07Z","query_name":"pool-phx.supportxmr.com.","query_type":"A"}
,"query_timestamp":"2023-08-06T00:56:07Z","query_name":"pool.supportxmr.com.","query_type":"AAAA"}
```


Figure 1. DNS Logging Example

Detection Phase

The cryptojacking detection phase combines the machine learning model and DNS logging collection. Figure 2 shows a flowchart describing the entire detection process. First, if the model detects a spike in CPU usage, then the DNS logs are checked to see if new domains are generated based on the timestamps. "New domains" are defined as domains visited during the CPU spike but not before. The newly generated domains are then compared to a subset of 100,000 domains in the Alexa Top Domains list [8]. This dataset is composed of the top URLs visited in terms of unique users and page views. Security researchers commonly use the Alexa Top Domains list to obtain samples of "benign" domains. A subset of 100,000 was chosen because only the top 100,000 domains were previously found to be statistically meaningful, whereas the domains ranking below 100,000 do not contain enough data to be commonly used. This means that the domain names for mining pools are not found in the top 100,000 [9]. If the new domains are part of the subset, it is not classified as a cryptojacking attack; otherwise, if they are not part of the subset, it is classified as a cryptojacking attack.

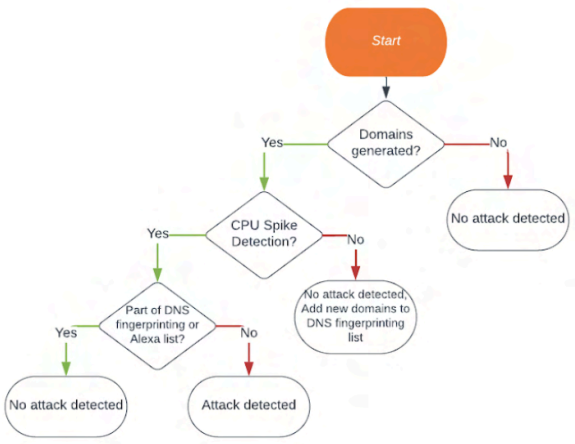

Figure 2. Flowchart describing multi-step cryptojacking detection method

III. Results

The three machine learning models were tested on the test set, consisting of a random sample of 870 rows. The gradient-boosted trees performed the best with an accuracy of 88.5%. The random forest classifier performed similarly with an accuracy of 88.0%, and the logistic regression achieved 86%. The gradient-boosted trees algorithm likely

performed the best because it is able to minimize errors and variance by combining the predictions of weak learners.

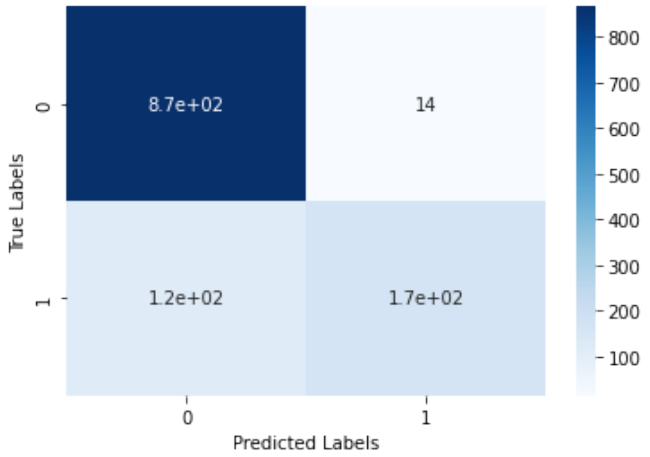

Figure 3. Confusion Matrix of Gradient-Boosted Trees Algorithm

Figure 3 shows a confusion matrix of the gradient-boosted trees, where 0 represents an attack and 1 represents no attack. We observe a high false positive rate, likely because of CPU utilization rates increasing due to workload spikes and non-malicious activity. However, with the DNS monitoring, the solution filters out all the false positives.

$$Precision = \frac{TP}{TP+FP} \quad (1)$$

$$Recall = \frac{TP}{TP+FN} \quad (2)$$

The precision for this model was 0.98 and the recall was 0.88, as calculated by formulas (1) and (2), respectively. This suggests that the model correctly identified 88% of all cryptojacking attacks, and when it predicted an attack, it was correct 98% of the time. The precision and recall indicate an effective and accurate model.

Feature Importance

Feature importance is a technique used in machine learning to assess the relevance of input features in making predictions. A score is calculated for each feature of the gradient boosting model, and this score determines the extent to which a feature contributes to the model's predictive accuracy. Different metrics were used to calculate each score, including the number of nodes, the number of root nodes, the sum of the split scores, and the average minimum depth of the first occurrence of a feature [10]. The top ten most important features are shown in Figure 4.

1	nvidia_smi_log.gpu.fb_memory_usage.free
2	nvidia_smi_log.gpu.bar1_memory_usage.free
3	nvidia_smi_log.gpu.clocks.video_clock
4	nvidia_smi_log.gpu.fb_memory_usage.used
5	nvidia_smi_log.gpu.bar1_memory_usage.used
6	nvidia_smi_log.gpu.clocks.sm_clock
7	nvidia_smi_log.gpu.pci.tx_util
8	nvidia_smi_log.gpu.clocks.graphics_clock
9	nvidia_smi_log.gpu.utilization.memory_util
10	nvidia_smi_log.gpu.temperature.memory_temp

Figure 4. Table of top 10 most important features of the gradient-boosted decision trees

These features are related to the memory usage on the GPU, the rate of transactions, the percent of time the GPU is being used, and the temperature and clock frequencies. High values for these features generally correspond to a cryptojacking attack because the computer is being used extensively. In addition, using GPU resources can generate heat, which is why the temperature should be monitored, and unusual clock frequency can indicate malicious activity [11].

When the gradient-boosted model was retrained with only the above subset of features, the resulting accuracy was 89%. Hence, the model is able to achieve similar accuracy using only this subset of features.

Application

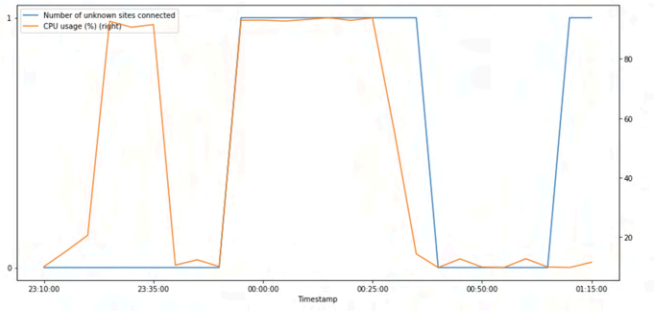

Figure 5. Graph showing a real application of CPU usage and DNS logs

Figure 5 shows an application of CPU usage and DNS logs collected on a machine running cryptojacking software. The orange line shows the CPU load in percent and the blue line shows the number of unknown sites a machine is connected to. When the CPU usage is high and the machine is connected to an unknown site (between roughly 23:45 and 00:35), it indicates a cryptojacking attack. From 23:10 to 23:40, although the CPU load is high, the machine is not connected to unknown sites, and therefore, it does not indicate an attack.

This model can be used by collecting data from a machine and deploying code available on an open-source

GitHub repository. The AWS Cloud Watch metrics can be used to monitor CPU usage and collect DNS logs.

IV. Discussion

This paper presents a novel solution to detect malicious crypto-mining effectively. This approach addresses the limitations of existing approaches by combining machine learning techniques with network monitoring, enabling a comprehensive and accurate detection process.

Current solutions are ineffective because the majority of them rely heavily on CPU monitoring. Attackers are easily able to evade and bypass detection mechanisms that rely on CPU monitoring by limiting usage, introducing idle states, or sharing resources. Evasions often lead to false negatives because low CPU activity is not reported as an attack. Additionally, CPU monitoring can lead to false positives because CPU usage can fluctuate due to workload spikes and other non-malicious activities. The proposed approach mitigates these effects by integrating machine learning with network monitoring. The machine learning model is beneficial because it enables adaptation — the model can learn from evolving strategies and a variety of factors. Some of the most important and relevant features found are memory usage, utilization, and temperature, while other techniques only monitor CPU utilization rates. In addition, the use of DNS logging can identify whether a system is connected to malicious domains, confirming whether a cryptojacking attack is occurring.

Some limitations of this study are that it has currently not been tested on large amounts of data. In addition, the data used in this study only comprised data involving the Monero cryptocurrency because of a lack of publicly available data. Since there are various types of cryptocurrencies, especially as new techniques and algorithms continue to be built, a broader range of datasets should be used to make the model more versatile and adaptable. As an extension of this research, future studies should seek to collect more data and perform more testing experiments. Companies may hope to build an API to automatically collect CPU metrics and DNS logs from a user's computer, making this solution employable.

This research holds both theoretical and practical applications in the field of cybersecurity. The use of machine learning highlights the future and possibilities of supervised machine learning algorithms – especially gradient-boosted trees. Furthermore, this tool has a wide scope for use in both organizations and personal devices. Companies that use a large amount of computing power can deploy this software in their systems, preventing unauthorized mining. In addition, individuals can utilize this software on their devices to prevent attacks, offering a defense against cryptojacking across various sectors.

V. References

[1] F. Fang et al., "Cryptocurrency trading: a comprehensive survey," Financial Innovation, vol. 8, no. 1, Feb. 2022, doi: https://doi.org/10.1186/s40854-021-00321-6. Available: https://jfin-swufe.springeropen.com/articles/10.1186/s40854-021-00321-6

[2] "Cryptojacking," *www.interpol.int*. https://www.interpol.int/en/Crimes/Cybercrime/Cryptojacking

[3] D. Thomas, "Cryptojacking Cases Increase Almost 400% In a Year," BeInCrypto, Jul. 26, 2023. https://beincrypto.com/cryptojacking-increases-fourfold-europe-us/

[4] Ahl, I. (2023, May 22). Permiso | Blog | Unmasking GUI-Vil: Financially Motivated Cloud Threat Actor. Permiso.io. https://permiso.io/blog/s/unmasking-guivil-new-cloud-threat-actor/

[5] G. Xu et al., "Delay-CJ: A novel cryptojacking covert attack method based on delayed strategy and its detection," Digital Communications and Networks, May 2022, doi: https://doi.org/10.1016/j.dcan.2022.04.030.

[6] "Morpheus/models/datasets/training-data/abp-sample-nvsmi-training-data.json at branch-23.11 · nv-morpheus/Morpheus," *GitHub*. https://github.com/nv-morpheus/Morpheus/blob/branch-23.11/models/datasets/training-data/abp-sample-nvsmi-training-data.json (accessed Aug. 15, 2023).

[7] "What is Boosting? Guide to Boosting in Machine Learning - AWS," *Amazon Web Services, Inc.* https://aws.amazon.com/what-is/boosting/

[8] "Alexa Top 1 Million Sites," *www.kaggle.com*. https://www.kaggle.com/datasets/cheedcheed/top1m

[9] W. Rweyemamu, T. Lauinger, C. Wilson, W. Robertson, and E. Kirda, "Clustering and the Weekend Effect: Recommendations for the Use of Top Domain Lists in Security Research,"

[10] "CLI User Manual — Yggdrasil Decision Forests documentation," *ydf.readthedocs.io*. https://ydf.readthedocs.io/en/latest/cli_user_manual.html (accessed Aug. 15, 2023).

[11] What is Cryptojacking and how does it work? (2023b, May 18). Usa.kaspersky.com. https://usa.kaspersky.com/resource-center/definitions/what-is-cryptojacking

Small Molecule Stabilization of the *CARD11* G-quadruplex Represses Transcription: Developing a Therapeutic Target for Diffuse Large B Cell Lymphoma

Aarohi Sonputri[1]

***Abstract*— Diffuse large B cell lymphoma (DLBCL) involves abnormal B cell growth in the lymphatic system. Abnormalities such as recurrent genetic mutations cause critical components of the BCR signaling pathway to be overactive. This constitutes an oncogenic defect that drives uncontrolled B cell growth. Caspase recruitment domain-containing protein 11 (CARD11) is a critical BCR pathway scaffold protein and its recurrent gain-of-function mutations are frequently found in DLBCL. This study aims to investigate the potential of *CARD11* gene silencing as a therapeutic for DLBCL treatment by targeting the DNA secondary structure- G-quadruplexes (G4s) formed within the gene, as G4s usually act as physical barriers to gene expression. Using circular dichroism (CD), stable G4's were identified within the highly guanine-rich promoter region. Small molecules were screened using a fluorescence-resonance energy transfer (FRET) assay to identify compounds that stabilize G4 structures. To quantify the effects of G4 stabilization on gene expression, qPCR was then used to determine that stabilization of G4s led to repression of transcription and subsequent reduction in mRNA levels of the oncogene *CARD11* and a few others,, which are crucial for DLBCL progression These findings highlight that stabilizing the G-quadruplex structures formed in the *CARD11* promoter region could inhibit DLBCL growth by silencing *CARD11* gene expression and downstream oncogenic signals in the BCR pathway.**

I. Introduction

Diffuse large B cell lymphoma (DLBCL) is a highly aggressive and heterogeneous subtype of non-Hodgkin lymphoma, characterized by the uncontrolled growth of abnormal B cells in the lymphatic system. DLBCL represents the most common form of non-Hodgkin lymphoma, accounting for approximately 30-40% of cases [1,5]. Despite significant advancements in DLBCL treatment, a substantial 60% of DLBCL patients still remain refractory to the standard combinatory treatment R-CHOP (*rituximab*, *cyclophosphamide*, *doxorubicin*, *vincristine*, and *prednisone*), or experience relapse after achieving initial remission [1,4,7].

The B cell receptor (BCR) signaling pathway plays a crucial role in DLBCL development and progression [6]. Upon encountering specific antigens, B cells activate their BCRs, leading to intracellular signaling cascades that promote cell survival and proliferation [1,2,3]. In Activated B cell (ABC) DLBCL, this pathway is constitutively active due to genetic mutations in other key component proteins of the BCR signaling pathway, such as *BCL2* and *MYC*, resulting in enhanced BCR signaling independent of antigen binding [3,6]. Upon activation, BCR sends signals downstream through a multi-protein complex that in turns activates other signaling pathways like the NFκB pathway, which is critical for cell survival and proliferation. The aberrant propagation of survival signals from uncontrolled BCR signaling is a key factor promoting the initiation and progression of DLBCL [1].

The present research focuses on the CARD11 protein, an important component of the multi-protein signaling complex. Since *CARD11* sits at a critical signaling node and its mutations play a vital role in driving lymphoma growth [1,2,4], it represents a promising therapeutic target. Specifically, silencing *CARD11* could overcome a central DLBCL growth mechanism by cutting off key survival signals at their origin - the mutated CARD11 protein itself.

Stabilized G-quadruplex structures (G4s), which are guanine-rich DNA or RNA sequences folded into stacked tetrads, within the *CARD11* gene promoter (Figure 1) likely downregulate *CARD11* and other oncogenes by physically blocking transcriptional machinery and interfering with regulatory elements, leading to reduced gene expression. These double stranded DNA secondary structures are extremely stable and can inhibit gene expression when localized to promoter regions, acting as roadblocks to RNA polymerases and other proteins attempting to bind. By screening a library of small molecules for the ability to selectively bind to and stabilize G4 structures, this innovative approach aims to silence the expression of genes involved in the development of DLBCL, offering a promising avenue for developing novel therapeutic strategies for aggressive DLBCL.

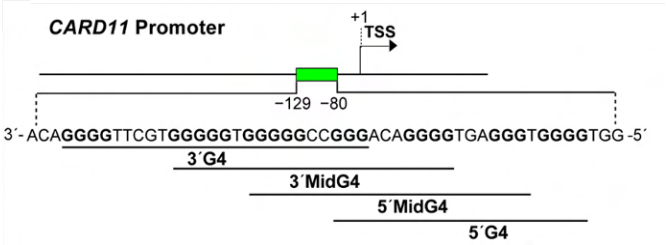

Figure 1. The *CARD11* promoter has potential G4-forming motifs near the transcription start site.

II. Materials and Methods

A. Oligonucleotides

Oligos from IDT and Eurofins were used for circular dichroism (CD) and fluorescence-resonance energy transfer (FRET) experiments. Their concentrations were determined by absorbance measurements at 360 nm using a nanodrop spectrophotometer and calculating the molar absorptivity (ε) via the Beer-Lambert law. Both CD and FRET samples were stored at 4°C.

B. CD Spectroscopy Analysis

We tested G4 formation in *CARD11* oligos using CD with varying KCl concentrations. Previous research has

[1] A.S. is with the Arkansas School for Mathematics, Sciences, and the Arts, Hot Springs, AR 71901 USA (corresponding author to e-mail: aarohi.sonputri@gmail.com).

revealed that potassium ions stabilize G4 structures, so varying potassium chloride concentrations would allow us to determine the optimal stability conditions of G4 and analyze the G4 folding dependence on potassium levels (Figure 2). Oligos were heated and cooled, and CD spectra data was collected at 263 nm using a Jasco-1100 spectropolarimeter. Data was baseline-corrected, smoothed using the Savitzky-Golay method, and thermal stability was then assessed by increasing the temperature by 1°C/min while recording molar ellipticities, allowing T_m determination within ±1°C using Prism software.

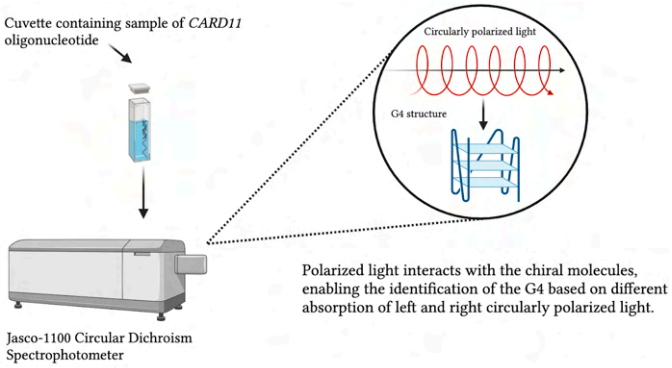

Figure 2. Visual representation of CD methodology to identify G4 structures within the *CARD11* oligonucleotide samples.

C. *Small Molecule Screening*

Custom Fluorescence Resonance Energy Transfer (FRET) probes were created to enable assessment of G4 stability changes induced by small molecules, requiring custom design to target the specific *CARD11* gene sequence. Probes were prepared with 8 small molecules at 40 µM in Dimethyl sulfoxide (DMSO) 16% mixed with FAM/TAMRA-labeled *CARD11* probes in 10mM NaCacodylate and 20mM KCl buffers to provide appropriate salt conditions known to facilitate G-quadruplex formation while enabling testing of the small molecule conditions. The probes underwent gentle centrifugation at 2000 rpm to mix the components while avoiding disruption of structure. Transferal to 96-well plates enabled high-throughput and controlled testing of multiple small molecule conditions simultaneously. The FRET assay was performed at 95°C, slightly below melting temperature, to potently evaluate stability modulations detectable by FRET signal changes. Data normalization on a 0-1 scale enabled standardized comparison across probes and conditions for comprehensive analysis. Curve fitting analysis was utilized to determine the logIC50 values for each small molecule, quantifying the molar concentration required to inhibit 50% of G-quadruplex structure stability. Comparison of the logIC50 values provided key insights into whether the small molecules preferentially disrupt or stabilize G4 structures, based on their binding affinity and potency.

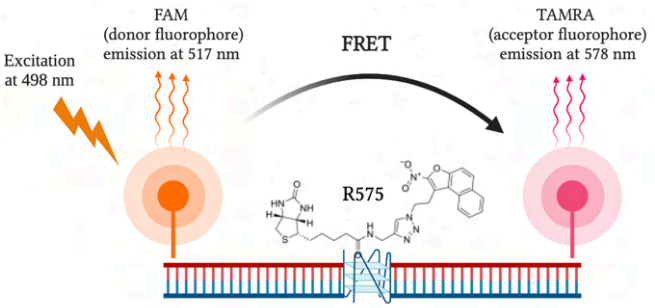

Figure 3. Visual representation of the FRET methodology to test for G4 stabilizing small molecules. R575 used as an example small molecule. In the FRET assay, the G-quadruplex folds upon cooling, bringing the FAM and TAMRA tags on the *CARD11* DNA together, while R575 binding further stabilizes the structure - keeping the tags consistently in close proximity and enabling ongoing energy transfer between them.

D. *Human Cell Lines*

The cell lines RIVA, HBL1, VAL, SUDHL6, and GM16113 from ATCC and DSMZ were stored in RPMI 1640 media with 10% FBS and 1% penicillin-streptomycin. They were grown at 37°C with 5% CO_2. Using these diverse DLBCL cell lines allows the testing of small molecule stabilization of the *CARD11* G4 on malignant cells from varying origins across patients (see Table 1).

Cell line	Cell line origin (biopsy status)
RIVA	Peripheral blood
HBL1	Pleural effusion
VAL	Bone marrow
SUDHL6	Peritoneal effusion
GM16113	Peripheral vein
GM22673	Peripheral vein

Table 1. Cell lines used alongside their biopsy origins.

E. *Gene Expression Measured Using qPCR*

Lymphoma cell lines were treated with small molecules 9037 or R575 to measure relative gene expression. TaqMan probes for genes including *CARD11* were used *in vitro* for this qPCR experiment. Master mixes were prepared with added cDNA for the qPCR. The cycle threshold (Ct) values were normalized to housekeeping gene TBP and compared to untreated controls, yielding ΔΔCt values. The relative gene expression changes were assessed based on these values.

F. *Statistical Analysis*

Data analysis was conducted using GraphPad Prism Software v 9.94. All experiments were performed in triplicate to ensure statistical significance and data

reliability. GraphPad Prism facilitated descriptive statistics, t-tests, ANOVA, and non-linear regression analyses. Visualizations, such as bar graphs and scatter plots, aided in interpreting trends and relationships within the data.

III. Results

The guanine-rich promoter oligonucleotide of *CARD11* displayed distinctive G4 CD peaks at ~260 nm (Figure 4A). Additionally, both these peaks and the oligonucleotides' melting temperatures were affected by the presence of a K+ gradient (Figures 4A-B). Consequently, the *CARD11* exhibits a Guanine rich sequence (3-4 runs of G consecutively), which is consistent with G4 formation (Figure 1). As the concentration of KCl increases, the molar ellipticity decreases, indicating a decrease in the stability of the G4 structures formed by the *CARD11* gene (Figure 4A). The peak at ~ 260 nm with 100mM KCl exhibits the highest molar ellipticity, suggesting that the G4 structure is most stable at this concentration (Figure 4A). As the KCl concentration decreases, the T_m values also decrease, indicating lower stability of the G4 structures, further demonstrating that G4 is most stable at 100mM KCl (Figure 4B).

FRET analysis was performed with the non-interactive small molecule 9037, and we see that 9037 decreased G4 stability in *CARD11*, *BCL2*, and *MYC* genes - confirming its non-stabilizing nature (Figure 4C). To further demonstrate 9037 as a non-interactive small molecule, qPCR was performed to reveal that 9037 did not significantly lower the fold change values in the key gene's expression while in comparison to the vehicle treatment control (VTC) of DMSO at 16% (see Figure 4D). Thus, in subsequent experiments, 9037 was used as a negative control to validate that the screening methodology could differentiate when a small molecule does not stabilize or silence *CARD11* G-quadruplex structures, in contrast to the positive impacts of stabilizing small molecules identified by the screen.

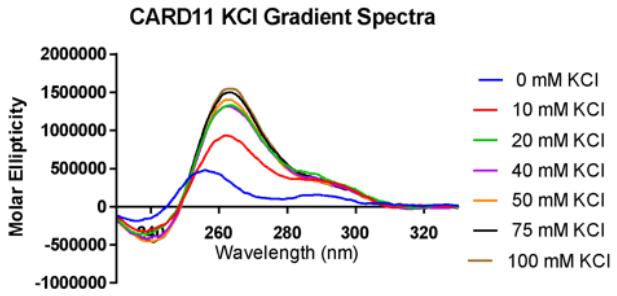

Figure 4A. Upstream G-rich sequence forms a K+-influenced G4 structure, confirmed by circular dichroism peak at ~260 nm.

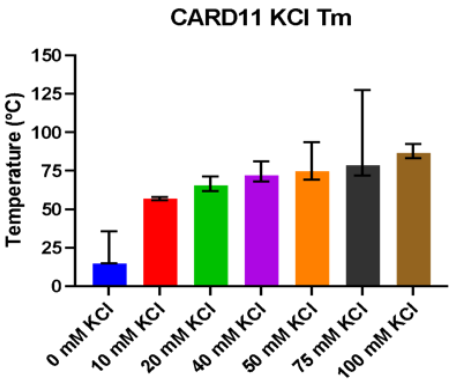

Figure 4B. Corresponding T_m values graphed.

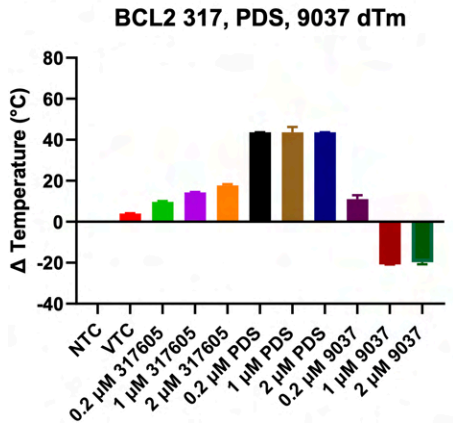

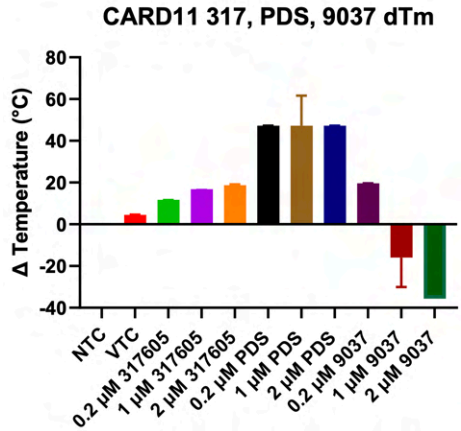

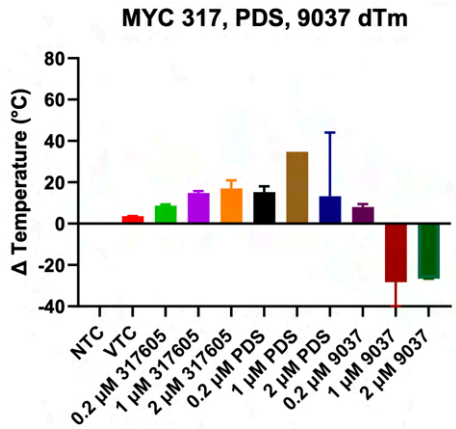

Figure 4C. FRET analysis compared the 9037 impacts (on key oncogenes alongside *CARD11*) to Puromycin Dihydrochloride Salt (PDS, 317605, NTC, and vehicle control: VTC (DMSO 16%).

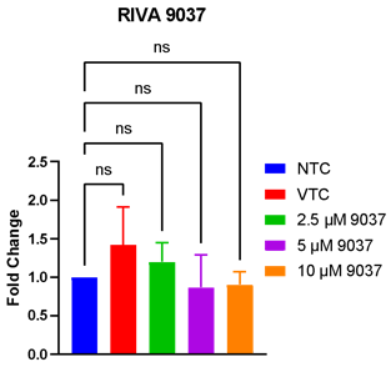

Figure 4D. Fold change *CARD11* mRNA with qPCR data with 9037 tested on RIVA cell line.

FRET assay revealed small molecules R575, 311153, 147481, and 317605 significantly increase G4 Tm, reinforcing structural stability. Small molecules 13248 and 309401 also stabilize G4 but to a lesser extent. Differences arise from diverse chemical structures, binding affinities, and interactions with *CARD11* promoter's G4 motifs. Molecular forces, functional groups, and configurations impact binding.

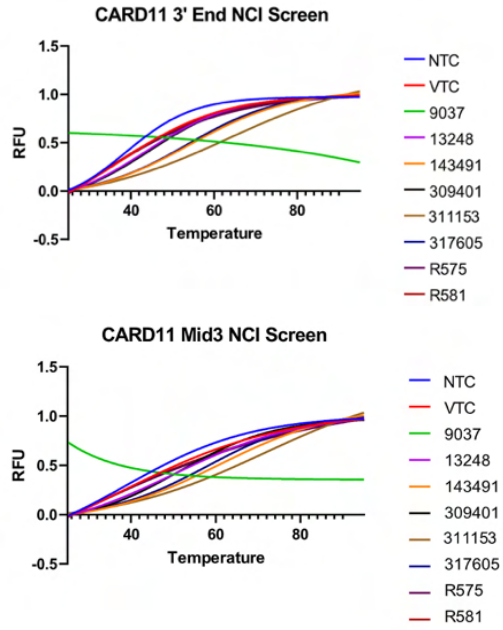

Figure 5. FRET melt curves obtained for small molecules compared to probe + 16% DMSO (vehicle control) at 2.5 µM concentration. Shifts rightwards indicate Tm increase ≥ 4°C, identifying potential candidates. FRET screen used probes in 10 mM NaCac and 20 mM KCl buffer, mimicking the *CARD11* gene's G4-forming conditions.

According to the FRET analysis, small molecule R575 enabled the FAM and TAMRA tagged *CARD11* DNA sequence to retain a consistent 0.7 raw fluorescent unit (RFU) energy transfer plateau from 60°C up to the highest tested temperature of 100°C, without exhibiting the rapid signal decrease that indicates structure melting seen for other small molecules (Figure 5). We thus conclude that R575 allows for stabilized G4 rigidity and continued folding across an expanded temperature range. Small molecule R575 was then investigated for its impact on genes *KRAS* and *TERT* (which contain G4 structures), and *UBC* and *EEF1A1* (which do not contain a G4 structure). In the RIVA cell line, derived from peripheral blood, 10 µM of R575 led to significant downregulation of *BCL2* and *CARD11* genes, indicating effective silencing (top panel, Figure 6). This suggests R575's potential to modulate *CARD11* gene expression, crucial in DLBCL progression. Similarly, the VAL cell line, derived from bone marrow, showed reduced *BCL2* expression with R575 (middle panel, Figure 6). Cell line GM16113, derived from peripheral vein, also experienced silencing effects on *BCL2, CARD11*, and *MYC* genes with R575 (bottom panel, figure 6).

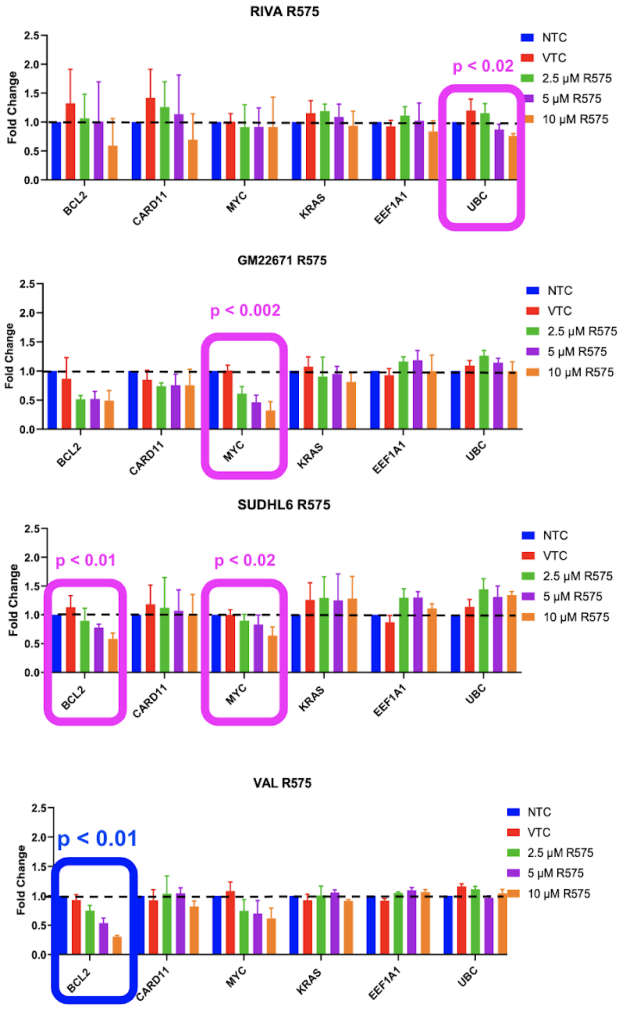

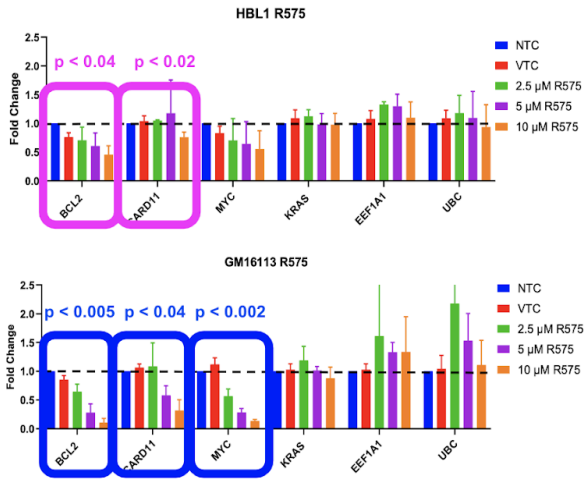

Figure 6. qPCR results for genes *BCL2*, *CARD11*, *MYC*, *MYD88*, *KRAS*, *TERT*, *UBC*, and *EEF1A1* in the RIVA (A), VAL (B), and GM116113 (C) cell lines with varied concentrations of small molecule R575. Boxed experiments show dose-dependent reduced levels of gene expression using ANOVA (purple) or two-sample t-tests (VTS vs. highest dose, pink) statistical analyses. Figures generated by student researcher.

IV. Conclusions

This study demonstrates the potential of targeting G-quadruplex structures within the *CARD11* promoter as a therapeutic strategy for DLBCL. We investigated G-quadruplexes forming in the *CARD11* gene using circular dichroism, identifying stable structures that can act as gene expression barriers. Through screening, the study found a small molecule R575 that substantially stabilizes G4. As stabilized G4 leads to gene silencing, there is no surprise that gene expression analyses revealed that R575 consistently downregulates *CARD11* across DLBCL cell lines, indicating potential for modulating oncogenic BCR signaling. We thus propose G4 in the *CARD11* promoter as a prospective therapeutic target for silencing *CARD11* and disrupting downstream signaling in DLBCL. Small molecule stabilization of these structures shows promises for precise, personalized treatment strategies. Further translational research on G4-targeted therapeutics *in vivo* is warranted to validate and optimize findings toward improved patient outcomes. This innovative approach signifies a potential paradigm shift towards direct DNA/RNA targeting to limit translation of key oncoproteins driving aggressive DLBCL growth.

Acknowledgment

I want to express my gratitude to Drs. Patrycja Krakowiak and Whitney Holden at the Arkansas School for Mathematics, Sciences, and the Arts, as well as Kennith Swafford and Dr. Samantha Kendrick at the Winthrop P. Rockefeller Cancer Institute, University of Arkansas for Medical Sciences (UAMS), for their unwavering support and resources throughout my research journey.

References

[1] Swafford K., Acharya, B., Xu, Y.Z., Raney, T., McCrury, M., Saha, D., Frett, B., & Kendrick, S. Targeting a Novel G-Quadruplex in the *CARD11* Oncogene Promoter with Naptho(2,1-b)furan-1-ethanol,2-nitro- Requires the Nitro Group.Genes,13(7),1144 https://doi.org/10.3390/genes13071144 (2022).

[2] Candelaria, M., & Dueñas-Gonzalez, A. Rituximab in combination with cyclophosphamide, doxorubicin, vincristine, and prednisone (R-CHOP) in diffuse large B-cell lymphoma. *Therapeutic advances in hematology*, *12*, 2040620721989579 (2021). https://doi.org/10.1177/2040620721989579

[3] Kendrick, S., Muranyi, A., Gokhale, V., Hurley, L. H., & Rimsza, L. M. Simultaneous Drug Targeting of the Promoter MYC G-Quadruplex and BCL2 i-Motif in Diffuse Large B-Cell Lymphoma Delays Tumor Growth. *Journal of medicinal chemistry*, *60*(15), 6587–6597. https://doi.org/10.1021/acs.jmedchem.7b00298 (2017).

[4] Davis, R. E. et al. Chronic active B-cell-receptor signalling in diffuse large B-cell lymphoma. Nature 463, 88-92, doi:10.1038/nature08638 (2010).

[5] Testoni, M., Zucca, E., Young, K. H. & Bertoni, F. Genetic lesions in diffuse large B-cell lymphomas. Ann Oncol 26, 1069-1080, doi:10.1093/annonc/mdv019 (2015).

[6] Davis, R. E. et al. Chronic active B-cell-receptor signalling in diffuse large B-cell lymphoma. Nature 463, 88-92, doi:10.1038/nature08638 (2010).

[7] De Cian, A., Guittat, L., Kaiser, M., Saccà, B., Amrane, S., Bourdoncle, A., Alberti, P., Teulade-Fichou, M. P., Lacroix, L., & Mergny, J. L. Fluorescence-based melting assays for studying quadruplex ligands. *Methods (San Diego, Calif.)*, *42*(2), 183–195. https://doi.org/10.1016/j.ymeth.2006.10.004 (2007)

Naringenin's Mitigation of Rotenone-Induced Cytotoxicity: a Potential New Candidate for Treating Parkinson's Disease

Judy Zhao[1]

***Abstract* — In the past five years, the prevalence of Parkinson's disease (PD) has increased by over 50% with an estimated 10 million people affected worldwide. Alpha-synuclein (αS) expression is a major hallmark of PD and has been linked to the downregulation of mitochondrial complex 1, neuronal death, and sporadic PD. Recent research has focused on polyphenols as potential targets for developing new treatments for PD because of their antioxidant properties. This study investigates the potential of the polyphenol naringenin to decrease αS expression, which would increase dopamine release in rotenone-induced PD. We tested naringenin against rotenone-induced cytotoxicity through caspase assays, colorimetric assays, and ELISA assays. We found that naringenin was able to mitigate both caspase activity and cytotoxicity in HTB-11 and U937 cells, representing neuronal and immune cells respectively. These findings suggest that naringenin has a protective effect on cells challenged by rotenone, potentially capable of slowing down the progression of PD.**

I. Introduction

Parkinson's Disease (PD) is a neurodegenerative disease caused by the selective degeneration of dopaminergic (DA) neurons in the substantia nigra of the midbrain [1]. The degeneration of DA neurons in PD is primarily due to apoptosis, with mitochondrial toxins exacerbating this process [4]. Important characteristics of PD include the appearance of alpha-synuclein (αS) and Lewy bodies in the neurons present in the substantia nigra pars compacta of the brain, which induces down-regulation of mitochondrial complex 1 and increased amount of reactivated oxygen species (ROS) [2].

Polyphenols are a diverse group of naturally occurring compounds found in various plant-based foods. Their antioxidant and anti-inflammatory effects make them potential therapeutic targets. These compounds are neutralizers of free radicals and protect cells from the oxidative damage implicated in numerous diseases, including cardiovascular conditions, neurodegenerative disorders, and cancer [5].

Naringenin, a polyphenol in the class of flavonoid, has emerged as a promising treatment option for PD. Scientists have demonstrated its ability to stimulate DA neurons and promote the production of glial cell line-derived neurotrophic factor (GDNF), supporting neuron growth and survival [8]. These studies also suggest that naringenin protects against dopaminergic neurodegeneration and oxidative damage by activating cellular defense mechanisms and inhibiting apoptotic pathways [8]. In addition, it has the ability to enhance the release of neurotrophic factors from astroglial cells, protect dopaminergic cells, improve motor skills, and reduce oxidative stress and neuroinflammation associated with PD [8]. However, these studies often investigate the effects of naringenin on neurons in general, not in the context of specific neurodegenerative diseases like PD.

The isoflavone rotenone is a naturally derived compound often used as pesticide and obtained from several plant species. Due to its lipophilic properties, it is able to inhibit mitochondrial complex 1 as well as the mitochondrial electron transport chain by crossing the blood brain barrier [11]. It has been found to kill DA neurons in a dose- and time-dependent manner by dramatically enhancing the release of lactate dehydrogenase (LDH) into the culture medium [6]. Additionally, rotenone can increase hallmarks of PD, such as αS expression, Lewy bodies, and dose-dependent ATP depletion. This means that rotenone plays a significant part in inducing PD through the creation of αS.

As mentioned above, flavonoids, as scavengers for highly reactive species such as free radicals, can increase oxidative damage and limit the expression of oxidative reactions. Naringenin in particular is able to mitigate mitochondrial oxidative stress damage, which plays an important role in neurodegeneration in PD [9]. On the other hand, rotenone was found to induce mitochondrial ROS production in isolated HL-60 cell mitochondria, primarily by blocking mitochondrial respiratory chain complex I [10]. If naringenin scavenged free radicals through mitochondrial complex 1, providing protection from rotenone, there is a possibility that it can lessen rotenone's impact in rotenone-induced PD.

In addition, we are interested in comparing the effects of naringenin to cannabidiol (CBD), as it is an established promising treatment for PD with anti-inflammatory and antioxidant effects [3]. CBD has been shown to improve motor symptoms related to PD and counter abnormal signaling in the PD-affected brain, playing a crucial role in the basal ganglia circuitry [3]. Studies have also demonstrated CBD's neuroprotective effects against rotenone -induced neuronal damage in primary cultures through its induction of cell stress and inhibition of the heme oxygenase (HO) reaction [7]. By inhibiting the HO reaction, CBD may enhance the cell stress response and confer full protection against oxidative stress in vivo [7].

We hypothesize that naringenin mitigates rotenone-induced immune and neuronal cell death through mitochondrial complex 1 at certain concentrations and can also reverse the effects of rotenone cytotoxicity. We wish to compare the effects of naringenin on neuronal and immune cells to that of CBD. To do so, we will conduct *In Silico* screening that determines the binding affinity of naringenin, rotenone and CBD to mitochondrial complex 1, and colorimetric assays that determine cell survival and cytotoxicity levels after treatment. We will also conduct the caspase assay which determines if naringenin and CBD are

[1]J. Z. is with Ward Melville High School, 380 Old Town Road, East Setauket, NY 11733-3482, and SCI Research Institute, Jericho (corresponding author to email: judy.c.zhao@gmail.com).

able to induce caspase mediated apoptosis, and the ELISA assay that determines the change in αS levels. A marker that will be used in these experiments are the caspases and endoproteases that are central to both intrinsic (mitochondria-mediated) and extrinsic (cell death receptor-mediated) apoptotic pathways, which have been shown to play a role in neuronal cell death. As apoptosis is dependent on caspases, new approaches to slowing the progression of neurodegenerative diseases have focused on caspase inhibition [4].

II. Materials and Methods

We used the virtual screening software Python Prescription (PyRx) to model the interactions between naringenin, CBD, and rotenone with mitochondrial complex 1 to determine if they intersect. CBD, rotenone and naringenin were all downloaded from PubChem in SDF 2D format. They were then converted into PDB format using the Online SMILES Translator and Structure File Generator. Then, the macromolecule (mitochondrial complex 1) was downloaded from the Protein Data Bank in PDB format. Both the ligands and the macromolecule were then input into the PyRx software, which processed the results. Finally, the Vina Wizard conducted a docking analysis within the PyRx workspace, and binding affinities (kcal/mol) and the upper and lower bond of the root-mean-square deviation (RMSD) were calculated.

The two cell lines used were u937 cells, which represented immune cells, and HTB-11 cells, which represented neuronal cells. Both cell lines were purchased from the American Type Culture Collection (ATCC), in Manassas. They were stored using a cell culture incubator, and incubated in an atmosphere of 5% CO2.

3-(4,5-Dimethylthiazol-2-yl)-2,5-Diphenyltetrazolium Bromide (MTT) assays were used to measure the cell proliferation rate, cytotoxicity, and quantification of cell growth and viability under treatment. Lactate Dehydrogenase (LDH) colorimetric assays additionally determined the percentage of damaged cells in a given sample. For both of the assays, the cell samples were placed in 96 well plates. The first row of the plate was set as the control, and the next three were treated with only naringenin at concentrations of 0.1uM, 1 uM and 10uM. The fifth row was treated with rotenone at concentrations of 1uM and 50uM. The last three rows were treated with a combination of both rotenone and concentrations of 0.1uM, 1 uM and 10 uM of naringenin. The cells were then incubated for 24 hours. This process was repeated with CBD for a MTT assay, where the first row of the plate was the control, the second was rotenone, the third was rotenone with CBD at 10uM, then rotenone combined with both CBD and naringenin at 10uM, then rotenone and naringenin at 10uM, and lastly, just CBD.

To calculate the percent change of the change in cell survival (viability percentage) for all the MTT assays, we used this formula:

$$-100 \times \frac{sample\ cell\ survival - control\ cell\ survival}{control\ cell\ survival}$$

In order to calculate the percent cytotoxicity compared to the original value of rotenone for the LDH assays, we used this formula:

$$100 \times \frac{sample\ released\ LDH - ROT\ released\ LDH}{sample\ total\ LDH - control\ released\ LDH}$$

To compare the means between the control group and various treatment samples, multiple T-Tests were performed. The p-values were then calculated using significance levels p=0.05, p=0.01, and p=0.001.The error bars on the graphs indicate standard deviations.

The Caspase-3 Colorimetric Assay was conducted to measure Caspase-3's activities to assess whether rotenone induces apoptosis. A chromophore p-nitroaniline (pNA) solution was added, which causes a deeper color change if there is more caspase and a lighter color change if there is less caspase. Following the cell culture procedures, cells were transferred to a six-well plate, and treated with their respective treatments (add 5 uL of NAR 100 uM, and NAR 10 uM to the wells). Then, we incubated the cells for 24 hours, after which the cells were collected in 1.5 ml tubes with 50ul of lysis buffer in each tube. Following the protocol of the assay kit provider (Caspase Colorimetric Apoptosis Assay, 2019), 50ul of assay buffer, 45 ul of lysis buffer, and 5ul of cell lysate were added to each well of a 96-well plate. Then, we added 5 uL of the pNA substrate solution, mixed the contents in each well, and took readings of the amount of absorbency at 0 minutes, 15 minutes, 45 minutes, and 1 hour with a microplate reader (iMark, USA) at 415 nm. Finally, we calculated the percent change of the caspase activity over the hour by this formula:

$$100 \times \frac{sample\ average\ absorbency - control\ average\ absorbency}{control\ average\ absorbency}$$

We measured αS and phosphorylated alpha-synuclein (p-Ser129) concentrations through an enzyme-linked immunosorbent assay (ELISA) to determine if either naringenin or CBD has an effect on the neuronal apoptosis caused by rotenone. p-Ser129 is often regarded as a helpful biomarker and also causes cognitive and motor dysfunction. A graph was generated to compare both the αS and p-Ser129 levels between the control and treatment groups.

III. Results

Molecular dockings of rotenone (ROT), naringenin (NAR), and cannabidiol (CBD) with the bovine mitochondrial cytochrome bc1 complex (1L0L) macromolecule found that all three ligands possess significant binding potential to mitochondrial complex 1

(Table 1), suggesting a strong bond between the ligands and the macromolecules in each pair.

Ligand	Macromolecule	Binding Affinity
NAR	1L0L	-9.1
ROT	1L0L	-8.9
CBD	1L0L	-8.8

Table 1. Binding Affinities of NAR, ROT and CBD molecularly docked to 1L0L assessed using PyRx showing strong bonds between the ligands and the macromolecules.

We also found that both naringenin and rotenone interact with mitochondrial complex 1 at approximately the same place (Figure 1), suggesting that naringenin can compete with rotenone at the binding site. Since rotenone causes apoptosis when bound to mitochondrial complex 1, we conclude that naringenin mitigates rotenone-induced apoptosis through interactions with mitochondrial complex 1.

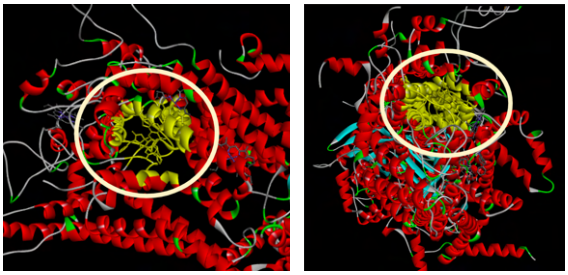

Figure 1. Interactions between mitochondrial complex 1, naringenin and rotenone. Left Panel: The area where mitochondrial complex 1 and rotenone intersect. Right Panel: The area where mitochondrial complex 1 and naringenin intersect

Next, we performed a MTT assay that examined u937 cells, which represent immune cells, and the amount of rotenone-induced cytotoxicity that different concentrations of naringenin were able to mitigate. We found that cells that were treated with 0.1uM naringenin significantly ($p<0.05$) reduced the increase of cytotoxicity caused by rotenone (Figure 2). Compared to the control, cells at 0.1uM naringenin + rotenone displayed a 7.6% increase in cytotoxicity, while rotenone combined with 1uM and 10uM of naringenin displayed greater increases of cytotoxicity (compared to the control) of 29.1% and 33.7%, similar to the 33.1% increase exhibited by cells with rotenone alone added (Figure 2). The results suggest that the concentration of 0.1uM of naringenin offers the best protective effects against the cytotoxicity induced by rotenone on u937 cells.

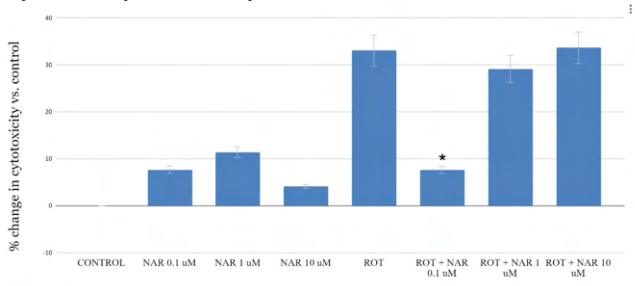

Figure 2. Naringenin significantly mitigated rotenone caused reduction of cell survival by 25.5% ($p<0.05$) at a concentration of 0.1 uM in u937 cells compared to original rotenone levels. *=$p<0.05$, NAR=naringenin, ROT = rotenone

A MTT assay was then conducted for the HTB-11 cells which represent neurons. We found that in cells incubated with rotenone, the treatment of 10uM naringenin significantly ($p<0.05$) mitigated rotenone-induced reduction of cell survival (Figure 3). Compared to the control, cells that were treated with 10uM naringenin + rotenone had a viability percentage (cell survival rate) of 90.6%, while rotenone combined with 0.1uM or 1uM of naringenin displayed viability percentage increases of 55.7% and 58.2%, even less than that exhibited by cells treated only with rotenone. The results suggest that a concentration of 10uM of naringenin + rotenone gives HTB-11 cells the best protective effects against rotenone on cell death.

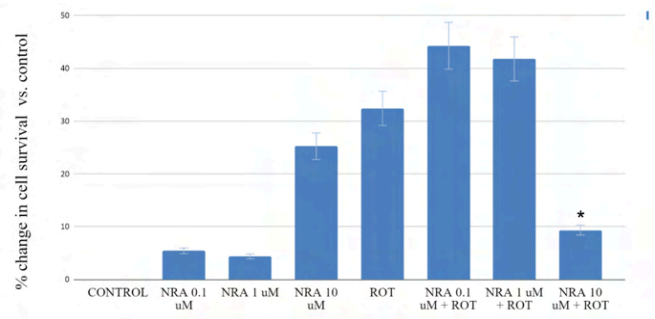

Figure 3. Naringenin significantly mitigated rotenone caused reduction of cell survival by 23.0% ($p<0.05$) in HTB-11 cells at 10uM compared to original ROT levels. *=$p<0.05$, NRA=naringenin, ROT = rotenone

After that, HTB-11 cells were treated with naringenin and rotenone at different concentrations in a LDH assay. We found that cells at 10uM naringenin + rotenone had a 42.2% increase in cytotoxicity compared to the original value of rotenone (Figure 4), which corresponds with the results obtained from our MTT assay with HTB-11 cells (Figure 3). Among the p-values collected from this data, only the results for naringenin and rotenone at 10uM were significant ($p<0.001$). The other p-values were all greater than 0.5, showing that naringenin didn't cause a significant amount of LDH to be released from the cells at NRA 0.1uM and 1uM.

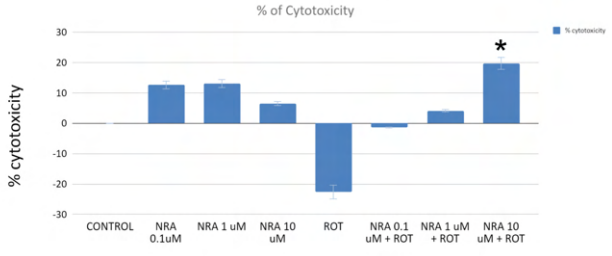

Figure 4. Naringenin at a concentration of 10uM significantly mitigated rotenone caused cytotoxicity by 42.2% ($p<0.001$) in HTB-11 cells. *=$p<0.001$ compared to ROT

An ELISA assay was used to monitor the amount of αS in cultured cells. We found that after treating the cells at

higher concentrations of naringenin, such as 10uM, there is a downregulation of αS expression compared to the control (Figure 5). Moreover, the percent change in αS for rotenone and naringenin at 100uM was 1.73% ($p < 0.001$) and 0.64% with rotenone and CBD at 100uM ($p < 0.05$). These are all significant given that the p-values compared to the original amount of rotenone are all less than 0.05. Similarly, the change in phosphorylated alpha-synuclein (p-Ser129) for rotenone and naringenin at 100uM was 0.49% ($p < 0.001$) and 0.14% with rotenone and CBD at 1000uM ($p < 0.01$). Lastly, the percent change in p-Ser129 for rotenone and CBD at 100uM is 0.13% ($p < 0.001$). These are also all significant, since the p-values compared to the control are all less than 0.05 (Figure 5). We observed that the percent change in both αS and p-Ser129 decreases as the concentration of naringenin increases in the presence of rotenone, suggesting that high concentration of naringenin is beneficial for decreased apoptosis of DA neurons and less expression of both αS and p-Ser129. Finally, the percent change in p-Ser129 decreases as the concentration of rotenone and CBD decreases, while the percent change in αS increases as the same concentration decreases. This suggests that naringenin is a more efficient treatment at mitigating αS expression in rotenone-induced PD.

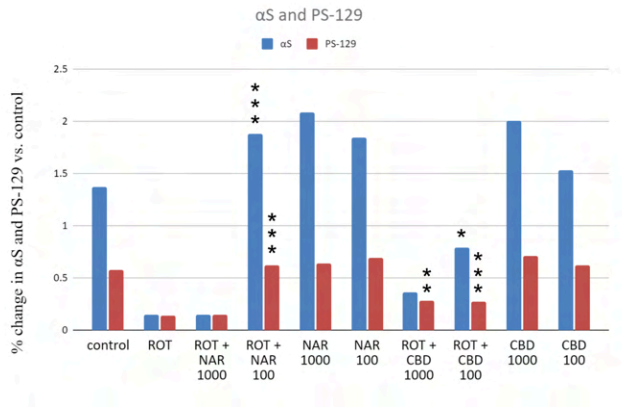

Figure 5. At a concentration of 100uM, naringenin also increased the amount of αS by 1.73% ($p<0.001$) and p-Ser129 by 0.49% ($p<0.001$). At a concentration of 1000uM of cannabidiol, the amount of p-Ser129 increased by 0.14% ($p<0.01$), and at a concentration of 100uM, the amount of αS increased by 0.64% ($p<0.05$) and p-Ser129 increased by 0.13% ($p<0.001$). *=$p<0.05$ compared to original amount of rotenone; **=$p<0.01$ compared to original amount of rotenone; ***=$p<0.001$ compared to original amount of rotenone. CBD = cannabidiol

From the Caspase-3 Colorimetric Assay, we found that 10uM of naringenin and rotenone increased caspase activity by 60% (Figure 6), which is a 22.6% decrease from caspase assay when treated with only rotenone. Additionally, naringenin and rotenone together at 100uM increased caspase activity by about 51% (Figure 6), which is a 30.6% decrease from only rotenone. The percent change of caspase activity increases as the concentration of rotenone and naringenin decreases, suggesting an inverse relationship between caspase activity and concentration of naringenin. As caspase activity levels are directly correlated to apoptosis rates, this means that the more naringenin was present, the less apoptosis occurred.

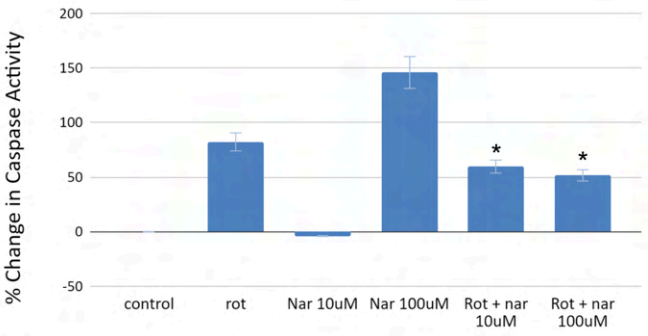

Figure 6. At a concentration of 100uM, naringenin mitigated rotenone-induced caspase activity by 30.6% ($p<0.05$), and at a concentration of 10uM, caspase activity was mitigated by 22.6% ($p<0.05$). *=$p<0.05$ compared to rotenone.

Finally, we compare the effects of CBD and naringenin in the presence of rotenone. The addition of rotenone at 10uM increased cytotoxicity in the cells by 54.58% (Figure 7). 10uM of CBD decreased % change in cytotoxicity to 34.40%, while 10uM of naringenin decreased cytotoxicity levels to 45.65% (Figure 7). Most noticeably, CBD and naringenin together decreased cytotoxicity to only 6.48%, much lower than any of the two used alone, suggesting a potential beneficial effect of combined treatment (Figure 7).

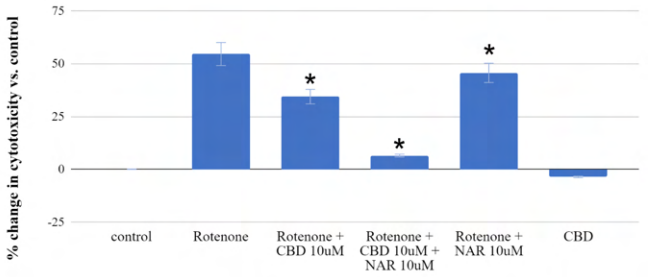

Figure 7. At a combined concentration of 10uM of cannabidiol and 10uM of naringenin in HTB-11 cells, rotenone-induced caspase activity was mitigated by 28.0% ($p<0.05$). *=$p<0.05$ compared to rotenone

IV. Conclusions

This research highlights the positive effects of naringenin towards decreasing rotenone-induced cytotoxicity.

In silico screening revealed strong binding potential of rotenone, naringenin, and cannabidiol to mitochondrial complex 1, indicating naringenin's ability to compete with rotenone at the binding site and mitigate rotenone-induced apoptosis. We proposed a model where naringenin and rotenone are observed to be able to interact at mitochondrial complex 1, where naringenin is able to scavenge the free radicals that rotenone produces.

In examining u937 immune cells through the MTT assay, we found that 0.1uM naringenin significantly reduced rotenone-induced cytotoxicity, indicating that this concentration of naringenin provides the most effective

protection against rotenone-induced cytotoxicity in u937 cells.

In HTB-11 cells which represent neurons, the MTT assay demonstrated that treatment with 10uM naringenin significantly mitigated rotenone-induced reduction of cell survival, providing the most effective protection against cell death compared to lower concentrations of naringenin.

Treatment of HTB-11 cells for an LDH assay showed that cells treated with 10uM naringenin + rotenone showed a significant increase in released cytotoxicity, indicating that lower concentrations of naringenin did not significantly increase LDH release from the cells.

The ELISA assay showed that higher concentrations of naringenin, particularly 10uM, reduced αS expression compared to the control, leading to a reduction in neuronal apoptosis. αS expression is also significantly decreased in both αS and phosphorylated alpha-synuclein (p-Ser129) levels compared to rotenone at 100uM and CBD at 100uM, showing an inverse relationship between rotenone/naringenin concentration and their effects on αS and p-Ser129 expression.

A similar inverse relationship was found between caspase activity and the concentration of naringenin through the caspase assay, which also suggests that higher concentrations of naringenin led to reduced caspase activity and thus, reduced apoptosis rates.

Finally, we observed that naringenin at 10uM and CBD at 10uM combined offer the best protection against rotenone-induced cytotoxicity, reducing cytotoxicity from 54.58% to 6.48%. The combined positive protective effects are much more pronounced than CBD or naringenin used alone

Our results have significant implications for rotenone-induced PD treatment, as they demonstrate that naringenin offers neuroprotective effects against rotenone-induced cytotoxicity, and this effect can be maximized when combined with CBD. Although the specific molecular pathways involved remain unclear, future mechanistic studies could investigate the downstream signaling cascades, oxidative stress markers, and apoptotic pathways, and how they contribute to the neuroprotective effects of naringenin. The current study primarily focused on in vitro cell culture models. Future research could involve in vivo studies using animal models of Parkinson's disease to continue to evaluate the neuroprotective effects of naringenin, which would provide a more comprehensive understanding of the potential therapeutic benefits of naringenin in a physiological context.

V. References

[1] Beitz, J. M. (2014, January 1). Parkinson's disease: a review. PubMed. https://pubmed.ncbi.nlm.nih.gov/24389262/

[2] Hajj, R., Schapira, A. H., & Toulorge, D. (2016). Molecular changes in the postmortem parkinsonian brain. ResearchGate. https://www.researchgate.net/publication/304908541_Molecular_changes_in_the_postmortem_parkinsonian_brain

[3] Kelly R, Bemelmans AP, Joséphine C, Brouillet E, McKernan DP, Dowd E. Time-Course of Alterations in the Endocannabinoid System after Viral-Mediated Overexpression of α-Synuclein in the Rat Brain. https://www.ncbi.nlm.nih.gov/pmc/articles/PMC8778740/pdf/molecules-27-00507.pdf

[4] Erekat NS. Apoptosis and its Role in Parkinson's Disease. https://www.ncbi.nlm.nih.gov/books/NBK536724/

[5] Pereira, L., & Cotas, J. (2023). Therapeutic Potential of Polyphenols and Other Micronutrients of Marine Origin. Marine drugs, 21(6), 323. https://doi.org/10.3390/md21060323

[6] Gille, G., Rausch, W.-D., & Radad, K. (2006, March 31). Rotenone induces cell death in primary dopaminergic culture by increasing ROS production and inhibiting mitochondrial respiration. PubMed. https://pubmed.ncbi.nlm.nih.gov/16580092/

[7]Duvigneau, J. C., Trovato, A., Müllebner, A., Miller, I., Krewenka, C., Krenn, K., Zich, W., & Moldzio, R. (2020). Cannabidiol Protects Dopaminergic Neurons in Mesencephalic Cultures against the Complex I Inhibitor Rotenone Via Modulation of Heme Oxygenase Activity and Bilirubin. Antioxidants (Basel, Switzerland), 9(2), 135. https://doi.org/10.3390/antiox9020135

[8]Nouri, Z., Fakhri, S., El-Senduny, F. F., Sanadgol, N., Abd-ElGhani, G. E., Farzaei, M. H., & Chen, J. T. (2019). On the Neuroprotective Effects of Naringenin: Pharmacological Targets, Signaling Pathways, Molecular Mechanisms, and Clinical Perspective. Biomolecules, 9(11), 690. https://doi.org/10.3390/biom9110690

[9]Yu, L. M., Dong, X., Xue, X. D , Zhang, J., Li, Z., Wu, H. J., Yang, Z. L., Yang, Y., & Wang, H. S., (2019). Naringenin improves mitochondrial function and reduces cardiac damage following ischemia-reperfusion injury: the role of the AMPK-SIRT3 signaling pathway. Food & function, 10(5), 2752–2765. https://doi.org/10.1039/c9fo00001a

[10]Li, N., Ragheb, K., Lawler, G., Sturgis, J., Rajwa, B., Melendez, J. A., & Robinson, J. P. (2003). Mitochondrial complex I inhibitor rotenone induces apoptosis through enhancing mitochondrial reactive oxygen species production. The Journal of biological chemistry, 278(10), 8516–8525. https://www.jbc.org/article/S0021-9258(20)86479-5/fulltext

[11] Tapasi Roy, Abhishek Chatterjee, Snehasikta Swarnakar, Rotenone induced neurodegeneration is mediated via cytoskeleton degradation and necroptosis,
Biochimica et Biophysica Acta (BBA) - Molecular Cell Research, Volume 1870, Issue 3, 2023, 119417, ISSN 0167-4889, https://doi.org/10.1016/j.bbamcr.2022.119417.

Remediating Carcinogenic Contamination Produced by Textile Waste Using Wood-decay Fungus

Yunseo Lee[1]

Abstract*—With 92 million tonnes of clothing discarded each year, the textile industry is responsible for 20% of global water pollution. Additionally, the manufacturing and disposal process, mostly occurring in developing nations, involves numerous toxins that may cause lung cancer as workers inhale them. However, wood-decay fungus, which secretes an enzyme capable of decomposing common soil pollutants, may offer a potential solution. Therefore, this research was conducted to study the feasibility of using wood-decay fungus as a bioremediator solution for fiber-related pollutants. In our experiment, contaminated water created by soaking worn-out T-shirts in distilled water revealed low dissolved oxygen (DO) and high dissolved carbon dioxide (COD) levels. In addition, when exposed to the contaminated water, lung cancer cell line A549 experienced increased cell growth and a long band of fragmented DNA. However, *Lentinula edodes* and *Trametes versicolor* (wood-decay fungi) placed in the contaminated water remediated the existing pollution. *L. edodes* was excluded from further experiments, as it suppressed the growth of other plants/biomass, revealing that it may be dangerous to be used as a solution in marine environments. Furthermore, A549 cells treated with *T. versicolor*-treated contaminated water had decreased lung cancer cell growth and less DNA damage. This data was collected by placing a net containing dry fungi next to running textile wastewater or by adding *T. versicolor* in dyeing and bleaching processes. In conclusion, *T. versicolor* remediates clothing waste pollutants in water, inhibits the proliferation of lung cancer cells, and prevents DNA damage. Understanding the effect of wood-decay fungi on clothing waste pollutants and may be significant in discovering new approaches to minimizing environmental impacts and protecting the health of garment workers in the textile industry.

I. Introduction

With the rapid rise of fast fashion, consumers now purchase 60% more clothing than they did 15 years ago [1]. Each year, 92 million tonnes of clothing are wasted, and this waste is responsible for 20% of global water pollution [3,4]. The manufacturing of fabrics uses heavy metals such as cadmium, lead, arsenic, and benzene that contaminate local water supplies that act as resources for irrigation and drinking [5]. When these pollutants enter the human body, through drinking or inhalation in garment hubs, they can cause respiratory, skin, and gastrointestinal health complications, as well as lung cancer [6]. Continuation of current consumer habits will lead to greater water pollution as well as pose risks of cancer for millions of textile factory workers. For example, an estimated 11.4 million women and girls in developing nations, like Bangladesh and Kenya, are victims of forced labor and work up to 15 hours a day, making them highly susceptible to exposure to these toxins [2].

[1] Yunseo Lee is with Chadwick International School, Incheon, 22002 South Korea. (email: m2lee2025@chadwickschool.org).

Wood-decay fungus offers a potential solution, as it secretes laccase, which decomposes environmental hormones that are similar in structure to lignin, cellulose, and hemicellulose [7]. Often called mycoremediation, wood-decay fungus, specifically white-rot fungus, is being used on a pilot scale to remediate soil contamination, implemented in both *ex situ* (biopiling, composting, etc.) and *in situ* (aerobic bioremediation) technologies [8].

This paper investigates the possibility of using the wood-decay fungi *Trametes versicolor* and *Lentinula edodes* as a bioremediating method for fiber-related pollutants, therefore preventing the proliferation of lung cancer cells and DNA damage. This will be assessed through water quality measurements alongside cell proliferation and DNA fragmentation tests.

II. Materials and Methods

1. Water Quality Measurement of Contaminated Water and Synthetic Dye

Contaminated water conditions were imitated by submerging worn-out cotton t-shirts in Erlenmeyer flasks with distilled water (DW) (Fig. 1A). To represent clothing dye used in garment hubs, synthetic dye was created using powdered Rit Dye with a 3% NaCl salt solution (Fig. 1C & 1D) [1]. White cloth was dyed yellow and placed in an Erlenmeyer flask with DW to see possible differences in water quality with regard to dye migration. All flasks were placed on a magnetic stirrer for two weeks (Fig. 1B & 1E).

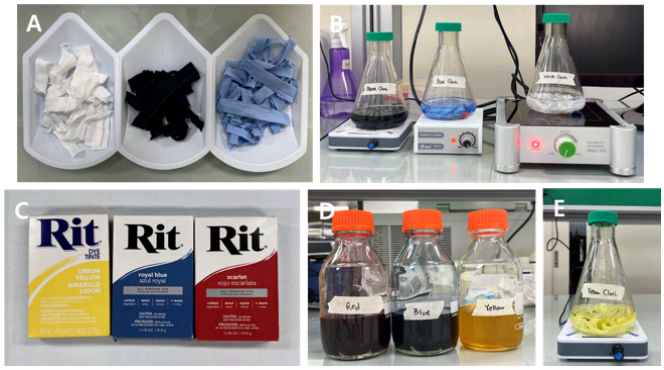

Figure 1. Contaminated water and synthetic dye solution preparation. (*A. Worn-out clothing; B. Clothing on magnetic stirrers; C. Powdered synthetic dye; D. Synthetic dye with 3% salt solution; E. Yellow-dyed cloth on magnetic stirrer*)

The water quality of each contaminated water was measured using a Water Monitoring Test Kit Set (ECOSAVER, Korea). Synthetic dyes were diluted by 0.1x until clear before their water quality was assessed using the most conventionally measured parameters: dissolved oxygen (DO), NO_2^-, NO_3, PO_4^{3-}, pH, and chemical oxygen demand (COD).

2. Remediation Effect of Wood-Decay Fungus on Waste Clothing Contaminated Water

The remediation effect was observed in two conditions: prevention (Pv) and purification (Pu). The former evaluated the effects of wood-decay fungus added at the same time as

waste clothing while the latter measured the effects of wood-decay fungus on already contaminated water.

For Pv conditions, powdered and whole *Lentinula edodes (L. edodes)* and *Trametes versicolor (T. versicolor)* were separately placed in 500-mL glass bottles with white cloth and DW. One bottle only had white cloth and DW as a control, and each container was left sitting for 2 weeks (Fig. 2B). A sample from each bottle was collected, centrifuged, and measured in DO and COD using a Water Monitoring Test Kit. For Pu conditions, white cloth-contaminated water from method 1 was added to separate 50 mL conical tubes with blended *L. edodes* (BLe), whole *L. edodes* (WLe), blended *T. versicolor* (BTv), whole *T. versicolor* (WTv), as well as one tube with only contaminated water as a control (Fig. 2A). After 2 weeks, COD levels were measured.

Figure 2. *T. versicolor* and *L. edodes* placed with waste clothing. (*A. Water contaminated with waste clothing for 2 weeks; B. Waste clothing submerged in DW and wood-decay fungi for 2 weeks; BLe=blended* L. edodes*; BTv=blended* T. versicolor*; WTv=whole* T. versicolor*; WLe=whole* L. edodes*; WC=waste clothing contaminated water*)

3. Wood-decay Fungus' Effect on Plant Growth (Biotoxicity)

Hydroponics was performed by placing cabbage seeds on a gauze soaked with liquid samples from Fig. 2A and 2B to see if the selected wood-decay fungi would negatively impact aquatic plant growth once used underwater. Cabbage seeds treated with samples from fungi-treated contaminated water had growth levels assessed after nine days of growth.

Growth levels of hydroponics results were evaluated based on the number of germinated seedlings and the level of plant growth.

4. Lung Cancer Cell Proliferation Test

The lung cancer cell line, A549 (KCLB 10185, BSL 1) was cultured in RPMI 1640 with 1% penicillin/streptomycin (P/S) and 10% FBS. The cells were seeded in two 6-well plates and treated with 1 µL or 10 µL of filtered waste clothing-contaminated water.

After 48 hours of incubation at 37 C° and 5% CO_2, the cell mixture was seeded in a 96-well plate. EZ-Cytox (DoGenBio, Korea) was added in each well and measured in absorbance using a microplate reader (Diatek, India) at 450 nm.

5. DNA Fragmentation Test

From the waste clothing contaminated water-treated cells in the previous method, DNA was extracted using a Genomic DNA Extraction Kit (AccuPrep, Korea). Gel electrophoresis was conducted and the DNA band was observed under a UV transilluminator (Accuris Instruments, USA).

6. Statistical Analysis

All cell proliferation tests were repeated three or more times and the values obtained were presented as mean ± SE and analyzed using a student *t*-test. Data with p values of 0.01 to 0.05 were marked as '*' and ' 0.05 to 0.001 as '**.', indicating significance.

III. Results

1. Water Pollution of Waste Clothing and Synthetic Dye Contaminants

DO levels for all clothing were lower than the control while COD levels increased by at least 6 ppm, indicating high pollution (Table 1). PO_4^{3-} levels also increased for white- and yellow-dyed cloth, which may contribute to eutrophication. Therefore, this test revealed that all clothing, especially white and freshly dyed cloth, contaminates water.

	Control	White cloth	Blue cloth	Black cloth	Dyed cloth
DO (ppm)	8	5	2	5	5
NO_2^- (ppm)	0	0	0	0	0
NO_3 (ppm)	0.1	0.1	0.1	0.1	0
PO_4^{3-} (ppm)	0.045	0.09	0	0.015	0.33
pH	6	7	6	6	6
COD (ppm)	2	8	20	15	8

Table 1. Water Quality Test Result of Water Contaminated with Different Colored Waste Clothing *(Contaminated water=worn out T-shirts was stored with DW for 14 days; Dyed cloth=white T-shirt stained with yellow synthetic dye)*

All dyes had DO levels lower than the control and PO_4^- unexpectedly increased at a concentration of $1x10^{-7}$ for certain colors (Fig. 3). Therefore, it was determined that there is a negative correlation between DO and synthetic dye but no clear correlation between dye concentration and PO_4^{3-} due to original colors of synthetic dyes interfering with results.

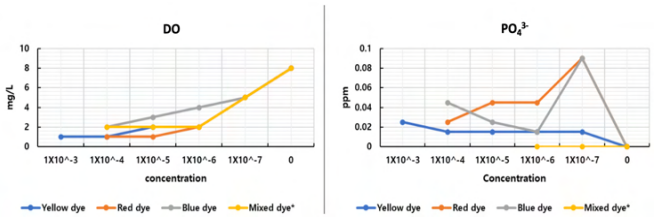

Figure 3. DO and PO_4^{3-} levels of synthetic dye at different concentrations.

2. Pollution Remediation Effect of Wood-Decay Fungus

For Pv conditions of wood-decay fungus, DO levels of *T. versicolor* and *L. edodes*-treated contaminated water showed a change in color but not a change to any indicator colors displayed on the monitoring kit. COD levels in both Pv and Pu conditions showed no change, revealing that wood-decay fungus was able to suppress further contamination from waste clothing.

3. Biotoxicity Results of Wood-decay Fungus Treated Contaminated Water

Contaminated water-exposed seeds had a growth level of 4 and contaminated water treated with whole and blended *T. versicolor* also had strong growth levels of 4 and 5. However, for *L. edodes*, the levels were at 1, meaning that it suppressed the growth of cabbage seeds. Therefore, *L. edodes* was excluded from the remaining experiments, as it would be harmful to plant life in aquatic biomes.

4. Effect of Waste Clothing Contaminant and Wood-decay on Lung Cancer Cell Growth

Cells that were exposed to contaminated water (Pv_control and Pu_control) had a positive trend in cell proliferation compared to DW-treated cells (Fig. 4). However, there was not much change for DC. As such, worn-out textile waste seems able to accelerate the growth of lung cancer cells.

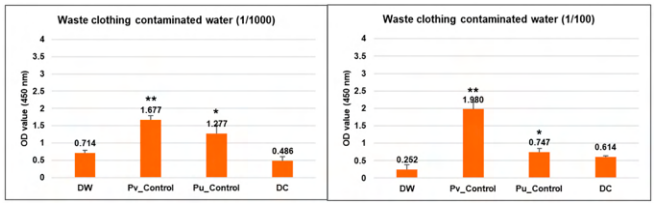

Figure 4. OD value of cells exposed to waste clothing contaminated water. (*Pv=prevention; Pu=purification; DC=dyed clothing, *=0.01<p<0.05; **=0.05<p<0.001*)

Second, for Pv conditions, though results for cells treated with blended *T. versicolor* were unclear, cells treated with whole *T. versicolor* showed a strong decrease in OD value by 91% and 93% in both 1/1000 and 1/100 concentrations. This result means that whole *T. versicolor* can effectively suppress the growth of lung cancer cells in preventive conditions.

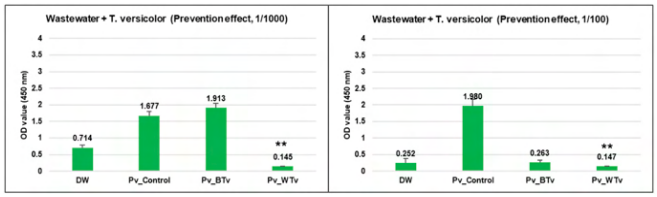

Figure 5. OD value of cells exposed to wood-decay fungus treated waste clothing contaminating water for Pv. (*Pv=prevention; BTv=blended T. versicolor; WTv=whole T. versicolor; **=0.05<p<0.001*)

Third, for Pu conditions, there was little to no change in OD value when cells were treated with *T. versicolor* at 1/100 concentration. Though cells treated at 1/1000 concentration of blended *T. versicolor* showed a 52.7% decrease and 25.2% decrease, for whole ones, a clear correlation was not determined due to the results' high p values.

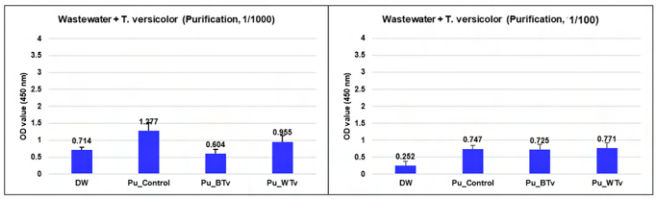

Figure 6. OD values of cells exposed to wood-decay fungus treated waste clothing contaminated water for Pu. (*Pv=prevention; BTv=blended T. versicolor; WTv=whole T. versicolor*)

5. DNA Fragmentation of Lung Cancer Cells Exposed to Waste Clothing Contaminated Water

Sample 1 (Pv_Control) showed a long band of DNA smearing with fragmentation lower than 100 bp, meaning that the waste clothing contaminants severely damaged the DNA. Comparing this to sample 2 (Pv_BTv), sample 2 was only fragmented until near 500 bp. This finding shows that blended *T. versicolor* was able to prevent DNA damage from waste clothing contaminants. For samples 3 and 6 (Pv_WTv and Pu_WTv), a single DNA band was present, meaning that there was no damage. These results show that waste clothing contaminants damage DNA, but whole *T. versicolor* prevents and stops this damage from occurring.

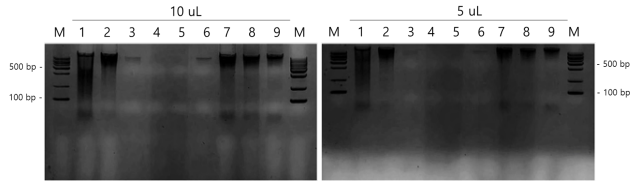

Figure 7. DNA fragmentation results of A549 cells exposed to waste cloth contaminated water with and without wood-decay fungus treatment. (*M=DNA size marker, 1-3=Pv of wood-decay fungus; 4-6=Pu of wood-decay fungus; 1 & 3=waste cloth contaminated water; 2 & 4=blended T. versicolor; 3 & 6=whole T. versicolor; 7=dyed cloth contaminated water; 8=distilled water; 9=control, No treatment; Left-hand side loaded with 10 uL of DNA product; Right-hand side loaded with 5 uL of DNA product*)

IV. Discussion and Conclusion

This research revealed *T. versicolor*'s ability to remediate water pollution caused by textile waste, suppress lung cancer cell growth, and prevent DNA damage from contaminants. Waste clothing contaminated water's water quality measurements were negative, with low DO and high COD levels, and the water proliferated the growth of lung cancer cells and damaged the cells' DNA. *T. versicolor* and *L. edodes* showed pollution remediation effects against the contaminants which can be due to the fungi's ligninolytic enzymes such as laccase [7]. Cell viability and DNA fragmentation tests showed that treating contaminated water with whole *T. versicolor* in preventive conditions suppresses lung cancer cell growth and protects those cells from further DNA damage. The results of this paper suggest that placing nets containing the dry fungi next to running clothing wastewater or incorporating the fungi into the dyeing or bleaching processes may help mitigate the effects of textile pollution. Toxins included in clothing manufacturing processes may also cause other respiratory, skin, and

gastrointestinal health concerns. Limitations of this study include the lack of variety in wood-decay fungus used due to insufficient time available for research. Therefore, further research should explore the remediation effect of multiple types of wood-decay fungus available in developing nations on specific categories of waste clothing pollutants.

References

[1] Martin, C. (2020, June 3). *The average person buys 60% more clothes and keeps them for about half as long as they did 15 years ago.* Hemp Clothing Australia.

[2] *What on Earth is a clothing supply chain?* Good On You. (2022, January 26)

[3] Igini, M. (2022, November 18). *10 stunning fast fashion waste statistics*. Earth.Org.

[4] Robinson, B., & Bryan RobinsonBryan E. Robinson is the owner of TshirtGrowth. He has sold t-shirts since 2006 through dropshipping. (2022, October 16). *35 T-Shirt Industry Statistics (2022)*. TshirtGrowth.

[5] CBC/Radio Canada. (2021, October 1). *Experts warn of high levels of chemicals in clothes by some fast-fashion retailers | CBC News*. CBCnews.

[6] Asher, W. *Unpacking toxic textiles*. Green America. (n.d.).

[7] Veloz Villavicencio, E., Mali, T., Mattila, H. K., & Lundell, T. (2020). Enzyme Activity Profiles Produced on Wood and Straw by Four Fungi of Different Decay Strategies. *Microorganisms*, *8*(1), 73.

[8] Turgeon, M. (2015, March 1). *Fact Sheet: Mycoremediation: White Rot Fungus*. Government of Canada.

Epigenetic Regulation of Head and Neck Squamous Cell Carcinoma: Insights from Transcriptome Analysis of *Nsd1* Knockout 3D Organoid Model

Kristine Lu[1], Chao Lu[2]

***Abstract* - Head and Neck Squamous Cell Carcinoma (HNSCC) are a prevalent form of cancer, affecting the oral cavity, larynx, and pharynx. HNSCC is commonly associated with tobacco use, alcohol consumption, and Human Papilloma Virus (HPV) infection. HPV Positive HNSCC generally exhibits better prognosis than HPV Negative HNSCC, which is frequently diagnosed at advanced stages with poor outcomes. Epigenetics, the study of heritable changes in gene expression that do not involve the sequence of base pairs in DNA, play a crucial role in HNSCC development. Specifically, the mutation of the gene *NSD1,* a gene that mediates histone modification, is often positively correlated with improved survival rates in HPV(-) HNSCC. This study aims to investigate the impact of *Nsd1* mutations on gene expression and pathways using murine oral-derived organoids, a 3D model that mimics head and neck squamous cancer cells' complexities. Through RNA sequencing and analysis, we compared wildtype organoids to organoids where we knocked out *Nsd1* at different stages of cancer progression. Our results suggest that *Nsd1* knockout leads to reduced inflammation, potentially contributing to weakened immune responses, and affects genes associated with Extracellular Matrix Organization, potentially influencing cancer cell migration and metastasis. Additionally, *Nsd1* may alter epithelial-mesenchymal transition, impacting cancer aggressiveness. This study provides valuable insights into the role of *Nsd1* in HNSCC and identifies potential targets for future research and therapeutic interventions.**

I. Introduction

HNSCCs (Head and Neck Squamous Cell Carcinomas) are the sixth most common cancer in the world. The majority of HNSCCs are found in Stage III and IV, where prognosis is poor, making it important to develop effective, less-toxic therapies.[1]

Our study concentrated on how HSNCCs are affected by epigenetics, the study of heritable changes in gene expression that do not involve the sequence of base pairs in DNA. Epigenetic changes consist of various chemical modifications of DNA and its associated proteins, altering gene expression patterns and phenotypic results. For example, the modification of histones, small proteins that maintain structure in chromatin, is widely considered to be a major factor in epigenetics. DNA is wound around histone octamers, keeping the DNA compact and allowing it to fit within the confines of the cell nucleus. When an epigenetic regulator chemically alters a histone protein, such as through the addition of a methyl group or acetyl group, it can affect how tightly wound DNA is, reducing or improving its transcribability and resulting in changes in gene expression, protein production, and cell state. Cancers are often associated with abnormality of certain epigenetic modifiers and modulators, making epigenetics a potential target for research and the development of new treatments.[2]

Nsd1 is a gene which plays a significant role in developmental epigenetics. One of the primary functions of *Nsd1* is to mediate the di-methylation at the 36th lysine residue of the Histone 3 protein, [H3K36me2], causing downregulation of transcription of nearby genes. Numerous studies[3, 4] have found that the *Nsd1* gene is frequently mutated in HNSCC, and that there is a positive correlation between mutations in *Nsd1* and the patient rate of recovery from HPV(-) HNSCC through the alteration of methylation levels of the H3K36me2 residue. In one such study[4], among 457 HPV(−) tumors, 13% contained alterations in the *Nsd1* gene. HNSCC patient samples with mutations in *Nsd1* exhibited reductions in H3K36me2. Recent studies[3,4] implicate that *Nsd1* mutations are associated with significantly improved patient survival rates. Mutations in *Nsd1* that lead to loss of function of the gene have also been found to correlate with the expression of several miRNAs and mRNAs important in cancer regulation and proliferation pathways. However, the mechanisms behind how these mutations in *Nsd1* ultimately lead to increased survival in HNSCC patients is still unclear, and further research is needed to clarify the pathways involved.

Our study aimed to identify genes and pathways which exhibited consistent and significant changes in expression when *Nsd1* was heavily mutated in carcinogenic head and neck squamous cells. While previous studies have been successful in analyzing the role of *Nsd1* through 2D cell cultures, we utilized oral-derived organoids (self-organized 3D tissue cultures that are generally derived from stem cells) to recapitulate features of primary mouse tongue epithelium in a 3D model encapsulating the key complexities of head and neck squamous cells. We procured samples of organoid cells at different stages of cancer growth in a mouse model of HNSCC and performed RNA sequencing. By analyzing the RNA-seq dataset, we compared the level of expression of various genes between cells with wildtype Nsd1 and cells where *Nsd1* was knocked out.

II. Materials and Methods

Deleting *Nsd1* gene in mouse tongue epithelium:

The Lu lab utilized Cre Recombinase, a specialized enzyme facilitating targeted genetic modifications by excising segments of DNA between selected loxP sites (which we introduced through genetic engineering), to delete exon 3 of the *Nsd1* gene in a conditional knockout mouse strain. Cre Recombinase was induced in the presence of a KRT5 promoter (a sequence which controls the expression of genes) by Tamoxifen (a commonly used inducer of Cre

[1]K.L. is with University High School, 4771 Campus Drive, Irvine, CA 92618, and Lu Lab @ Columbia University (corresponding author to e-mail: kaynelu921@gmail.com).
[2]C.L. is with Lu Lab @ Columbia University

Recombinase), which was administered via oral gavage 3 times a week. To ensure that the deletion and recombination of DNA had successfully occurred, the mice also carry an mTmG allele. mTmG mice allow us to determine the effectiveness of Cre-recombinase using color fluorescence.

Generation of *Nsd1* knockout organoids, RNA extraction and sequencing:

We treated *Nsd1* wildtype and *Nsd1* knockout mice with 4NQO (r-nitroquinoline 1-oxide) (a potent carcinogen) in their drinking water to induce cancer growth. Mouse tongue tissue from control and *Nsd1* KO mice following tamoxifen administration were then dissociated into single cells and sorted to allow for isolation of epithelial cell populations. Cells were seeded and added to the media, which was changed every two days, and cells were passaged to form organoids, which provide a more physiologically relevant model than cell populations for study. Passaging involves dissociating and moving cells between culture vessels in order to promote and maintain healthy organoid growth and prevent overcrowding. We established 3D organoid cultures from mice at 0, 16, or 32 weeks of 4NQO treatment, which are considered as normal, precancerous, and cancerous, respectively.

RNA extraction and sequencing analysis:

Once our organoids had developed, we disrupted the organoid cells to release the RNA using Trizol, taking appropriate measures to protect the RNA from degradation. This step aimed to capture the genetic information present in cells, particularly RNA involved in gene expression. We then extracted it using a standard RNA extraction kit and purified it to remove impurities. Extracted RNA samples were used to prepare for sequencing libraries using Illumina kits. The libraries were sequenced using NextSeq 400.

The raw sequencing data obtained from the RNA-sequencing was processed using FastQC, a widely used tool for assessing the quality of sequencing data. FastQC measured the per-base sequence quality, identifying regions of inaccurate data, as well as sequence length distribution, which ensures uniform coverage and detects anomalies in our RNA sequences. The GC content refers to the proportion of guanine and cytosine nucleotides in the RNA sequence, and discrepancies were identified and data was adjusted accordingly. FastQC also helped identify redundant sequence stretches which were removed. We performed necessary trimming and filtering to pre-process the data. The reads were then aligned to a mm10 reference genome using HISAT2 alignment algorithms. This process involved mapping the reads to their corresponding genomic locations in the mouse genome. Subsequently, the characteristic sequences in the aligned reads were quantified using the tool, featureCounts, to assess gene expression patterns.

We performed differential gene expression analysis of our processed data to determine using DESeq2, a widely used tool for RNA sequencing data analysis. DESeq2 first performs data normalization, adjusting for differences in sequencing depth between samples to ensure accurate comparisons. It then estimates dispersion to account for variability in gene expression across samples, before matching a generalized linear model framework to the dispersion-adjusted, normalized data to identify genes that show significant changes in expression levels between different batches of cells and cells of different time frames. This analysis allowed for the identification of genes that were significantly upregulated or downregulated in *Nsd1* KO cells compared to wild-type cells. We utilized DESeq2 to generate tables of differentially expressed genes, log-fold changes between data points, and p-values. Statistical tests, such as negative binomial distribution-based analysis, were applied to determine the significance of gene expression changes. These tests, particularly the negative binomial distribution-based analysis implemented in DESeq2, were selected for their suitability in handling the unique characteristics of RNA-seq data. The negative binomial distribution is well-suited for modeling RNA Sequencing data by accommodating overdispersion and accurately reflecting the variability observed in gene expression levels. A link to the R script used can be found here.

We then further analyzed the differentially expressed genes using Enrichr, a gene set analysis server widely used in gene analysis. This analysis helped identify key pathways and biological processes associated with *Nsd1* mutation and their potential implications in cancer progression.

Data Visualization:

PCA Plots, Heatmaps, and Lists of significantly upregulated and downregulated genes were generated based on statistical analysis results using data visualization libraries in R including ggplot2, DESeq2, gplots, and more.

III. Results

Our data consisted of 16 sets of RNA-seq samples from different organoid cultures at different stages of cancer development. We had 4 data points from 0 weeks into cancer development, 5 points from 16 weeks into development, and 7 points from 32 weeks into cancer development. Each data point consisted of a list of affected genes and their levels of expression, varying based on amount of time into cancer development and *Nsd1* KO vs. Wild-type. PCA plots/clustering showed that 0-week and 16-weeks organoids had similar levels of overall gene expression to each other, while 32-week organoids showed large differences from the 0/16 week data points. (Fig. 1). This is likely due to the progression of cancerous mutations over time.

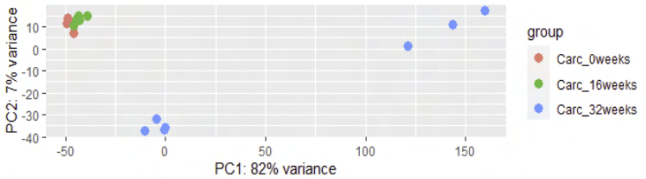

Figure 1: PCA Plot comparing organoids at 0 weeks, 16 weeks, 32 weeks of 4NQO carcinogen treatment. Generated from R

To confirm, we analyzed and compared the 0/16 week wild-type data and 32 week wild-type data as a control

group. Inputting our data into Enrichr, a gene analysis tool, we showed that at 32 weeks, there was an upregulation of genes involved in the RAC1 GTPase Cycle (associated with cytoskeletal structure and cell proliferation), inflammatory response pathways, and Allograft Rejection (rejection of foreign cells), which suggests increased activation of signaling pathways associated with cellular movement, immune response, and potential rejection-like processes (Figure 2).

On the other hand, our data also showed significant downregulation of genes related to oxidative phosphorylation, cyclin and cell-cycle regulation, and mitochondrial translation elongation pathways, indicating a shift away from normal cellular energy production and controlled cell division (Figure 3). This deviation from typical cellular processes aligns with the "hallmarks of cancer," reflecting dysregulation in energy metabolism and cell cycle control, which are common features in cancerous cells.These changes align with characteristics observed in cancer, particularly in terms of enhanced cell mobility and immune-related responses. Overall, these findings suggest a molecular signature consistent with cancer progression in the 32-week organoids compared to the 0/16-week ones. The observed alterations in gene expression patterns validate the effectiveness of the analysis methods employed, supporting the conclusion that the organoid cultures were evolving in line with the intended experimental design.

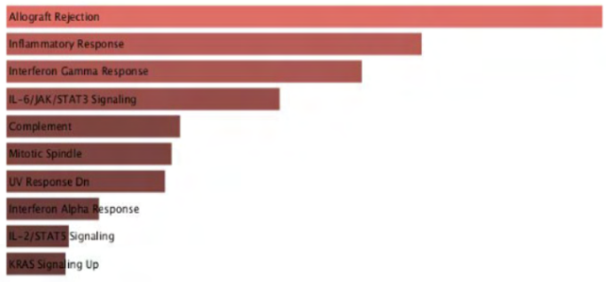

Figure 2: Significantly Upregulated Genes in MSigDB Hallmark 2020 Pathways in 32-weeks organoids, sorted by P-Value.

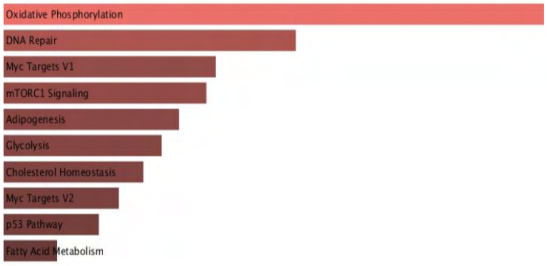

Figure 3: Significantly Downregulated Genes in MSigDB Hallmark 2020 Pathways in 32-weeks organoids, sorted by P-Value.

We also noticed in a PCA plot where the *Nsd1* KO genotype was annotated (Figure 4) that, at 32 weeks, but not at 0/16 weeks, *Nsd1* KO cell organoids varied greatly from WT organoids in their gene expression patterns.

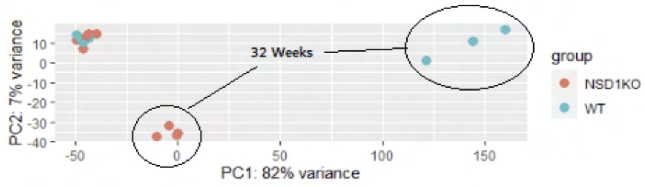

Figure 4: PCA Plot comparing Nsd1KO and WT organoids. Generated by R

A heatmap generated through unsupervised clustering, which identifies patterns in gene expression even without labeled categories, showed similar results, where wild-type 32-Weeks organoids showed high variance of gene expression compared to *Nsd1* KO organoids at 32 weeks, which clustered much closer to 0/16-week organoids (Figure 5).

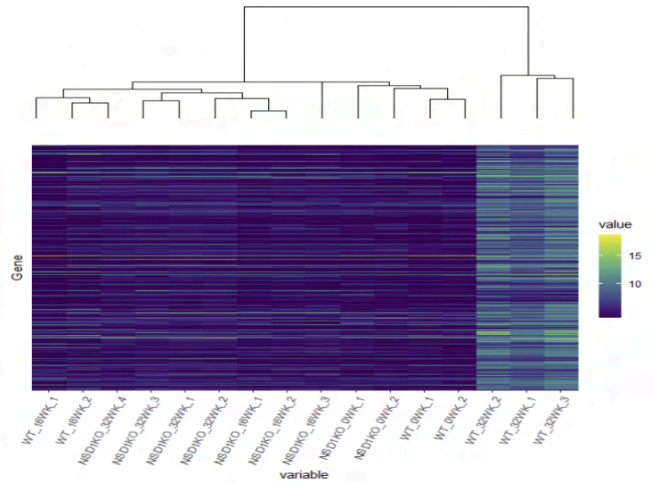

Figure 5: Gene expression heatmap of WT/Nsd1KO organoids over 0/16/32 weeks, clustered by similarity, generated by R.

We proceeded to compare differentially expressed genes of 32-weeks wild-type organoids and 32-weeks *Nsd1* KO organoids. We found significant downregulation of genes in the Allograft Rejection, inflammatory response pathways, and inflammatory response in cells when *Nsd1* was knocked out (Figure 6). This implies that inflammation, a hallmark of cancer, is lowered and tumor tissue doesn't trigger as great of an immune response in cells where *Nsd1* is knocked out. This is consistent with previous studies that report DNA methylation resulting in immune-cold phenotypes[5].

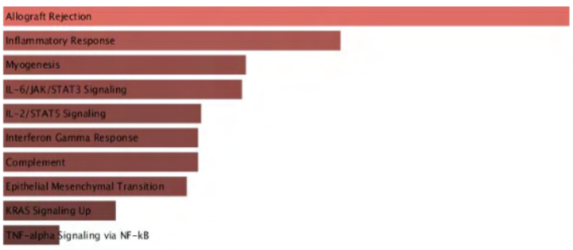

Figure 6: Significantly Downregulated Genes in MSigDB Hallmark 2020 Pathways in *Nsd1* knockout organoids, sorted by P-Value.

In addition, 32-weeks *Nsd1* KO organoids displayed an upregulation of Extracellular Matrix (ECM) Organization genes (eg. Apical Junction) which are responsible for monitoring cell movement (Figure 7). This upregulation is influential in controlling the movement and spread of cancer cells from the primary tumor in the beginnings of metastasis[15] . Our results align with previous studies investigating the relationship between *Nsd1* and cancer, which imply that the *Nsd1* gene may contribute to ECM modeling associated with tumor metastasis.

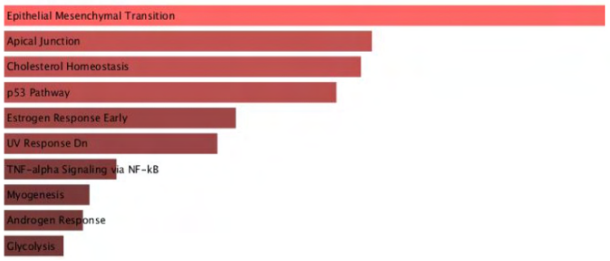

Figure 7: Significantly Upregulated Genes in MSigDB Hallmark 2020 Pathways in Nsd1 knockout organoids, sorted by P-Value.

We also observed a significant upregulation in the epithelial mesenchymal transition (EMT) pathway genes (Figures 7 and 8), which allows epithelial cells to undergo changes and transform into a mesenchymal cell phenotype. Mesenchymal cells are multipotent stem cells with a dynamic cytoskeleton and which exhibit cellular plasticity, and are characterized by extensive migratory capabilities. Studies[8, 9, 10] have shown that EMT is involved in tumor progression and metastasis, as well as initial angiogenesis (the formation of new blood vessels around a tumor, enhancing tumor growth) sprouting. In our *Nsd1* KO organoids, genes which generally promote EMT such as Snai1, Cdh2, Col11a1, Mmp16, Zeb1, Zeb2 and others were significantly downregulated, while genes which inhibit EMT including Cldn4, Cldn3, Epcam, Patj, Ocln, and more were significantly upregulated (Figure 10). Thus, it can be speculated that *Nsd1* may be regulating genes that promote EMT, so that when it is heavily mutated or knocked out, tumor cells have less EMT and metastasize less rapidly.

A graph of select significant genes and their Log2 fold changes is shown below (Figure 8). Negative Log2 Fold Changes signify significant downregulation, while positive changes signify significant upregulation.

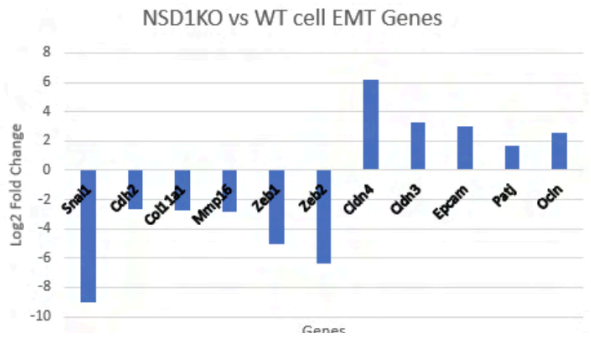

Figure 8: Log2 Fold Changes of EMT genes comparing Nsd1 KO vs. WT organoids.

IV. Discussion

Based on the results of our analysis, we can speculate that there is a correlation between loss of *Nsd1* and changes in EMT pathway as well as a downregulation of inflammation response. Our results align with previous studies[11, 12, 13] that suggested a relationship between the EMT pathway and inflammation in carcinogenesis. Cancer cells which have undergone EMT have altered cell-cell junction complexes (complexes allowing for cell communication and associated with preventing overgrowth) and become more aggressive, stimulating the production of proinflammatory factors such as IL-1 and TNF, by cancer cells. Consistent with our findings, studies show that a decrease in EMT is associated with a decrease in inflammation[16].

Similarly, we noticed a correlation between EMT pathway expression and ECM Organization pathways. Shared genes in the ITGB family, Laminin Subunit Alpha genes, and more were present in both EMT pathways and Extracellular Matrix Organization pathways.

ITGB1, Integrin Subunit Beta 1, and ITGAM, Integrin Subunit Alpha M, are protein-coding genes which interact with the ECM. In particular, ITGB forms a heterodimeric complex (a protein composed of two different polypeptide chains) with an alpha subunit of integrins, allowing integrins to interact with ligands in the ECM. This allows it to regulate various cellular processes including migration, proliferation, and survival. Mutations and dysregulations of ITGB have been implicated in various aspects of cancer development and metastasis. In *Nsd1* KO organoids, ITGB1 is significantly upregulated compared to in wild-type cells.

Another gene family including LAMB3, LAMC2, LAMB1, and LAMA5 encodes for different subunits of the laminin protein family. Laminins are proteins with sugar molecules attached (glycoproteins) that play a crucial role in the formation of the basement membranes in the extracellular matrix. Laminin-encoding genes are involved in both the EMT pathways and the ECM Organization pathways, and are a component in determining cell growth, communication, and movement. Reduced expression of LAMA5 has been found in some types of cancer, and restoring its expression has been shown to inhibit tumor growth and metastasis. LAMA5, LAMB1, LAMB3, and LAMC2 were among significantly upregulated genes in organoids where *Nsd1* was knocked out.

Clinically, several studies have linked both lower metastatic potential and increased chemotherapy responsiveness to genes involved in the EMT pathway. However, the exact extent of EMT's role in these observations requires further investigation.

Our data also revealed the upregulation and downregulation of many genes that are not part of the above pathways, including upregulations in pathways associated with T-cells, NK cells and others in *Nsd1* KO cells, and downregulations in other pathways. However, The significance of these pathways in cancer pathophysiology is still not clear and warrants further studies.

In summary, it was observed that *Nsd1* KO organoids at 32 weeks had a lower level of cancer aggressiveness compared to wild-type cells at the same time point. The downregulation of genes associated with inflammation pathways in *Nsd1* KO organoids suggests that they trigger a weaker immune response than wild-type cells, which the body reacts strongly to. In contrast, upregulation of genes associated with ECM organization in *Nsd1* KO organoids indicates an effect on the mobility of cancer cells during the early stages of metastasis. Furthermore, *Nsd1* may promote epithelial-mesenchymal transition (EMT) (the process where epithelial cells gain migratory properties and become mesenchymal stem cells), allowing cells higher migratory capability. In *Nsd1KO* organoids, we found that genes that promote EMT were significantly downregulated, while those that inhibit EMT were upregulated.

The decrease in inflammation and inhibition of EMT and ECM Organization Pathways in *Nsd1* knockout mouse HNSCC organoids are consistent with clinical reports of a better prognosis in human HNSCC when *Nsd1* is heavily mutated. These findings have significant implications for cancer management and treatment, as *Nsd1* presents a promising target for biomarker development and therapeutic intervention, to recognize genetic signs and intervene before cancer development[12]. However, further research is needed to fully understand the mechanisms by which *Nsd1* functions in cancer progression, and to determine the optimal strategies for targeting this gene in cancer therapy.

References

1. Jemal A, Bray F, Center MM, Ferlay J, Ward E, Forman D. Global cancer statistics. *CA Cancer J Clin* 2011;61:69–90.
2. Weinhold B. Epigenetics: the science of change. Environ Health Perspect. 2006 Mar;114(3):A160-7. doi: 10.1289/ehp.114-a160. PMID: 16507447; PMCID: PMC1392256.
3. Nargess Farhangdoost, Cynthia Horth, Bo Hu, Eric Bareke, Xiao Chen, Yinglu Li, Mariel Coradin, Benjamin A. Garcia, Chao Lu, Jacek Majewski, Chromatin dysregulation associated with Nsd1 mutation in head and neck squamous cell carcinoma, Cell Reports, Volume 34, Issue 8, 2021, 108769, ISSN 2211-1247,
4. Pan, C., Izreig, S., Yarbrough, W. G., & Issaeva, N. (2019). Nsd1 mutations by HPV status in head and neck cancer: differences in survival and response to DNA-damaging agents. Cancers Head Neck, 4, 3. PMID: 31321084; PMCID: PMC6613249.
5. Brennan K, Shin JH, Tay JK, Prunello M, Gentles AJ, Sunwoo JB, Gevaert O. NSD1 inactivation defines an immune cold, DNA hypomethylated subtype in squamous cell carcinoma. Sci Rep. 2017 Dec 6;7(1):17064. doi: 10.1038/s41598-017-17298-x. PMID: 29213088; PMCID: PMC5719078.
6. Oshi, M., Le, L., Angarita, F.A., Tokumaru, Y., Yan, L., Matsuyama, R., Endo, I., & Takabe, K. (2021). Association of allograft rejection response score with biological cancer aggressiveness and with better survival in triple-negative breast cancer (TNBC). Journal of Clinical Oncology, 39(15_suppl), 561. https://doi.org/10.1200/JCO.2021.39.15_suppl.561
7. Krossa I, Strub T, Aplin AE, Ballotti R, Bertolotto C. Lysine Methyltransferase Nsd1 and Cancers: Any Role in Melanoma? Cancers (Basel). 2022 Oct;14(19):4865. doi: 10.3390/cancers14194865. PMID: 36230787; PMCID: PMC9563040.
8. Huang, Y., Hong, W. & Wei, X. The molecular mechanisms and therapeutic strategies of EMT in tumor progression and metastasis. *J Hematol Oncol* 15, 129 (2022). https://doi.org/10.1186/s13045-022-01347-8
9. Ribatti D, Tamma R, Annese T. Epithelial-Mesenchymal Transition in Cancer: A Historical Overview. Transl Oncol. 2020 Jun;13(6):100773. doi: 10.1016/j.tranon.2020.100773. Epub 2020 Apr 22. PMID: 32334405; PMCID: PMC7182759.
10. Masao Saitoh, Involvement of partial EMT in cancer progression, *The Journal of Biochemistry*, Volume 164, Issue 4, October 2018, Pages 257–264, https://doi.org/10.1093/jb/mvy047
11. Suarez-Carmona M, Lesage J, Cataldo D, Gilles C. EMT and inflammation: inseparable actors of cancer progression. Mol Oncol. 2017 Jul;11(7):805-823. doi: 10.1002/1878-0261.12095. Epub 2017 Jun 26. PMID: 28599100; PMCID: PMC5496491.
12. Ricciardi, M., Zanotto, M., Malpeli, G. *et al.* Epithelial-to-mesenchymal transition (EMT) induced by inflammatory priming elicits mesenchymal stromal cell-like immune-modulatory properties in cancer cells. *Br J Cancer* 112, 1067–1075 (2015). https://doi.org/10.1038/bjc.2015.29
13. Md Shariful Islam, Md Reaz Morshed, Golap Babu, Md Asaduzzaman Khan. The role of inflammations and EMT in carcinogenesis, Advances in Cancer Biology - Metastasis Volume 5, 2022,100055,ISSN 2667-3940, https://doi.org/10.1016/j.adcanc.2022.100055.
14. Yang C, Wang K, Liang Q, Tian TT, Zhong Z. Role of Nsd1 as potential therapeutic target in tumor. Pharmacol Res. 2021 Nov;173:105888. doi: 10.1016/j.phrs.2021.105888. Epub 2021 Sep 16. PMID: 34536546.
15. Popova NV, Jücker M. The Functional Role of Extracellular Matrix Proteins in Cancer. Cancers (Basel). 2022 Jan 4;14(1):238. doi: 10.3390/cancers14010238. PMID: 35008401; PMCID: PMC8750014.
16. Suarez-Carmona M, Lesage J, Cataldo D, Gilles C. EMT and inflammation: inseparable actors of cancer progression. Mol Oncol. 2017 Jul;11(7):805-823. doi: 10.1002/1878-0261.12095. Epub 2017 Jun 26. PMID: 28599100; PMCID: PMC5496491.

Decision Bias in Recognition Memory: How Memory-Selective Neurons Encode Criterion Shifts

Cloris Shi[1], Evan Layher[2]

Abstract— **Humans make recognition-based decisions by assessing stimuli familiarity while considering strategic biases. For example, in the legal system, people balance eyewitness memory against the consequences of mistakenly identifying the wrong suspect. Under uncertain memory, individuals can flexibly shift criteria to optimize decisions based on the situation. Prior single-neuron research has characterized memory-selective (MS) neurons that accurately distinguish new and familiar stimuli, but it remains unclear whether these neurons respond differently under various decision biases. Here, we recorded extracellular action potentials of single neurons across frontal and temporal cortices while subjects performed an image recognition task with criterion manipulations. Firing rate patterns of MS neurons were decoded using a Support Vector Machine (SVM) classifier to identify selectivity during pre-stimulus and stimulus periods. In all recorded brain regions, we identified MS, visually-selective, and criterion-selective neurons. Furthermore, MS neurons encoded criterion shifts and image categories, suggesting that memory is integrated in parallel with other stimuli within the single neurons. These findings reveal that MS neurons are influenced by decision biases and other stimulus features that encompass the nuances of memory-based decision-making.**

I. Introduction

Recognition memory allows us to identify familiar objects, individuals, and events. It is an important component of declarative memory, or memory that is selectively and consciously retrieved. Recognition memory is often impaired in individuals with amnesic or neurodegenerative conditions like Alzheimer's disease, so recognition tasks are routinely used for assessments of human cognition [1]. Under uncertainty, memory-related decisions rely on integrating information from two aspects: (1) strength of familiarity with the stimulus and (2) the external context in which the stimulus is presented [2]. In other words, memory recall is often integrated with metacognitive decision processes when people decide whether to report or withhold uncertain evidence of familiarity. Hence, decision-making requires the interplay of memory strength and context.

Signal detection theory, a mathematical model, provides a framework to quantify the distinction between the retrieval and the decisional components of recognition memory. In this model, a human indicates a "remember" response by making a high-confidence "old" judgment. Adaptive decision-making involves setting a decision criterion along the familiarity continuum, a threshold above which a human will classify an item as a prior encounter [4]. In an old-new recognition memory task, a liberal criterion accepts items as old despite little memory evidence, while a conservative criterion accepts fewer items as old and requires more memory evidence. Shifting criteria allows an agent to make optimal decisions in different scenarios.

The neuroscience of recognition memory has remained elusive. Neuroimaging studies of recognition memory have long overlooked the role of criterion-shifting, a flexible and highly individualistic characteristic that introduces response bias during evaluation [5]. In fact, participants engage in decision biases during tasks even in the absence of instruction. To better disentangle memory and decisional processes, it is necessary to control for decision biases in our experimental design through deliberate manipulations.

Variation in criterion-shifting between individuals suggests the existence of a biological basis encoding criterion. Some individuals will consistently maintain either a liberal or conservative criterion, while others are more flexible in adapting their criterion to optimally adhere to shifting priorities. Using a behavioral task to deliberately encourage criterion shifts, we have identified criterion-sensitive regions across widespread fronto-parietal regions by using functional magnetic resonance imaging (fMRI) [6]. Neuroimaging like fMRI uses hemodynamics, or changes in blood flow measured with blood-oxygen-level dependent (BOLD). Hemodynamics serves as a useful proxy because neuron activity increases with greater blood perfusion of the brain. However, neuroimaging displays the activity of populations of neurons, so improved techniques are needed to understand the dynamics of specific single neurons.

Single neuron recording provides much better temporal and spatial resolution than non-invasive neuroimaging or electroencephalograms. Prior single-neuron studies have suggested that single cells, or neurons in this case, can encode stimulus identity (visually-selective) and familiarity (memory-selective) with abstract concepts. Memory-selective neurons, which fire differently in response to previously seen concepts, are in the hippocampus and amygdala [7]. However, it remains unknown how neurons selectively integrate memory retrieval and decision biases, and whether both signals are engaged dynamically when required.

Here, we aimed to uncover the existence of criterion-selective neurons, which are cells that respond differently under liberal and conservative criteria. Then, we sought to understand how visually-selective and memory-selective neurons respond under controlled criterion-shifts to determine if memory and decisional aspects of recognition are processed in parallel.

II. Methods

A. Behavioral Task Design

Patients with drug-resistant epilepsy received electrodes for intracranial monitoring based on clinical criteria. Each macro-electrode contained eight 40 μm diameter microwires, from which broadband 0.1 to 9000 Hz extracellular signals were recorded at a 32 kHz sampling rate (ATLAS system, Neuralynx Inc.). Subjects (ages 24–65 (M=40); 5 female, 1 male, 1 non-binary) were 7 epilepsy patients from Cedars-Sinai Medical Center. The institutional review boards of Cedars-Sinai Medical Center and the California Institute of Technology approved all protocols.

[1] Cloris Shi is with Troy High School, 2200 Dorothy Ln, Fullerton, CA 92831 (corresponding author to e-mail: clorisfshi@gmail.com)
[2] Evan Layher is with the Department of Psychological and Brain Sciences, University of California, Santa Barbara, CA 93106 and Department of Neurosurgery, Cedars-Sinai Medical Center, Los Angeles, CA 90048.

Participants performed a recognition memory task with criterion manipulations (Appendix 1A, B). Each subject viewed 256 images per session, which had 16 test blocks of 16 images retrieved from the LaMem database [8].

Each block began with a study phase. Subjects memorized a series of 32 images, shown once (16 images) or twice (16 images). Discriminability or difficulty of memory recall was considered "easy" for images displayed twice and "hard" for images displayed once.

In the test phase, subjects decided whether the image had been present in the study phase and how confident they were. Correct responses for old or new items are "hits" or "correct rejections," while incorrect responses for an old or new item are "false alarms" or "miss" respectively.

Two error schemes were implemented to alternatively encourage liberal or conservative criteria shifts. While implementing a liberal criteria, one minimizes misses, while under a conservative criteria, one minimizes false alarm. Subjects' performance were evaluated based on two parameters: (1) difficulty of the task, assessed by discriminability (d_a), and (2) strategy of the subject, assessed by criterion placement (c) and criterion shift (C).

A normal, equal-variance signal detection theory model evaluated task performance per individual (Appendix 1.C.). Discriminability (d_a), differences in discriminability across conditions (Δd_a), criterion placement (c_a), and criterion shifting (C) is computed across all conditions. Hit rate (*HR*) and false alarm rate (*FAR*) were computed from summation of the total hit (H), miss (M), correct rejection (CR), and false alarm (FA) rates within each trial:

$$HR = \frac{H}{H+M} \quad (1)$$

$$FAR = \frac{FA}{CR+FA} \quad (2)$$

$$d_a = \left(\frac{2}{1+s^2}\right)^{1/2}[z(HR) - sz(FAR)] \quad (3)$$

$$c_a = \frac{-\sqrt{2}s}{(1+s^2)^{1/2}(1+s)}[z(HR) + z(FAR)] \quad (4)$$

$$C = c_a(conservative) - c_a(liberal) \quad (5)$$

$$\Delta d_a = d_a(moderate) - d_a(low) \quad (6)$$

where z is the density of standard normal distribution and s is the standard deviation ratio between old item and new item distributions. We set s = 0.8, which is the mean ratio computed for recognition memory tests [9].

B. Spike Sorting

Extracellular action potentials from neurons were recorded in subjects during the task. Raw signals were bandpass filtered 300–3,000 Hz. Spikes were detected and sorted offline using OSort (v4.1), a semi-automatic, template-matching algorithm [10]. OSort used an adaptive threshold to rudimentarily filter putative neurons, but spikes could be interrupted by electrical noise or neurons firing in synchrony. Thus, manual offline sorting remained necessary with a qualitative rubric (Appendix 2.A). We recorded 955 single neurons in five brain regions: medial temporal lobe (MTL; n=334), medial frontal cortex (MFC; n=288), posterior temporal cortex (PTC; n=158), orbitofrontal cortex (OFC; n=104), and insular cortex centromedian thalamic nucleus (INS, CM; n=71) (Appendix 2.B).

C. Statistical and Decoding Analysis

Neuron selectivity was determined by comparing firing rates between two 1s windows: (1) pre-stimulus phase defined -1000–0 ms before image onset and (2) stimulus phase from 200–1200 ms after image onset (t=0 ms). Recorded stimulus period is offset by 200 ms from image onset to compensate for the time neurons need to encounter and process visual stimuli [11].

We assessed four types of neuron selectivity: image category, criterion, memory, and confidence. A neuron was considered visually-selective (VS) if the firing rate differed across the four visual categories using a 1×4 analysis of variance (ANOVA) test at p<0.05. A memory-selective (MS) cell differentially fires when correctly classifying new and old stimuli; confidence-selective neurons respond differently in low and high confidence scenarios, as assessed using paired t-tests. A criterion-selective (CS) neuron fires distinctively in conservative and liberal criteria trials either in pre-stimulus or stimulus test phases.

Single-trial population decoding was performed on high-firing neural populations (>0.4 Hz) assembled across sessions. Firing rates for each cell were first detrended and then normalized. A 10-fold cross validation linear support vector machine (SVM) classifier for neural decoding was implemented in MATLAB (R2023a). The decoder randomly selected 80% of the neural population to analyze, and performance was tested on the remaining 20% to estimate the variance of random decoding. Time-resolved decoding was further performed on spike counts measured in a 200-ms moving window from -1000–1200 ms. The decoder's performance was evaluated against the 95th percentile of a null distribution. Performance was defined as average accuracy at selecting the correct category.

III. Results and Discussion

A. Task Performance

We sought to understand neuron responses to stimuli and behaviors. Discriminability manipulations successfully altered task difficulty between hard and easy discriminability conditions. Mean image discriminability (d_a) across hard discriminability trials (Mean (M)=1.16, Standard Deviation (SD) =0.943) remained significantly lower compared to easy ones (M=1.68, SD=1.18) (MΔ = -0.52, 95% CI [-0.66, -0.38]) confirming that viewing stimuli once versus two times during the study phase effectively modulated task difficulty for subjects.

Criterion (c) assesses the direction and magnitude of decision biases. Mean c in the conservative condition (M=0.066, SD=0.41) was significantly greater than the mean c in the liberal condition (M =-0.25, SD = 0.49), showing that the penalty system shifted criterion placement (MΔ = 0.32, 95% CI [0.26, 0.38]).

A criterion shift (C) between conservative and liberal sessions was more prominent across all subjects during uncertain memory. Mean C in hard discriminability conditions (M=0.40, SD=0.53) was significantly higher than mean C in easy discriminability ones (M=0.24, SD=0.53) (MΔ = 0.16, 95% CI [0.091, 0.23]). We conclude that participants rely more heavily on memory strength during easier tasks but use strategic criteria shifts when it is difficult to discriminate images.

A. *Neuron Selectivity*

Electrodes recorded a total of 955 single neurons and 2,917,842 action potentials. This was assessed using a standard analysis of variance (ANOVA) test that identified 787 (82%) selective neurons in the pre-stimulus (62%) and stimulus (38%) phases. Selective neurons are defined as neurons that exhibited statistically significant differences in firing rate pattern in response to various stimuli, such as image category, criterion placement, memory familiarity, and recollection confidence. In total, neurons encoded 2,351 selectivities, suggesting that one neuron could encode multiple selectivities.

Among stimulus-phase neurons, VS neurons (n=171), shown in Figure 1B, constituted the largest proportion (35%). Among VS cells, decoding analyses revealed that neurons were selective to memory (p<0.001) during the stimulus but not pre-stimulus phase. The concurrent processing of memory in VS cells suggests that the parameters of each image category are represented as a memorized concept. These findings matched concept cells that encode abstractions like the categories of our task [3]. As such, VS cells served as the control group on which decoding accuracy was evaluated for MS and CS neurons.

MS neurons were identified during the stimulus phase of test periods. Their firing rates differ between trials where an accurate old or new response was given (Figure 1A). There were 18% of stimulus-phase neurons significantly (p<0.05) modulated by memory, similar to prior studies [12]. Memory-selectivity was decoded through a SVM classifier (p<0.001) across all defined brain regions but most appeared in the MTL (45%). This matches the current understanding of the MTL as the main site for the encoding and integration of memory. The decoding classifier revealed that MS neurons were also selective to confidence (p = 0.0035; Figure 2A), suggesting that memory may be encoded in gradations by familiarity. Visually-selective MS neurons constituted 30% of the MS population, and SVM decoding in Figure 2B supports that memory recall relies on simultaneous categorization (p < 0.001).

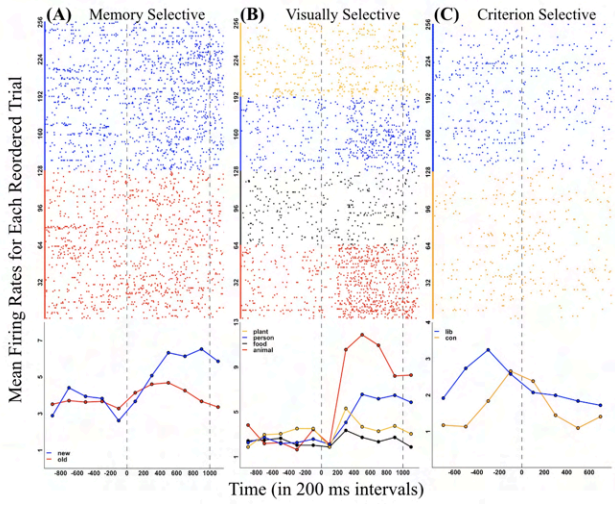

Figure 1. Example raster plots of mean firing rate of single neurons that are selective (p<0.05) to (A) memory (new > old) or (B) image category (plant > other categories) in stimulus period when image is shown, and (C) criterion (conservative > liberal) in the response period before decision is made.

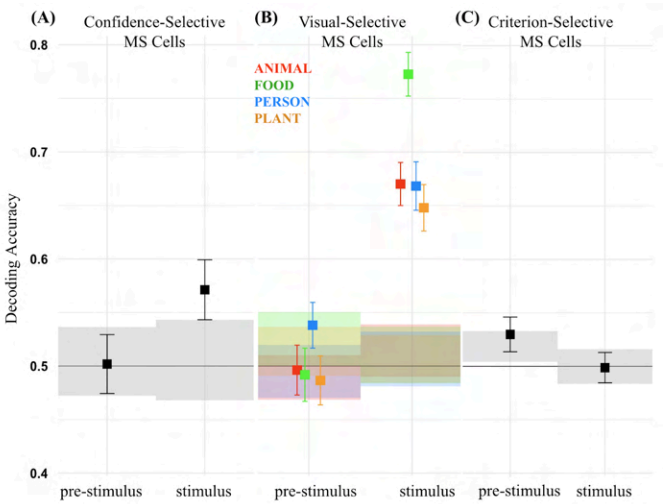

Figure 2. Significantly improved decoding performance suggests MS neurons encode confidence, visual category, and criterion. Decoding analysis depicts the mean of 100 iterations compared to the 95th percentile of a random (0.5) classifier (shaded). (A) Confidence selectivity in MS neurons (8%) during stimulus phase (p=0.0035). (B) Visual selectivity in MS neurons (30%) during stimulus phase (p<0.001). (C) Criterion-selectivity in pre-stimulus MS neurons (p=0.018).

Criterion-selective neurons, in Figure 1C, fire differently between liberal and conservative trials (p<0.001). They constituted 25% (193/787) of the total neuron population. During the pre-stimulus phase, criterion-selectivity within 17% of MS neurons was detected (Figure 2C), suggesting decision biases implemented before image onset and indicating the presence of anticipatory cells that filter memory recall. VS neurons, however, do not encode criterion, indicating a unique overlap of memory with decision bias. In the stimulus phase, criterion-selectivity was not significant among MS cells. While decision biases are implemented in the absence of image, criteria are not processed concurrently with memory in image presence.

IV. Conclusions

Single neuron actions and interactions are the building blocks of brain activity, and the clinical sequelae of most cognitive diseases stem from the dysfunction or failure of individual neurons. In our study on recognition memory, single neuron recording has helped elucidate how patients make context-informed decisions and recall information. To our knowledge, this paper is the first to characterize criterion-selective (CS) neurons. We identify that CS neurons influence memory recall when subjects set a decision bias before an image is seen. The encoding of criteria at the single-neuron resolution suggests a biological basis of individualistic decision thresholds. This finding supports the existence of criterion-related brain regions identified through neuroimaging by identifying a single-neuron basis of criterion-encoding [6]. As a result, our results also support the application of single-neuron recording to the monitoring of memory-related pathological development. Developing neural maps of decision-making pathways can support precision medicine, allowing for personalized treatment for neurodegenerative diseases. To this end, single unit recordings have been used to determine the structure of basal ganglia in Parkinson's patients,

creating a map of information flow throughout the brain and allowing physicians to monitor disease progression [13].

Further, our research also reveals that an individual neuron can encode multiple sources of information, defying categorization as selective to only one category of stimuli. We find that memory-selective neurons are influenced by criterion, confidence, and category, suggesting that single neurons are highly nuanced because they integrate various sources of information when processing memory signals. The potential of an individual neuron to harbor multiple varieties of stimuli provides an exciting opportunity to evaluate how such a synchronization of signals is affected by pathology. Thus, our research supports using single-neuron electrode recording to decipher the neural code underlying human behavior, understanding how cells respond to different stimuli.

There exists several limitations to our proposed single-neuron model of memory-based decision making. Electrode recording remains a solely clinical intervention, and it is unknown if our observed structure of memory pathways translates to a healthy population. Although we took care to record neurons from healthy brain regions of epileptic patients, it is possible that pathological tissue could be found at undetected sites. To this end, we seek to expand our sample from seven patients to a larger population. We further aim to replace the manual aspects of pre-processing data using OSort with machine-learning algorithms in neuron classification. Although it remains standard for a human evaluator to verify neurons using a qualitative rubric, we seek to completely automate neuron classification, allowing for single-neuron data to be quickly accessible after collection.

We also note that our dataset includes a disproportionately higher number of neurons across the frontoparietal lobe. In these regions, we found memory-selective neurons that responded when decision biases were implemented in recognition-based judgments. Thus, future research can explore increased electrode monitoring in the medial temporal and frontal lobes, regions in the brain where greater concentrations of neurons were identified. This may aid in localizing subdomains of memory or criterion activity and tracking memory-encoding pathways between neurons.

Already, single-neuron research has been used in humans to treat psychiatric and neurologic diseases. Deep brain stimulation (DBS), which uses electrodes targeting single neurons, has shown promise in treating chronic pain, motor disorders, Parkinson's disease, Alzheimer's disease, and depression. For these patients, single-neuron research can provide treatment tailored to an individual's criterion-shifting and memory networks. Thus, this study is positioned at the forefront of a paradigmatic transition towards a more highly-resolved and computationally-driven approach to studying macroscopic behaviors in human cognition.

V. Acknowledgements

We thank the Miller Lab and staff at Cedars-Sinai Epilepsy Monitoring Center for assistance. We thank Dr. Lina Kim of the UC Santa Barbara Research Mentorship Program for her guidance.

VI. References

1. Brown, M. W., Warburton, E. C., and Aggleton, J. P. (2010). Recognition memory: material, processes, and substrates. Hippocampus, 20(11), 1228-1244.
2. Fechner, H. B., Pachur, T., Schooler, L. J., Mehlhorn, K., Battal, C., Volz, K. G., & Borst, J. P. (2016). Strategies for memory-based decision making: Modeling behavioral and neural signatures within a cognitive architecture. *Cognition*, 157, 77-99.
3. Tajika, H. (2001). Recognition memory, psychology of.
4. Aminoff, E. M., Clewett, D., Freeman, S., Frithsen, A., Tipper, C., Johnson, A., ... & Miller, M. B. (2012). Individual differences in shifting decision criterion: A recognition memory study. *Memory & Cognition*, 40, 1016-1030.
5. Layher, E., Dixit, A., & Miller, M. B. (2020). Who gives a criterion shift? A uniquely individualistic cognitive trait. *Journal of Experimental Psychology: Learning, Memory, and Cognition*, 46(11), 2075–2105. https://doi.org/10.1037/xlm0000951
6. Layher, E., Santander, T., Chakravarthula, P., Marinsek, N., Turner, B. O., Eckstein, M. P., & Miller, M. B. (2023). Widespread frontoparietal fMRI activity is greatly affected by changes in criterion placement, not discriminability, during recognition memory and visual detection tests. *NeuroImage*, *279*, 120307.
7. Minxha, J., Adolphs, R., Fusi, S., Mamelak, A. N., & Rutishauser, U. (2020). Flexible recruitment of memory-based choice representations by the human medial frontal cortex. *Science*, 368(6498), eaba3313.
8. Khosla, A., Raju, A. S., Torralba, A., & Oliva, A. (2015). Understanding and predicting image memorability at a large scale. In Proceedings of the IEEE international conference on computer vision (pp. 2390-2398).
9. Ratcliff, R., Sheu, C. F., & Gronlund, S. D. (1992). Testing global memory models using ROC curves. *Psychological review*, 99(3), 518.
10. Rutishauser, U., Schuman, E. M., & Mamelak, A. N. (2006). Online detection and sorting of extracellularly recorded action potentials in human medial temporal lobe recordings, in vivo. *Journal of neuroscience methods,* 154(1-2), 204-224.
11. DiCarlo JJ, Zoccolan D, Rust NC. How does the brain solve visual object recognition? Neuron. 2012 Feb 9;73(3):415-34. doi: 10.1016/j.neuron.2012.01.010. PMID: 22325196; PMCID: PMC3306444.
12. Faraut, M., Carlson, A. A., Sullivan, S., Tudusciuc, O., Ross, I., Reed, C. M., ... & Rutishauser, U. (2018). Dataset of human medial temporal lobe single neuron activity during declarative memory encoding and recognition. *Scientific data*, 5(1), 1-11.
13. Boraud, T., Bezard, E., Bioulac, B., & Gross, C. E. (2002). From single extracellular unit recording in experimental and human Parkinsonism to the development of a functional concept of the role played by the basal ganglia in motor control. *Progress in neurobiology*, 66(4), 265-283.

APPENDIX

1. Behavioral Tasks

A. Task Design

The task consisted of 4 study-test phase cycles. In each cycle, our 2 (discriminability condition: low vs. high) x 2 (criterion condition: conservative vs. liberal) factorial design created a total of 4 conditions, repeated 4 times for a total of 16 blocks.

Images were shown for 1000 ms, separated by a variable period. This was to prevent anticipatory memory signals in neurons in the case that we had used a predictable crosshair period. Questions (8 questions/block) assessing image category were interspersed between stimuli to ensure subjects remained attentive throughout the task.

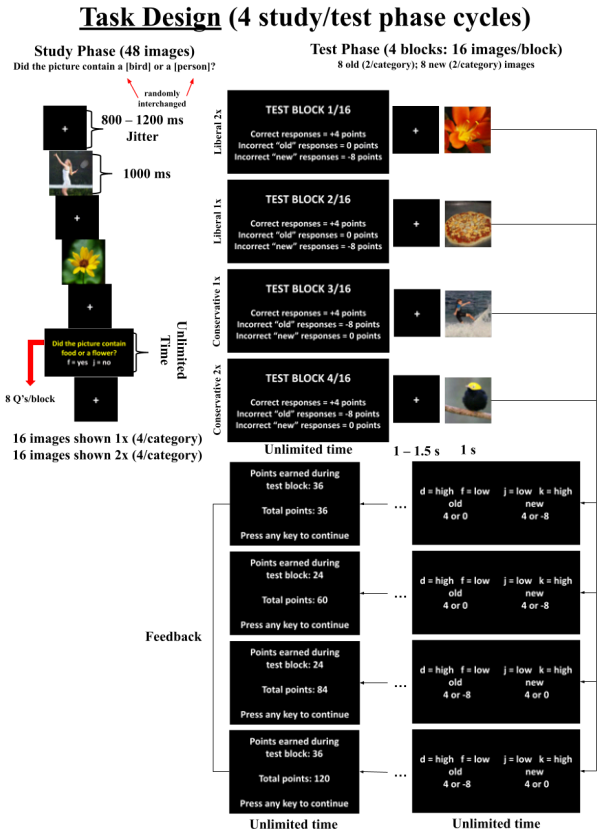

B. Image Selection and Modification

Images retrieved from the LaMem database were modified in two ways to ensure that memorability varied solely on image content [11]. First, images were center cropped to a consistent size (400x400 pixels) as dimensions may affect memorability to an unknown, albeit small, degree. Next, stimuli were selected if their memorability score ranged from 0.60–0.91 out of a 0–1 scale, ensuring that images displayed were memorable enough so participant memory capabilities could be adequately characterized.

Images were assigned a memorability score from 0–1 (M=0.755) labeled by a convolutional neural network algorithm trained on human rankings. Memorability for selected task images (0.60–0.91, M=0.759) were equally stratified across four levels: 0.60–0.67, 0.68–0.75, 0.76–0.83, 0.84–0.91. We used non-overlapping image sets for patients completing multiple sessions.

During all test blocks, displayed images belonged evenly across subject category (4 images/category) within memorability levels (4 images/level). Below are sample images used in trials:

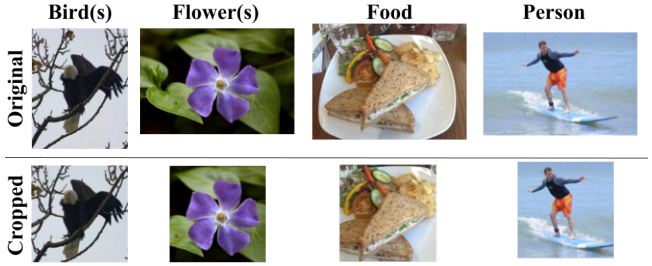

C. Behavioral Evaluation

Performance on a behavioral task can be evaluated with several equations. A normally distributed, equal-variance signal detection theory model, shown below, was used to calculate hit rate (HR) and false alarm rate (FAR) per subject to characterize task performance per individual.

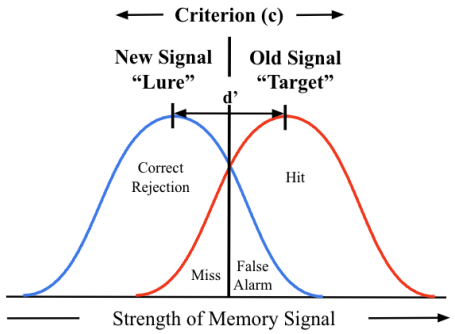

2. Neuron Spike Data Processing

A. Manual Spike Sorting Criteria

Neurons were evaluated on various criteria, including minimum firing rate, minimum amplitude, waveform coherence, power spectrum corruption, regularity of spiking rate, and firing frequency within a 3 ms interval. Here is a representative neuron.

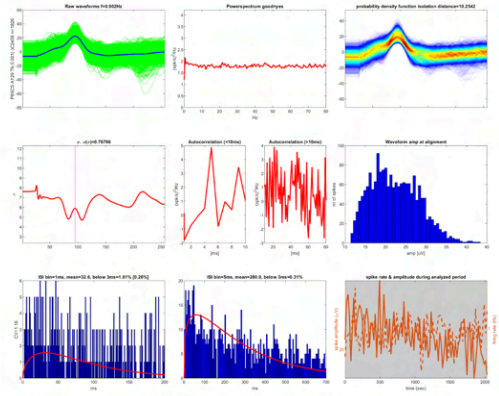

B. Brain Regions and Specific Recording Sites

We aggregated different brain regions where electrodes were planted into five generalized brain domains. Electrodes were recorded in left (L) and right (R) sides of the brain, omitted below:

Medial Frontal Cortex	Medial Temporal Lobe	Posterior Temporal Cortex
Anterior cingulate cortex (ACC)	Amygdala (A)	Fusiform Face Area (FFS)
Supplementary motor association area (SMA)	Hippocampus (H)	Posterior temporal (PT)
	Parahippocampal gyrus (PHG)	
Orbitofrontal Cortex	**Other**	
Orbitofrontal (OFC, OF, OFI)	Insular cortex (INS)	
	Centromedian nuclei (CM)	

A Generative-Adversarial Approach to Low-Resource Language Translation via Data Augmentation

Linda Zeng[1]

***Abstract*—Language and culture preservation are serious challenges, both socially and technologically. In response to this issue, this paper takes a data-augmenting approach to low-resource machine translation, helping to diversify the field and preserve underrepresented cultures. Since low-resource languages, such as Aymara and Quechua, do not have many available translations that machine learning software can use as a reference, machine translation models frequently make errors when translating to and from low-resource languages. Because models learn the syntactic and lexical patterns underlying translations through processing the training data, insufficient amount of data hinders them from producing accurate translations. In this paper, I propose the novel application of a generative-adversarial network (GAN) to automatically augment low-resource language data. A GAN consists of two competing models, one learning to generate sentences from noise and the other interpreting whether a given sentence is real or generated. The paper shows that even when training on a very small amount of language data (< 20,000 sentences) in a simulated low-resource setting, such a model is able to generate original, coherent sentences, such as "ask me that healthy lunch im cooking up," and "my grandfather work harder than your grandfather before." This GAN architecture is effective in augmenting low-resource language data to improve the accuracy of machine translation and provides a reference for future experimentation with GANs.**

I. Introduction

Languages play a vital role in preserving cultural beliefs and traditions. As technology becomes increasingly prevalent, it is crucial for translation software to reflect the world's linguistic diversity, ensuring that valuable cultural identities are not left behind. However, current state-of-the-art translation models frequently make mistakes when translating to and from "low-resource languages" [1], or languages that do not have enough digital data that machine learning algorithms can use as reference. For example, many American indigenous languages, such as Aymara and Quechua [2], are underrepresented in datasets, resulting in models trained on them generating incorrect translations.

Previous approaches have focused on bridging the gaps between high-resource and low-resource languages through transfer-learning and cross-lingual pretraining [1]–[3], which have limited efficacy depending on the similarity between the high-resource and low-resource languages being used. The direction of data augmentation focusing solely on low-resource language generation has not been fully explored and holds promise for breakthrough [4].

Artificially increasing the size of datasets with original, generated samples allows translation models to receive more variety and volume in training, improving their generalizability. Both monolingual and parallel data augmentation is important for Neural Machine Translation (NMT), which refers to translation powered by neural networks. Training on monolingual corpora in addition to parallel data has been used to improve NMT models [5]–[7], especially in low-resource NMT [8]. As a result, this paper introduces a system for monolingual data augmentation.

In contrast to the human labor of creating new sentences in low-resource languages by hand, a generative-adversarial network (GAN) is capable of autonomously generating as much new data in a low-resource language as needed. Previous studies have implemented GANs for machine translation [9-12], but at the time of our research, no previous models have used them for translation of low-resource languages.

In this study, I propose applying a GAN to monolingual low-resource language data augmentation to improve translation quality. My model generates new synthetic language data for low-resource languages and is the first to combine GANs, data augmentation, and low-resource NMT.

II. Model Architecture

My design consists of two models: an encoder-decoder and a GAN, which contains a generator and a discriminator. Figure 1 displays a preliminary example of the model workflow.

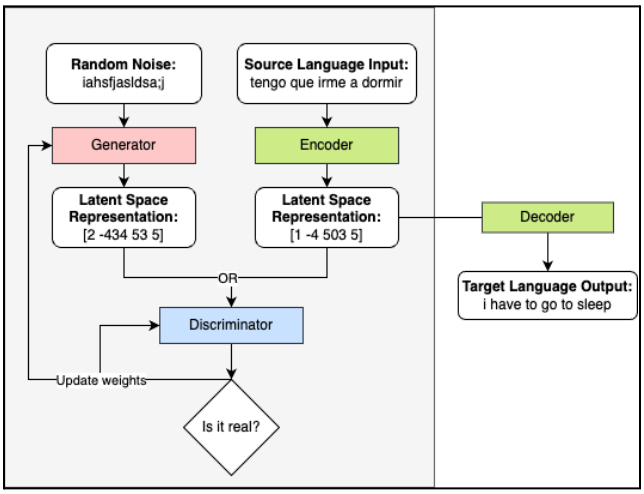

Figure 1. *Overall workflow with basic examples.*

First, the encoder-decoder learns to translate from a source language to the target language using the training data. In Figure 1, the source language is Spanish, and the data point is "tengo que irme a dormir." The encoder transforms the source language into a latent space representation, an abstract representation of the sentence's

[1]L.Z. is with The Harker School, 500 Saratoga Ave, San Jose, CA 95129 (corresponding author to email: 26lindaz@students.harker.org).

meaning, and then the decoder "decodes" the representation into the target language—in this case, "i have to go to sleep" in English. Similar sentences are positioned closer together in this internal latent space, which reflects samples' external meanings regardless of language. After the encoder-decoder finishes training, a batch of sentences in the source language from the dataset are fed into the trained encoder, and generates latent space representations. Figure 1 shows a simplified version of the representation: [1 -4 503 5].

Next, we train the GAN using the encoder-decoder as a tool, as shown in the left box in Figure 1. The generator takes in a batch of random noise, a list of randomly generated numbers between -1 to 1 which, by themselves, have no meaning (the figure represents noise as gibberish). Then, the generator tries to create sentence meanings out of the noise by transforming them into latent space representations, shown as [2 -434 53 5] in Figure 1.

The discriminator receives either the encoder's or the generator's latent space representation, without knowing from which model the representation comes from. The discriminator predicts whether a given encoding is real (from the encoder) or fake (from the generator), and then compares its prediction with the encoding's real label to evaluate its own performance. Depending on the discriminator's success or failure, the generator also adjusts its weights and learns to create encodings more similar to the encoder's in order to fool the discriminator. This process continues until ultimately, through trial-and-error, the generator learns to generate latent space representations so similar to the real ones that the discriminator is not able to tell them apart. As a result, the generator is able to generate unlimited new latent space representations from only noise and no extra data. Like the encoder's encodings, these representations can then be decoded by the decoder into real sentences in the target language.

Figure 2 displays the neural-network architectures underlying the encoder-decoder, generator, and discriminator.

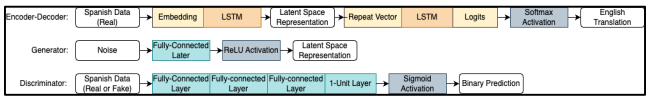

Figure 2. *Generator, discriminator, and encoder-decoder architectures.*

The encoder-decoder uses a long-short term memory (LSTM) network for both the encoder and decoder. Long-short term memory (LSTM) networks [13] are a special type of neural networks that learn when to remember information that may be important later on in a data sequence. In NMT, since related words may be placed far from each other in a sentence, encoder-decoders commonly use LSTMs because LSTMs can capture the long-term dependencies between such words.

In between the major LSTM layers of the encoder-decoder, the embedding layer learns to map words with analogous meanings to similar numerical vectors, the repeat vector copies each latent space representation into the decoder, and the logits layer maps' numerical outputs into probabilities. Last, a softmax activation function normalizes the probabilities, producing the output.

The generator consists of a dense layer, which is a layer of fully connected units, and a ReLU activation function, which is commonly used in GANs to optimize efficiency and capture complex data distributions. The generator's main purpose is to learn through trial and error to mimic the encoder's encodings despite only being given noise as input.

The discriminator consists of three dense layers and then a one-unit dense layer, which allows it to produce a prediction of whether the input is from the encoder or the generator. Each of these hidden layers include a ReLU activation function to capture complexity. Finally, the model uses a sigmoid activation function to categorize its prediction into a 1 (for encoder) or 0 (for generator). Using trial-and-error, the discriminator learns how to differentiate encodings of natural source language data (from the encoder) from synthetic encodings (from the generator).

The combined GAN model feeds its noise input to the generator and the generator's encoding output into the discriminator. The discriminator's prediction is used to update the weights for both models. Ultimately, once both models optimize their performances, the generator's outputs serve as novel data points for data augmentation.

III. Data

The data used in this study was derived from a Tatoeba dataset [14] processed by a third-party [15]. The training, validation and test data were given only to the encoder-decoder while the GAN operated solely on noise and the encoder-decoder's output.

To mimic the characteristics of low-resource languages using English and Spanish, I reduced the amount of data from 253,726 sentence pairs to only 20,000. Of the 20,000, 18,000 sentence pairs were used to train the encoder-decoder, 1,000 were kept as validation data to verify accuracy and prevent overfitting during the training process, and the last 1,000 sentence pairs served as test data and were not seen or used until after training and hyperparameter tuning for the encoder-decoder. I retained only words, lowercase, and no punctuation. Using Keras's built-in Tokenizer [16], I then split each sentence into a list of probabilities. I found the longest sentence and padded the rest with zeros to the same length.

IV. Experimental Setting

This section describes conditions, procedures, hyperparameters, and observations relevant to training.

I imported all of the model layers from the Python Keras library [16]. Through experimentation, I chose the encoder-decoder's two LSTM layers to contain 64 units. To minimize overfitting, I included weight decay, which shrinks the weights of neural networks, and dropout, which drops out a few randomly selected neurons during training. These values were empirically determined for each layer in the encoder-decoder. For the encoder LSTM, I used a type of weight decay known as L2 regularization with a value of 5e-5, and a dropout of 0.5. For the decoder LSTM, I used an L2 regularization of 1e-5 and a dropout of 0.5. The model

was compiled with a categorical cross entropy loss function and an Adam optimizer [17] with a learning rate of 2e-3 and weight decay rates of beta1 0.7 and beta2 0.97. The encoder-decoder trained in batches of 30 samples for 400 epochs on the training data.

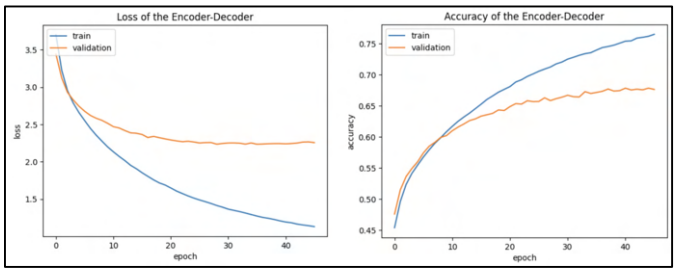

Figure 3. *Loss and accuracy of the encoder-decoder.*

While training, the encoder-decoder reached an accuracy of 92.8%, and a peak accuracy of 71.4% on validation data. Figure 3 shows the progression of training and validation loss and accuracy through epochs.

The generator's dense layer contained 64 units. The model was compiled with a categorical cross entropy loss function and an Adam optimizer with learning rate 4e-4. The discriminator's three dense layers each had 1,024 units, followed by a single-unit layer that represented its prediction. The model was compiled with a binary cross entropy loss function and an Adam optimizer with a learning rate of 1e-4. The combined GAN compiled with a binary cross entropy loss function and an Adam optimizer with a learning rate of 1e-4. With a batch size of 1900, the GAN trained across 8,000 epochs.

Shown in Figure 4, while training, the GAN's loss values plateaued for both the generator and the discriminator, indicating that the models reached convergence and were both performing optimally against each other. Its final loss values hovered around 0.581 for the generator and 0.438 for the discriminator.

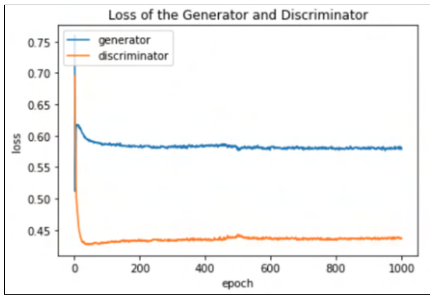

Figure 4. *Loss of the GAN.*

Once the generator and discriminator were performing optimally, the decoder was run on the generator's encodings, converting their meanings into probabilities. Each probability mapped to the closest word in the tokenizer's dictionary of probability word pairs, forming sentences.

Hyperparameter Tuning

In order to find the hyperparameters for optimal results, I experimented by first varying values by a factor of either 2 or 10 and testing every combination. To optimize for time, I used 5,000 sentences and 80 epochs. For the learning rates of the encoder-decoder, generator, discriminator, and GAN, as well as the weight decay, I tried a range of values from 1e-1 to 1e-8, decreasing in magnitude by a factor of 10 each time. When varying the number of units and batch sizes for the encoder-decoder's LSTM layers, the generator's dense layer, and the discriminator's dense layers, I chose powers of 2 between 16 and 2048. For the encoder-decoder's dropouts, I tried a range from 0.5 to 0.8.

After finding the approximate values to optimize performance, I tested more specific values within the ideal range I found, isolating each of the models and incrementing values. Once reaching optimal parameters, I increased the training data and epochs to further improve the models.

V. Results

Encoder-Decoder Performance

On the test data, the encoder-decoder had a final accuracy of 69.3%. This accuracy is respectable, considering the fact that the model was trained on less than 20,000 sentences, which is less than one-tenth of the size of other low-resource language datasets, whose sizes are between 0.2 to 1 million [3][18].

As this paper focuses more on the data-augmentation aspect than the machine translation part of this research, accuracy was used instead of BLEU score [19], a metric that assesses the quality of a machine translation relative to a human-curated translation by counting overlapping n-grams. Using accuracy, the value of incomplete yet coherent translations could be considered and did not affect results as strongly as BLEU scores would have caused it to.

GAN Performance

After training, the GAN was able to successfully generate coherent sentences, such as sentences 1, 2, and 3 labeled "good" in Table 1. Generated samples generally centered around its own cohesive theme, which is an indication of the model's successful understanding of word meanings. From random noise, the generator was able to create its own completely new and logical sentences, a significant feat considering the lack of training data.

Sample Generated Sentences	
my grandfather work harder than your grandfather before	good
to consider quit job is this dream man	good
ask me that healthy lunch im cooking up	good
maryam discovered hes hes am am are are	repetition
home actually was everything everything listen actually everything	repetition
cheerful weird yourself punished music alone everybody everybody	nonsensical
those in so friends so complicated english comes	nonsensical
stressed gloves eating eating worried online online online	unrelated

Table 1. *Raw Samples by the GAN.*

Error Analysis and Future Work

The model made a series of errors, shown in lines 4–7 in Table 1. The severity of errors decreased as the GAN trained for more epochs. Thus, future models may train for a larger number of epochs to examine whether errors can be reduced

further. I propose future work for three main errors: repeated words, nonsensical grammar, and unrelated words.

Repeated words occur in most MT models due to the model trying to generate words that are close in context to each other, which is necessary [20]. Once the decoder translates the latent space representations into probabilities, they may be reduced to the same word. Future work should involve training the model to remember the previous probabilities it generated and to vary them.

Some sentences are grammatically incorrect or nonsensical with randomly placed words. Due to the low-resource setting, the model did not learn enough context to understand how to place these words. For example, in Table 1, the model predicted "weird" to follow "cheerful." The model likely assigned similar embeddings to these two words since they are both adjectives that may have been used in comparable contexts. However, while the adjectives may be used interchangeably as modifiers for a person, they cannot follow each other directly. Future work should attempt to train the model on which semantically related words can be placed together syntactically.

The model occasionally groups unrelated words together. It has not seen a word (e.g. "gloves" in Table 1) enough to understand its usual context (i.e. being put on people's hands). Future work should focus on incorporating a dictionary of words into the model so that it better understands words' meanings.

In the future, I plan to post-process the samples by cleaning and inserting punctuation and capitalization. I also plan to test this method's performance in a true low-resource setting.

VI. Conclusion

This work takes strides to address data inequality in neural machine translation, using a generative-adversarial approach to augment low-resource languages. Experiments show promising results: using less than 20,000 sentences, the GAN was able to generate unlimited, coherent sentences. These new sentences can be added to the original corpus to improve the accuracy of machine translation. Improvements can be made on this research to increase comprehensiveness when evaluating the model's performance and to minimize the repetition and incoherence in many of the generated sentences.

This innovative approach has the potential to bring about more robust language translations for minority populations. Because of this GAN architecture's ability to generate an unlimited amount of original sentences despite being trained on minimal data, it can be used as an effective tool to augment low-resource language data, allowing translation software to train on more sentences and therefore generate more accurate translations. The next steps of this research are to explore this model's feasibility on a variety of low-resource languages from a diverse set of language families. This novel application of a GAN to low-resource language translation serves as a reference for future work that combines GANs and Natural Language Processing, specifically MT.

VII. Acknowledgement

I would like to thank my teachers, Anu Datar and Ricky Grannis-Vu, for their ongoing support and encouragement.

VIII. References

[1] J. Gu, H. Hassan, J. Devlin, and V. O. Li, "Universal neural machine translation for extremely low resource languages," in *Proceedings of the 2018 Conference of the North American Chapter of the Association for Computational Linguistics: Human Language Technologies, Volume 1 (Long Papers)*. New Orleans, Louisiana: Association for Computational Linguistics, Jun. 2018, pp. 344–354. [Online]. Available: https://aclanthology.org/N18-1032

[2] F. Zheng, M. Reid, E. Marrese-Taylor, and Y. Matsuo, "Low-resource machine translation using cross-lingual language model pretraining," in *Proceedings of the First Workshop on Natural Language Processing for Indigenous Languages of the Americas*. Online: Association for Computational Linguistics, Jun. 2021, pp. 234–240. [Online]. Available: https://aclanthology.org/2021.americasnlp-1.26

[3] B. Zoph, D. Yuret, J. May, and K. Knight, "Transfer learning for low-resource neural machine translation," in *Proceedings of the 2016 Conference on Empirical Methods in Natural Language Processing*. Austin, Texas: Association for Computational Linguistics, Nov. 2016, pp. 1568–1575. [Online]. Available: https://aclanthology.org/D16-1163

[4] M. Fadaee, A. Bisazza, and C. Monz, "Data augmentation for low-resource neural machine translation," in *Proceedings of the 55th Annual Meeting of the Association for Computational Linguistics (Volume 2: Short Papers)*. Vancouver, Canada: Association for Computational Linguistics, Jul. 2017, pp. 567–573. [Online]. Available: https://aclanthology.org/P17-2090

[5] J. Zhang and C. Zong, "Exploiting source-side monolingual data in neural machine translation," in *Proceedings of the 2016 Conference on Empirical Methods in Natural Language Processing*. Austin, Texas: Association for Computational Linguistics, Nov. 2016, pp. 1535–1545. [Online]. Available: https://aclanthology.org/D16-1160

[6] R. Sennrich, B. Haddow, and A. Birch, "Improving neural machine translation models with monolingual data," in *Proceedings of the 54th Annual Meeting of the Association for Computational Linguistics (Volume 1: Long Papers)*. Berlin, Germany: Association for Computational Linguistics, Aug. 2016, pp. 86–96. [Online]. Available: https://aclanthology.org/P16-1009

[7] D. Cai, Y. Wang, H. Li, W. Lam, and L. Liu, "Neural machine translation with monolingual translation memory," in *Proceedings of the 59th Annual Meeting of the Association for Computational Linguistics and the 11th International Joint Conference on Natural Language Processing (Volume 1: Long Papers)*. Online: Association for Computational Linguistics, Aug. 2021, pp. 7307–7318. [Online]. Available: https://aclanthology.org/2021.acl-long.567

[8] A. Currey, A. V. Miceli Barone, and K. Heafield, "Copied monolingual data improves low-resource neural machine translation," in *Proceedings of the Second Conference on Machine Translation*. Copenhagen, Denmark: Association for Computational Linguistics, Sep. 2017, pp. 148–156. [Online]. Available: https://aclanthology.org/W17-4715

[9] Z. Yang, W. Chen, F. Wang, and B. Xu, "Improving neural machine translation with conditional sequence generative adversarial nets," in *Proceedings of the 2018 Conference of the North American Chapter of the Association for Computational Linguistics: Human Language Technologies, Volume 1 (Long Papers)*. New Orleans, Louisiana: Association for Computational Linguistics, Jun. 2018, pp. 1346–1355. [Online]. Available: https://aclanthology.org/N18-1122

[10] Z. Zhang, S. Liu, M .Li, M. Zhou, and E. Chen,"Bidirectional generative adversarial networks for neural machine translation," in *Proceedings of the 22nd Conference on Computational Natural Language Learning*. Brussels, Belgium: Association for Computational Linguistics, Oct. 2018, pp. 190–199. [Online]. Available: https://aclanthology.org/K18- 1019

[11] Z. Yang, W. Chen, F. Wang, and B. Xu, "Unsupervised neural machine translation with weight sharing," in *Proceedings of the 56th Annual Meeting of the Association for Computational Linguistics (Volume 1:*

Long Papers). Melbourne, Australia: Association for Computational Linguistics, Jul. 2018, pp. 46–55. [Online]. Available: https://aclanthology.org/P18-1005

[12] A. Rashid, A. Do-Omri, M. A. Haidar, Q. Liu, and M. Rezagholizadeh, "Bilingual-GAN: A step towards parallel text generation," in *Proceedings of the Workshop on Methods for Optimizing and Evaluating Neural Language Generation*. Minneapolis, Minnesota: Association for Computational Linguistics, Jun. 2019, pp. 55–64. [Online]. Available: https://aclanthology.org/W19-2307

[13] S. Hochreiter and J. Schmidhuber, "Long short-term memory," *Neural Computation*, vol. 9, no. 8, pp. 1735–1780, 1997.

[14] Tatoeba: Collection of sentences and translations. Tatoeba.org. [Online] Available: https://tatoeba.org/en/

[15] C. Kelly and L. Kelly, "Interesting Things for ESL/EFL Students (Fun English Study)," 2023. Manythings.org. [Online]. Available: https://manythings.org.

[16] F. Chollet *et al.* (2015) Keras. [Online]. Available: https://github.com/fchollet/keras

[17] D. P. Kingma and J. Ba, "Adam: A method for stochastic optimization," 2017. [Online] Available: https://arxiv.org/abs/1412.6980

[18] S. Ranathunga, E.-S. A. Lee, M. P. Skenduli, R. Shekhar, M. Alam, and R. Kaur, "Neural machine translation for low-resource languages: A survey," 2021. [Online] Available: https://arxiv.org/abs/2106.15115

[19] K. Papineni, S. Roukos, T. Ward, and W.-J. Zhu, "Bleu: a method for automatic evaluation of machine translation," in *Proceedings of the 40th Annual Meeting of the Association for Computational Linguistics*. Philadelphia, Pennsylvania, USA: Association for Computational Linguistics, Jul. 2002, pp. 311–318. [Online]. Available: https://aclanthology.org/P02-1040

[20] Z. Fu, W. Lam, A. M.-C. So, and B. Shi, "A theoretical analysis of the repetition problem in text generation," 2021. [Online] Available: https://arxiv.org/abs/2012.14660

Investigating the Origins of Niche Shift in Bagheera kiplingi

Shaochi S. Chuang[1]

***Abstract*— As a predominantly herbivorous forager among a wide range of predators, the jumping spider Bagheera kiplingi's diet of Beltian bodies, a detachable nutrient-filled tip found on certain species of Vachellia trees, is unique among the more than 6,000 members of the family Salticidae. The jumping capabilities of Salticidae spiders is widely accepted to be an evolutionary trait designed to help them capture far-away prey. Therefore, the herbivory of B. kiplingi presents a fascinating area of study as its ability to digest high-fiber, nutrient-poor plant material could provide key insights into the evolutionary processes behind niche shifts. Analysis of the dietary habits of Bagheera prosper, B. kiplingi's closest relative, characterizes this species as an obligate carnivore. Moreover, polymerase chain reaction using nifH primers has resulted in the successful amplification of DNA from surface-sterilized B. kiplingi, but not from B. prosper or Frigga crocuta (another spider species that has been found on Vachellia collinsii plants). These results document the first discovery of nitrogen-fixing activity within an arachnid and support the hypothesis that B. kiplingi benefits from the presence of symbiotic bacteria in its gut to supplement a low-nitrogen diet. Additionally, behavioral analysis of B. kiplingi's diet in controlled settings suggests that they require regular inoculations of ant larvae in order to survive on plant material, supporting the hypothesis that B. kiplingi obtains a portion of its microbiome through consuming ant larvae. This hypothesis is further reinforced by an analysis of B. kiplingi's mouth structures via scanning electron microscopy indicating that they do not have physical adaptations that are generally associated with herbivory. Meanwhile, video behavioral analysis of B. kiplingi behavior in comparison to B. prosper and F. crocuta provides evidence for the optimal foraging theory and the locomotor crossover hypothesis.**

I. Introduction

Bagheera kiplingi is a species of jumping spider, also known as a salticid, that resides in Mesoamerica from Mexico to Costa Rica [1]. Past studies have demonstrated that *B. kiplingi* possess a uniquely herbivorous diet consisting of roughly 60-90% plant tissue from the Beltian bodies of *Vachellia* trees with the remainder consisting of mainly larvae of *Pseudomyrmex* ants that live in mutualistic relationships with these trees, in addition to small flies and occasional cannibalism [1]. In contrast, the over 50,000 other species of spiders are carnivores, with only rare exceptions, such as the orb-weaving spider that occasionally consumes pollen from its web as a juvenile [2]. *B. kiplingi* is the only consistent forager to have been described [1], making its primarilly-diet a fascinating area of study.

While no other arachnid is known to be herbivorous, prior research suggests that the vast majority of plant-eating arthropods benefit from symbiotic relationships with bacteria in their digestive tracts: particularly those that can digest cellulose and fix nitrogen [3]. Modifications to the mouth and digestive tracts are also common, including broader and flatter mouthparts to grind down plant material and added length and surface area in the gut that permit populations of specialized bacteria to thrive [4,5].

Microbial transmission has been documented to occur in two main ways: vertical transmission where a parent passes microbes directly to offspring [6], and horizontal transmission where bacteria are usually acquired from members of the same species through infection [7]. In rare instances, interspecies transmissions of bacteria symbionts have been observed, such as between the pika and the yak in Tibet [8]. It has been proposed that *B. kiplingi* accelerated its adoption of a plant-based diet through the consumption of ant larvae, which provide an infusion of bacteria that allows it to temporarily digest cellulose and fix nitrogen [9].

To test this, DNA analysis of the *B. kiplingi* microbiome was used to compare them to their sister species, *Bagheera prosper* [10], and a distantly related species of salticid, *Frigga crocuta,* that has also been observed living on *Vachellia* trees in Panama (where *B. kiplingi* has not been found). Further experiments studying *B. kiplingi's* diet under different controlled environments along with morphological analysis using scanning electron microscopy (SEM) were also used to supplement the previous findings.

As an additional objective, *B. kiplingi's* unique position in the ecosystem was capitalized upon to contribute to the field of behavioral ecology as their behaviors were compared to that of *B. prosper* and *F. crocuta*. Considering that the two species are documented obligate carnivores and share either a common evolutionary history (*B. prosper*) or a common habitat (*F. crocuta*) with *B. kiplingi* [10], an analysis of the three spiders' behaviors provide a strong platform for analyzing the validity of the optimal foraging theory (OFT) and the locomotor crossover hypothesis (LCH). Under both frameworks, *B. kiplingi*, an herbivore, is expected to move more to access stationary Beltian bodies, its main food source, while reorienting less due to reduced energy demands for food detection [11,12,13].

This potential shift in niche—the trophic and behavioral position of an organism within its ecosystem [14]—could provide new insights into how evolution may proceed, particularly if other spiders with similar habitats and common lineages might still be carnivores.

II. Methods and Materials

DNA Analysis

Sample Collection. For this study, *B. kiplingi, Pseudomyrmex peperi* adults*, P. peperi* larvae, and *Vachellia collinsii* leaves were collected from Akumal, Mexico. This location was chosen because prior studies suggested that Mexican *B. kiplingi* from this region were more herbivorous than *B. kiplingi* found elsewhere [1]. Samples of *B. prosper* were collected from the University of Oklahoma Biological Station (UOBS) at Lake Texoma—the site of prior studies of *B. prosper*— and samples of *F. crocuta, Pseudomyrmex spinicola,* and *V. collinsii* were collected from El Cortezo in central Panama [1]. *P. spinicola* was collected due to prior studies that document them as a part of *B. kiplingi's* diet, however, not enough were collected to conduct DNA

[1] S.C is with Princeton High School, Princeton NJ, 08540

extraction and analysis [1]. All collected samples were stored in 95% ethanol to preserve DNA before extraction [15].

DNA Extraction. DNA was extracted from *P. peperi* adults (n=5), *P. peperi* larvae (n=5), and *V. collinsii* Beltian bodies (n=2) using the Zymo Research Quick-DNA Tissue/Insect Kit and its listed procedures (Catalog: D6016). For the extraction of DNA from the spiders- *B. kiplingi* (n=3), *B. prosper* (n=4), *F. crocuta* (n=4)- samples were surface sterilized to ensure all sequenced DNA was from inside the spider and therefore reflective of its microbiome and not its environment. This was done in a UVC Sterilization Cabinet for 15 minutes on each side. Afterward, each specimen was split into Head/Legs and Abdomen with a flame-sterilized blade. The resulting samples then underwent the same DNA extraction procedures as the other specimens.

Polymerase Chain Reaction (PCR) and Purification. PCR was performed on each DNA sample using the iProof PCR kit (Catalog: 1725331) and its listed procedures with *nifH* primers to target nitrogen-fixing bacteria. After a 30-second denaturation at 98°C, the reaction mixture was run through 35 cycles of denaturation for 10 seconds at 98°C, annealing for 30 seconds at 53°C, and extension for 30 seconds at 72°C, followed by incubation for 10 min at 72°C and then a permanent hold at 10˚C until the samples were retrieved.

After PCR, the DNA samples were purified using the QIAGEN QIAquick PCR Purification Kit (Catalog: 28106) and the procedures listed within.

DNA Sequencing and Analysis. The purified samples were then sent to Genewiz in South Plainfield, NJ for DNA sequencing and analysis.

Controlled Environment Analysis of Diet

Set-up and Analysis. In Akumal, Mexico, *V. collinsii (*with *B. kiplingi* residing on it) were stripped of all ants and netted to prevent *B. kiplingi* from leaving or *Pseudomyrmex* ants from entering. These plants were then separated into two groups: a plant-only (n=15) group where *B. kiplingi* only had access to their usual food source of Beltian bodies, and a flies (n=15) group where flies from the genus *Drosophila* were provided as an additional food source. These flies were chosen for two reasons: their similarity to the non-ant insect food source that *B. kiplingi* has been observed to consume [1], and their similarity to the nectar-stealing flies that are the principal prey of *F. crocuta* [1]. The diet and feeding behavior as well as the duration of survival of *B. kiplingi* from each group were documented.

Scanning Electron Microscopy (SEM) Analysis of Mouth Structures

Specimen and Analysis. A specimen of *B. kiplingi* was sent to the Smithsonian Tropical Research Institute's Electron Microscopy Laboratory to analyze its mouth structures. The results were then compared to previously reported structures of the carnivorous salticid, *Phidippus clarus* [16].

Behavioral Analysis

Video Collection. Behavior of *B. kiplingi* (n=31) in Akumal recorded by Christopher Meehan in 2007 was compared to the recorded behavior of *B. prosper* (n=14) at UOBS, and *F. crocuta* (n=12) in El Cortezo. Videos capturing the spider for longer than 5 minutes were kept and used in the research. For data analysis, videos were split into 5-minute segments as the analysis units.

Video Analysis. 3 major behaviors were documented at 10-second intervals of the 5-minute videos: stationary (quiet), rotation without changing location (reorient), or changing location at a distance equal to or greater than one body length (move) was documented. These procedures were adapted from a previous study on the behavior of a different salticid, *Phidippus audax* [17]. The data was then analyzed using a Tukey Honestly Significant Difference (HSD) test and standard error.

III. Results

DNA Analysis

DNA sequencing returned clear sequences for *P. peperi* and *B. kiplingi,* confirming the effectiveness of the extraction, amplification and purification procedures. In addition, *nifH* was successfully amplified in all samples of *B. kiplingi* and *P. peperi* but was not detected in any samples of *B. prosper* or *F. crocuta*.

Controlled Environment Analysis of Diet

In the plants-only group, *B. kiplingi* were not observed to consume any Beltian bodies and all died within two weeks of the start of the experiment. In the flies group, *B. kiplingi* were also not observed to consume any Beltian bodies but were able to survive on a fly-only diet for up to 6 months.

Scanning Electron Microscopy Analysis of Mouth Structures

SEM analysis of *B. kiplingi's* mouth structure showed that they were nearly identical to other jumping spiders, possessing fanged chelicera with venom ducts and bristles in and around their mouth (Fig. 1).

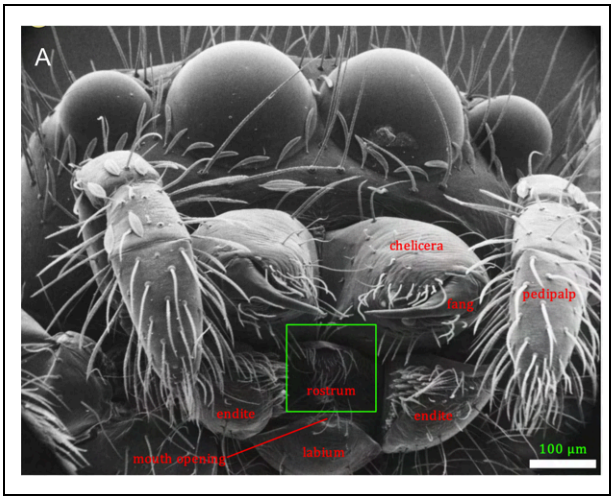

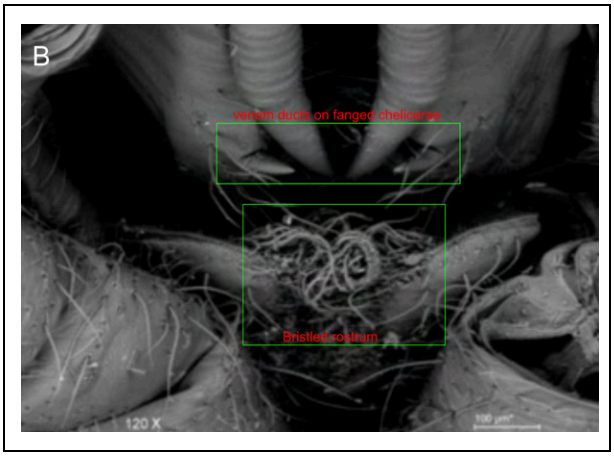

Figure 1. Comparison of external mouth structures in *P. clarus* and *B. kiplingi*. **A**. *P. clarus*, bristles on its rostrum and venomous fanged chelicerae [16]. **B**. *B. kiplingi*, with visible bristles on the rostrum and venom ducts on fanged chelicerae (Image credit: Mark Eastburn, Jorge Ceballos).

Behavioral Analysis

No difference was found in the occurrence of quiet behavior over the span of 5 minutes between *B. kiplingi* ($\bar{x}$=6.6±0.98), *B. prosper* ($\bar{x}$=6.9±1.57), and *F. crocuta* ($\bar{x}$=7.1±1.57) (Fig. 2). In terms of reorientation, *B. kiplingi* ($\bar{x}$=13.7±0.87) was found to reorient more than *B. prosper* ($\bar{x}$=8.3±1.44) but less than *F. crocuta* ($\bar{x}$=18.1±1.4) over 5 minutes (Fig. 2). The opposite was true for movement, with *B. kiplingi* ($\bar{x}$=9.4±1.17) moving more than *F. crocuta* ($\bar{x}$=4.9±1.88) but less than *B. prosper* ($\bar{x}$=15±1.78) over 5 minutes (Fig. 2).

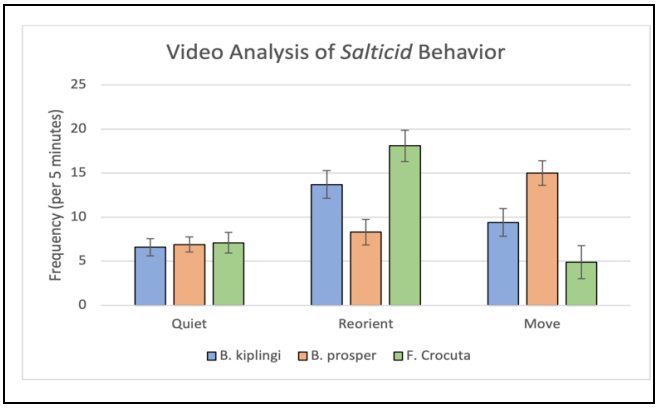

Figure 2. Comparison of the frequency of quiet, reorient, and movement behavior between *B. kiplingi, B. prosper,* and *F. crocuta* sampled at 10-second intervals over 5 minutes.

IV. Discussion

The amplification of *nifH* genes in *B. kiplingi* reveals the first discovery of nitrogen-fixing activity within an arachnid. While past studies on spiders have found strains of *Burkholderia* bacteria—some of which have nitrogen-fixing abilities—they were unable to determine the specific species of bacteria present, leaving ambiguity as to whether the detected bacteria were actually nitrogen-fixing or merely closely related to nitrogen-fixing bacteria [18]. Meanwhile, *nifH*'s specificity to only nitrogen-fixing bacteria confirms that *B. kiplingi* does have nitrogen-fixing bacteria within its body [19]. Furthermore, the lack of *nifH* amplification in *B. prosper* and *F. crocuta* also supports the results, ruling out the possibility of contamination for *nifH* amplification in *B. kiplingi*. The absence of *nifH* in both *B. kiplingi's* sister species and a species of spider that resides in similar environments also suggests that *B. kiplingi* is unique in its niche.

In the controlled environment experiments, since the spiders in the plant-only group were not observed to consume Beltian bodies, this disputes the possibility of both vertical and horizontal intraspecies microbial transmission in *B. kiplingi,* as both would have continued in this environment; instead, it suggests that the spiders rely on an external source to remain herbivorous.

The lack of herbivory in the fly group demonstrates that *B. kiplingi* is able to survive on a purely carnivorous diet, conflicting with the herbivorous nature of *B. kiplingi* in the wild. This directs us to examine *B. kiplingi's* diet as a whole, where the consumption of ant larvae stands out as the largest carnivorous portion of the diet.

With both the DNA analysis and past studies confirming the presence of nitrogen-fixing bacteria in *Pseudomyrmex* adults and larvae [20], as well as studies that indicate ants pass down their microbiome through vertical transmission (meaning that all larvae no matter age would possess the microbes) [21], the finding that *B. kiplingi* were positive for nitrogen-fixing bacteria suggests that the consumption of ant larvae is connected to its microbiome. This provides a strong case for the hypothesis that microbial transmission occurs between *B. kiplingi* and *Pseudomyrmex* larvae through a predator-prey interaction.

From SEM images, the similarity in mouth structures between *B. kiplingi* and *P. clarus* indicates that *B. kiplingi* has retained its carnivorous morphology but has not evolved herbivorous morphology to physically process its diet, such as broader fangs [4]. This supplements the previous findings by suggesting that *B. kiplingi's* herbivory is not reliant on a physical transformation.

While initially the behavioral comparison between *B. kiplingi* and *B. prosper* appears contradictory to the predictions of OFT and LCH as *B. prosper* reoriented less and moved more than *B. kiplingi*, the frameworks do not consider the behaviors of *B. kiplingi* in response to *Pseudomyrmex* aggression [1]. Crucially, hostility from the ants would likely necessitate higher levels of vigilance in *B. kiplingi* [1], prompting it to reorient more and move less to avoid being detected by the ants. Meanwhile, *B. prosper*, an active predator, would still need to move frequently to search for food. Conversely, the behaviors of *B. kiplingi* compared to *F. crocuta* do remain consistent with predictions from OFT and LCH. Because *F. crocuta* also resides on *Vachellia* plants and likely faces the same behavioral pressures from *Pseudomyrmex* ants as *B. kiplingi*, the fact that their behaviors align with expected behaviors provides strong support for OFT and LCH.

V. Significance and Future Objectives

This research not only contributes to the currently under-researched field of niche evolution, but it also documents the first instance of nitrogen-fixing activity in an arachnid, presenting a significant discovery for the field of microbiology, arachnid behavior, and ecology. Future studies should investigate how the presence of nitrogen-fixing bacteria impacts the diet and behavior of its host.

Furthermore, the diet and SEM analyses suggest that *B. kiplingi* relies primarily on their microbiome to consume plants. These findings hint at the possibility that *B. kiplingi* derived this microbiome, which breaks down plant tissue, from *Pseudomyrmex* larvae. This is evidence for the first example of horizontal microbiome transfer from prey to predator between animals, representing a new possible pathway of how microbes may begin to associate with hosts.

This data also represents the possibility of a new class of predator-prey relationships where the primary goal is microbiome acquisitions as opposed to energy gain. The results from this study should be considered in future research on predator-prey interactions and behaviors, rapid evolution into new niches, and microbiome retention.

Since the detailed mechanisms of *B. kiplingi's* herbivory remains a mystery, future research will employ metagenomic sequencing and more in-depth behavioral manipulation experiments to confirm the occurrence of predator-prey microbial transmission and identify the specific species of microorganisms involved.

Lastly, the video behavioral analysis not only provides significant support for OFT and LCH it also advances the understanding of how predator-prey interactions influence changes in an organism's feeding habits. To further test the frameworks on *B. kiplingi,* future experiments should be conducted under controlled conditions without ants to document their baseline behaviors.

VI. Acknowledgments

I would like to thank Mark Eastburn for mentoring me through this research project, assisting with the collection of samples and videos, and guiding my analysis. I would also like to thank the Princeton High School Research Program for supporting my research with lab space, lab time, sourcing materials, and funding. Lastly, I would like to thank Dr. Ren-Chung Cheng from the Department of Life Science and Dr. Kai-Jung Chi from the Institute of Biophysics at National Chung-Hsing University for their expertise and advice.

VII. References

[1] Meehan, C., Olson, E., Reudink, M., Kyser, T. K., & Curry, R. (2009). Herbivory in a spider through exploitation of an ant–plant mutualism. Current Biology, 19(19), R892–R893. https://doi.org/10.1016/j.cub.2009.08.049

[2] Smith, R. B., & Mommsen, T. P. (1984). Pollen Feeding in an Orb-Weaving Spider. Science, 226(4680), 1330–1332. https://doi.org/10.1126/science.226.4680.1330

[3] Calderón-Cortés, N., Quesada, M., Watanabe, H., Cano-Camacho, H., & Oyama, K. (2012). Endogenous Plant Cell Wall Digestion: A Key Mechanism in Insect Evolution. Annual Review of Ecology, Evolution, and Systematics, 43(1), 45–71. https://doi.org/10.1146/annurev-ecolsys-110411-160312

[4] Elias, S. A. (2023). Insect Mouthparts - an overview | ScienceDirect Topics. Www.sciencedirect.com. https://www.sciencedirect.com/topics/veterinary-science-and-veterinary-medicine/insect-mouthparts#:~:text=Insects%20have%20evolved%20a%20wide

[5] van Borm, S., Buschinger, A., Boomsma, J. J., & Billen, J. (2002). Tetraponera ants have gut symbionts related to nitrogen–fixing root–nodule bacteria. Proceedings of the Royal Society of London. Series B: Biological Sciences, 269(1504), 2023–2027. https://doi.org/10.1098/rspb.2002.2101

[6] Gonella, E., Crotti, E., Rizzi, A., Mandrioli, M., Favia, G., Daffonchio, D., & Alma, A. (2012). Horizontal transmission of the symbiotic bacterium Asaia sp. in the leafhopper Scaphoideus titanus Ball (Hemiptera: Cicadellidae). BMC Microbiology, 12(S1). https://doi.org/10.1186/1471-2180-12-s1-s4

[7] Wcislo, W. T., & Tierney, S. M. (2009). Behavioral environments and niche construction: the evolution of dim-light foraging in bees. Biological Reviews, 84(1), 19–37. https://doi.org/10.1111/j.1469-185x.2008.00059.x

[8] Rosenberg, E., & Zilber-Rosenberg, I. (2021). Reconstitution and Transmission of Gut Microbiomes and Their Genes between Generations. Microorganisms, 10(1), 70. https://doi.org/10.3390/microorganisms10010070

[9] Science. (2009). First Omnivorous Spider Says "No Thanks" to Insects. AAAS Articles DO Group. https://doi.org/10.1126/article.31555

[10] Ruiz, G., & Edwards, G. B. (2013). Revision of Bagheera(Araneae: Salticidae: Dendryphantinae). Journal of Arachnology, 41(1), 18–24. https://doi.org/10.1636/k12-67.1

[11] Sweeney, K., Cusack, B., Armagost, F., O'Brien, T., Keiser, C. N., & Pruitt, J. N. (2013). Predator and prey activity levels jointly influence the outcome of long-term foraging bouts. Behavioral Ecology, 24(5), 1205–1210. https://doi.org/10.1093/beheco/art052

[12] Kreiter, N., & Wise, D. H. (1996). Age-related changes in movement patterns in the fishing spider, Dolomedes triton (Araneae, Pisauridae). Journal of Arachnology, 24(1).

[13] Smith, H. M. (2009). The Costs of Moving for a Diurnally Cryptic Araneid Spider. The Journal of Arachnology, 37(1), 84–91. https://www.jstor.org/stable/40233844

[14] Emerson, B. C., & Gillespie, R. G. (2008). Phylogenetic analysis of community assembly and structure over space and time. Trends in Ecology & Evolution, 23(11), 619–630. https://doi.org/10.1016/j.tree.2008.07.005

[15] Stein, E. D., White, B. P., Mazor, R. D., Miller, P. E., & Pilgrim, E. M. (2013). Evaluating Ethanol-based Sample Preservation to Facilitate Use of DNA Barcoding in Routine Freshwater Biomonitoring Programs Using Benthic Macroinvertebrates. PLoS ONE, 8(1), e51273. https://doi.org/10.1371/journal.pone.0051273

[16] Hill, D. (2011). The jumping spider mouth (Araneae: Salticidae) . Peckhamia, 97(1). https://peckhamia.com/peckhamia/PECKHAMIA_97.1.pdf

[17] Hollis, J. H., & Branson, B. A. (1964). LABORATORY OBSERVATIONS ON THE BEHAVIOR OF THE SALTICID SPIDER PHIDIPPUS AUDAX (HENTZ). Transactions of the Kansas Academy of Science. Kansas Academy of Science, 67, 131–148. https://pubmed.ncbi.nlm.nih.gov/14248840/

[18] Hu, G., Zhang, L., Yao, Y., & Peng, Y. (2019). Taking insight into the gut microbiota of three spider species: No characteristic symbiont was found corresponding to the special feeding style of spiders. Ecology and Evolution, 9(14), 8146–8156. https://doi.org/10.1002/ece3.5382

[19] Gaby, J. C., & Buckley, D. H. (2012). A Comprehensive Evaluation of PCR Primers to Amplify the nifH Gene of Nitrogenase. PLoS ONE, 7(7), e42149. https://doi.org/10.1371/journal.pone.004214

[20] Eilmus, S., & Heil, M. (2009). Bacterial Associates of Arboreal Ants and Their Putative Functions in an Obligate Ant-Plant Mutualism. Applied and Environmental Microbiology, 75(13), 4324–4332. https://doi.org/10.1128/aem.00455-09

[21] Bringhurst, B., Allert, M., Greenwold, M., Kellner, K., & Seal, J. N. (2022). Environments and Hosts Structure the Bacterial Microbiomes of Fungus-Gardening Ants and their Symbiotic Fungus Gardens. Microbial Ecology, 86(1374–1392 (2023)). https://doi.org/10.1007/s00248-022-02138-x

Inhibition of Superbug Formation by Blocking Transmission of Bacterial Necrosignal Using Kimchi LAB Metabolites

Ann Lee[1]

Abstract— **Multidrug resistance of superbugs has become one of the greatest threats to global health. Previously, it was understood that bacteria that survive direct exposure to antibiotics acquire antibiotic resistance traits and become superbugs. However, a 2020 study by Bhattacharyya et al. introduced a novel mechanism of superbug formation: dying bacteria transfer resistance-enhancing factor AcrA to living bacteria through a process called necrosignaling. In this study, we investigate whether the metabolites released by kimchi lactic acid bacteria (LAB) of various fermentation stages could block the transfer of necrosignals and therefore inhibit the creation of superbugs. To test this hypothesis, dying *E. coli* was applied on one side of LB agar plates and kimchi metabolites were injected into their borders. Agar diffusion tests were performed with *E. coli* on the other side of the agar plates. It was found that *E. coli* evolved into multi-resistant bacteria under necrosignal conditions, and kimchi LAB metabolites of all three fermentation stages blocked the transmission of these signals, resulting in a reduction in bacterial growth. Notably, LAB metabolites of kimchi in the second, or moderate, fermentation stage were the most effective. These results demonstrate that the LAB metabolites found in kimchi block the transmission of necrosignals, prompting further research into the use of kimchi postbiotics as a potential health food or medical treatment to counter multidrug resistance.**

I. Introduction

Superbugs, or multidrug resistant bacteria, pose severe threats to global health and food security, infecting 2.8 million people in the U.S. and resulting in 35,000 deaths in 2019 [1]. However, the survival of bacterial swarms and the rise of multidrug resistance remains relatively unfamiliar. Until now, it had been understood that bacteria that survive direct exposure to antibiotics acquire antibiotic resistance and become a superbug [2]. However, a 2020 study by Bhattacharyya et al. introduced a novel mechanism of superbug formation: dying bacteria release resistance-enhancing substance AcrA, a specific molecule found in a type of pump within the bacterial cell called RND efflux pump that interacts with the outer membrane of live cells (Figure 1) [3]. This interaction stimulates the live cells to expel or pump out drugs, such as antibiotics, from inside the cell through a process called necrosignaling [3].

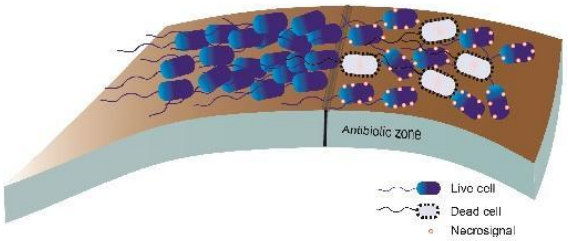

Figure 1. Dying bacteria cells releasing necrosignals to enhance antibiotic resistance in living cells

Necrosignaling occurs as a form of microbial communication called quorum sensing, which allows bacteria to coordinate responses through signaling molecules [3]. Thus, disrupting this communication could deter the transfer of resistance-enhancing signals.

Studies investigating promising compounds to prevent quorum sensing have discovered that bacteria in kimchi possess antimicrobial and anti-biofilm properties [4]. Specifically, during the process of fermentation, the bacteria release various byproducts known as lactic acid bacteria, or LAB, metabolites. Some of these LAB metabolites significantly inhibit the formation of biofilms, or communities of bacteria that stick together to form a protective shield against antibiotics, by disrupting quorum sensing. As the concentration of these metabolites increased, they became even more effective at interfering with quorum sensing, indicating their potential ability to target microbial communication pathways like necrosignaling [5].

In this study, we use agar diffusion tests to examine if kimchi LAB metabolites inhibit bacterial necrosignaling and determine the fermentation stage of kimchi that most effectively prevents these chemical signals, ultimately revealing a novel candidate for future treatment of multi-resistant superbugs. Through the examination of clear zone sizes formed when bacteria are exposed to antibiotics, we also aimed to analyze the antibacterial efficacy of kimchi LAB metabolites.

II. Methods

To prepare bacteria culture media MRS and LB agar, a mixture containing 27.5g of MRS powder, 7.5g of agar powder, and 500 mL of distilled water (DW), and another mixture with 10g of LB powder, 7.5g of agar powder, and 500 mL DW were autoclaved and left to cool. To make MRS and LB broth, one mixture containing 100 mL of DW and 27.5 g MRS broth powder and another mixture containing 500 mL of DW and 10g of LB broth powder were autoclaved and left to cool.

Three types of kimchi were prepared according to different fermentation levels: kimchi with fermentation grade 1 for shortest (24 hours), 2 for medium (30 days), and 3 for longest (1 year) period of fermentation. Samples of kimchi soup were incubated in both aerobic and anaerobic conditions (Figure 2). 30 uL of kimchi soup and MRS broth were cultured in conical tubes. After being removed from the incubator, bacterial colonies in MRS plates were

[1]Ann Lee is with the Seoul International School, 15 Seongnam-daero 1518beon-gil, Sujeong-gu, Seongnam-si, Gyeonggi-do, South Korea 13113 (corresponding author to email: annslee814@gmail.com).

classified based on form, margin, elevation, color, transparency, and size.

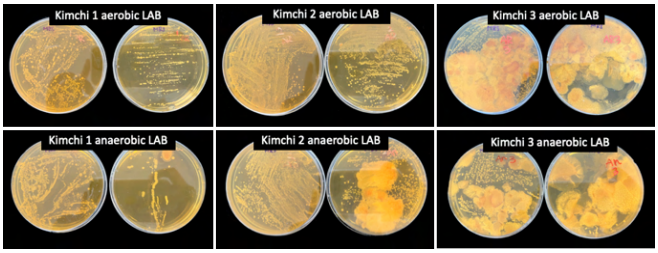

Figure 2. Kimchi LAB colonies on MRS agar plates after culture

Petri dishes were divided into three sections for antibiotic susceptibility tests and halves for border crossing assays. We note that if the size of the clear zones formed during any of these tests were too large, they could leak into neighboring sections of the petri dish and compromise experimental data. Thus, it was important that clear zones larger than half of the radius of the petri dish do not form. As the petri dish used in this study was 4.5 cm in radius, 2.25 cm would be the maximum diameter a clear zone could cover without spilling over to other sides. Since 0.01x dilutions of ampicillin and meropenem and 0.001x dilutions of ceftezole produced clear zones closest to 2 cm, these specific concentrations were selected for further use (Figure 3).

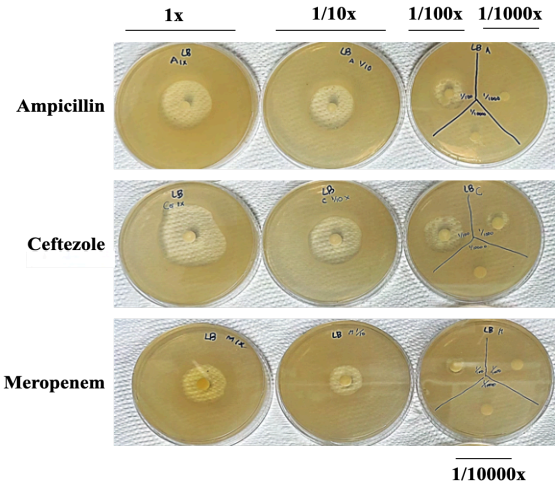

Figure 3. Clear zones formed by different dilutions of antibiotics

To test the antibiotic susceptibility of *E.* coli, three types of antibiotics, ampicillin, meropenem, and cephalosporin, were first diluted to various concentrations. *E. coli* stock solution was spread out onto agar plates, and paper discs were placed on each surface for antibiotic treatment (Figure 4). Each agar plate was incubated at 30°C for 48 hours.

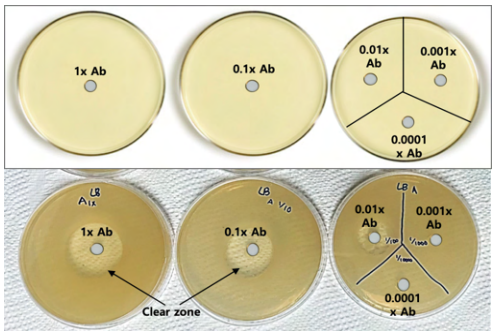

Figure 4. Placement of paper discs based on dilutions of antibiotic treatment

To test the antibiotic susceptibility of *E. coli* under the influence of necrosignals, LB agar plates with cultured *E. coli* were prepared according to different experimental conditions (Figure 5). Bacterial colonies were extracted from three locations (A, B, C) to be spread on new LB agar plates. After antibiotic treatment and incubation, the diameters of clear zones were measured as an indication of the inhibition of bacterial growth.

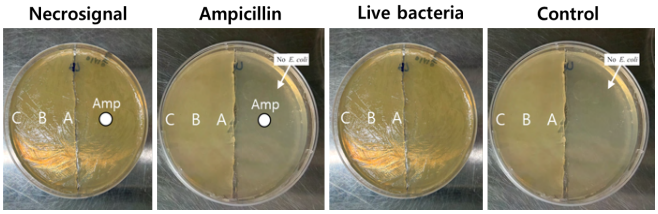

Figure 5. Method for testing antibiotic resistance of bacteria in different experimental conditions

The absorbance values of kimchi cultivated solutions were obtained, and 1 ABS per 1 mL was measured. Then, with a 0.2 um syringe filter, LAB was removed from cultivated solutions to recover the kimchi LAB metabolites.

In order to confirm if superbug formation would be inhibited, the midline of cultured LB agar plates were cut and saturated with kimchi LAB metabolites (Figure 6). Bacterial colonies from three locations were spread on new LB agar plates. After antibiotic treatment and incubation, the diameter of each clear zone was measured.

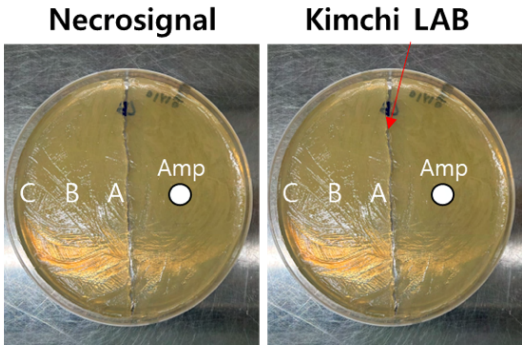

Figure 6. LB agar plates with and without kimchi LAB metabolites in border based on experimental conditions

Finally, kimchi samples with only LAB metabolites or together with LAB were prepared. Then, these samples were

autoclaved at 121°C, 1.2 atm., refrigerated at -75°C, and irradiated to simulate the packaging conditions of kimchi. These metabolites were injected into the cut midlines of cultured LB agar plates (Figure 7). Bacterial colonies from location B were applied on new LB agar plates. After treatment with antibiotics and incubation, the diameters of clear zones were measured to test the active range of kimchi LAB metabolites.

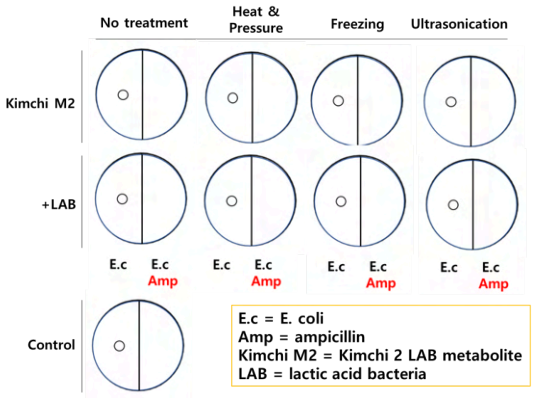

Figure 7. Method of detecting active range of kimchi LAB metabolites

III. Results

We first found that necrosignals induce antibiotic resistance of bacteria. The diameters of clear zones under necrosignal condition were shorter than that of ampicillin, live bacteria, or control conditions, especially in distance B, which represents a moderate distance between the isolated bacterial colonies and the line where kimchi LAB was injected. (Figure 8). Notably, it was found that ceftezole and meropenem under necrosignal conditions inhibited an area of bacterial growth of diameters 0.9 cm and 0 cm, respectively, in contrast to live bacteria condition, in which clear zones had diameters of 1.9 cm and 1.3 cm, respectively (Figure 9 B and C). The differences in these clear zones show that bacteria exposed to necrosignals under 'necrosignal conditions' developed resistance, as clear zones represent the extent to which antibiotics prevented the growth of visible bacterial colonies on agar plates.

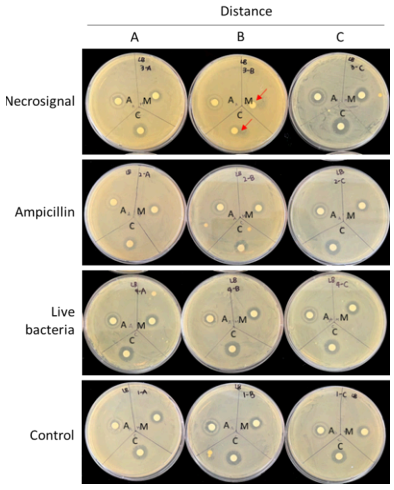

Figure 8. Qualitative effect of necrosignal on multi-drug resistance of bacteria

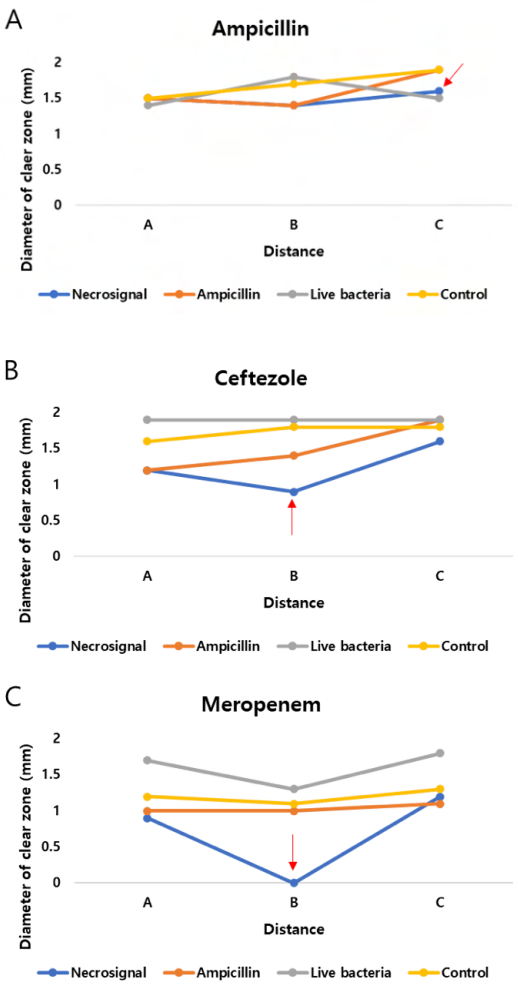

Figure 9. Diameters of clear zones formed by antibiotics depending on distance from border and experimental conditions

Koreans enjoy various types of kimchi with different fermentation stages: freshly made (24 hours), moderately fermented (30 days), and highly fermented (1 year) kimchi. Classification of kimchi LAB colonies and analysis of LAB proliferation revealed that the type and amount of kimchi LAB colonies varied widely based on fermentation stage and culture conditions (Figure 10 and 11).

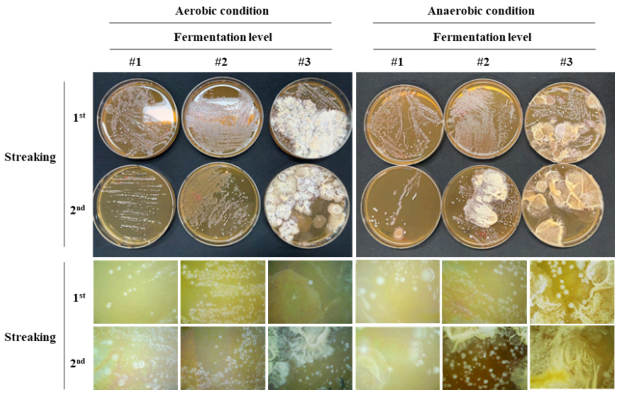

Figure 10. Kimchi LAB culture in aerobic and anaerobic conditions

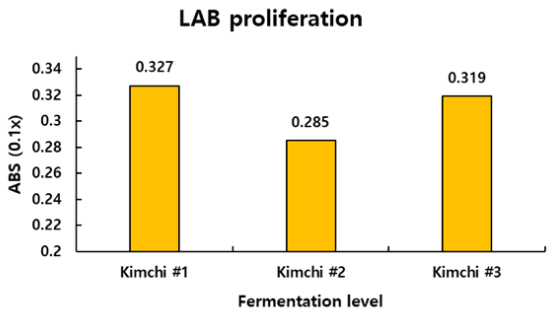

Figure 11. LAB proliferation (ABS, or absorbance, per 1 mL) of kimchi with different fermentation periods

Most importantly, in the antibiotic susceptibility test of *E. coli* by necrosignal, we concluded that kimchi LAB metabolites inhibit transmission of necrosignals. In comparison to necrosignal conditions, larger clear zones appeared in the presence of kimchi LAB metabolites (Figure 12). For example, in distance B, the diameters of clear zones under necrosignal conditions (control) were lowest, 1.4, 0.9, and 0 cm for ampicillin, ceftezole, and meropenem, respectively (Figure 13 A, B, and C). In contrast, the diameters of clear zones with exposure to kimchi metabolites were higher than the control. Furthermore, in distance A, necrosignals reduced the diameter of clear zones formed by ampicillin, ceftezole, and meropenem to 1.5, 1.2, and 0.9 cm, respectively, much lower than when kimchi LAB metabolites were present (Figure 13 A, B, and C).

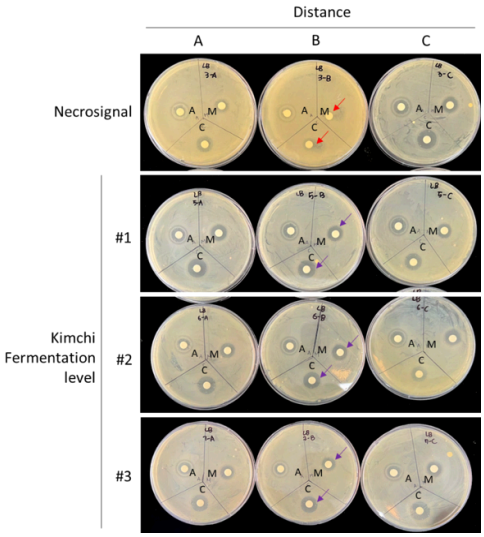

Figure 12. Qualitative effect of Kimchi LAB Metabolites on Inhibition of Necrosignal

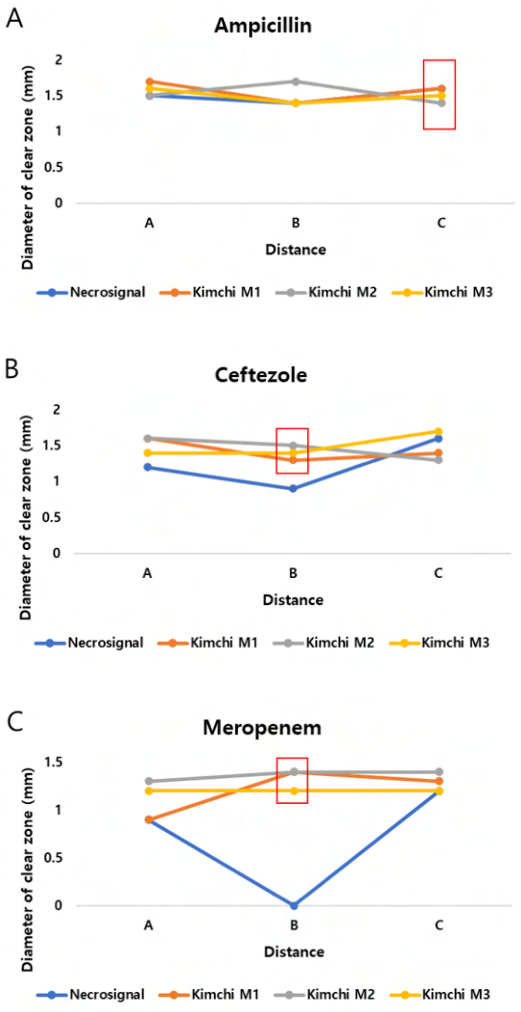

Figure 13. Diameters of clear zones formed by antibiotics depending on distance from border and inclusion of kimchi LAB metabolites

Finally, Kimchi LAB metabolites maintained necrosignal inhibitory activity even under high temperatures, deep freezing, and ultrasonic conditions. Clear zones formed by ceftezole and meropenem under necrosignaling conditions were smaller in diameter (Figure 14 B & C) than those under various treatment conditions.

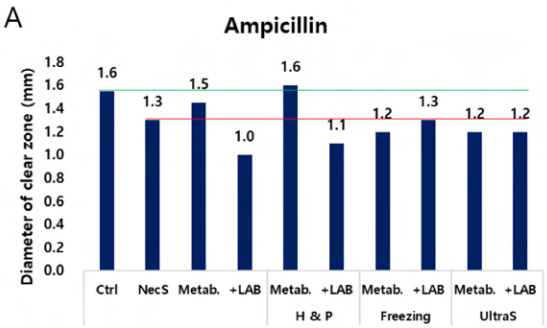

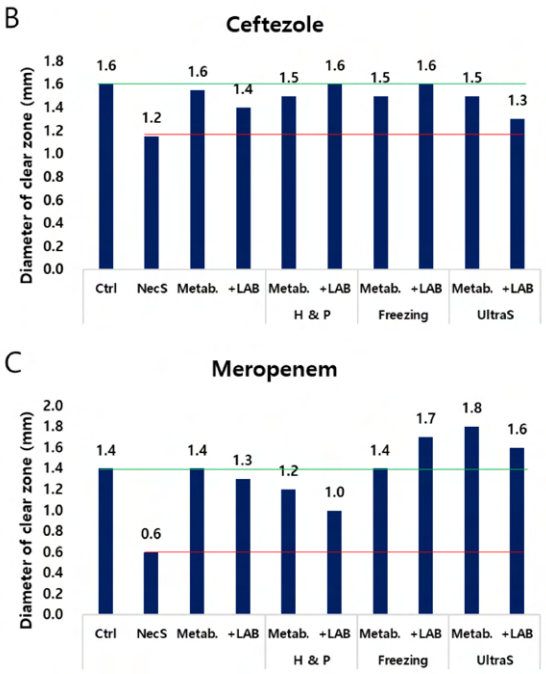

Figure 14. Diameter of clear zones formed by antibiotics depending on treatment of kimchi LAB metabolites in comparison to necrosignaling conditions (red lines) and control (green lines)

IV. Discussion

Our study found that necrosignals enhance the survival of bacteria in the presence of antibiotics, thus inducing the transformation from regular bacteria to superbugs. We discover that kimchi's LAB metabolites have necrosignaling-inhibiting effects. This could be due to that during kimchi LAB fermentation, the major metabolites produced are a heterogeneous mixture of lactic acid and ethanol, which works to break down structures of proteins in bacteria, along with bacteriocins and exopolysaccharides that are known to have antimicrobial effects [6].

While this experiment demonstrated that kimchi LAB metabolites inhibit necrosignal transmission, the effectiveness of these substances under environmental stressors (i.e. when the conditions deviate from typical kimchi fermentation conditions) was still uncertain. We must carefully assess the range of LAB metabolites' inhibitory activity because if kimchi is to be incorporated into future medications, it must withstand various processing and packaging treatments, subjected to heating and pressure, deep freezing, and ultrasonication. We tested some of these conditions as shown in Figure 14 and concluded that kimchi LAB metabolites overall maintain necrosignal inhibitory activity when subjected to high temperature, deep freezing, and ultrasonic conditions and are made up of very durable substances. However, we note that the clear zones made by ampicillin under necrosignaling conditions (Figure. 14 A), were greater in size than those under various treatment conditions, deviating from the pattern shown in Figure 14 B and C. This could be due to the fact that the bacteria were previously exposed to ampicillin in order to produce dying bacteria, making this result dispensable.

We also noted that the results of this study were different from what we expected. According to Inatsu et al, when Staphylococcus aureus, a gram-positive bacterium, was inoculated with kimchi for a prolonged time (i.e. fermentation occurred for a long time), the *S. aureus* level decreased rapidly to minimum detectable level [7]. In my study, however, bacterial growth was limited mostly effectively when exposed to moderately-fermented kimchi. One factor that could have accounted for this difference was the presence of dying bacteria in my study. While my study analyzed necrosignaling, which involves the transfer of chemical signals from dying to living bacteria, Inatsu et al only considered the effect of kimchi fermentation stages on bacterial proliferation.

V. Conclusion

The primary purpose of this study was to detect whether dying bacteria secrete necrosignals for living bacteria to become multi-resistant bacteria, and, if detected, to discover whether kimchi LAB metabolites can effectively suppress necrosignaling between dying and living bacteria. First, border crossing assays confirmed that necrosignals enhance survival of bacteria in the presence of antibiotics, thus inducing the transformation from regular bacteria to superbugs. In addition, it was found that LB agar plates treated with kimchi LAB metabolites had larger clear zones, proving that kimchi LAB metabolites suppress the transfer of necrosignals, especially those of moderate fermentation. Hence, through this research, it was discovered that kimchi LAB metabolites have repressing effects against the transfer of necrosignals and maintain this inhibitory activity even under extreme conditions, thus being a novel candidate for future treatment of multi-resistant superbugs. However, as this study was limited to revealing the overall effects of kimchi LAB metabolites, future research should be conducted to identify and confirm the exact chemical components of kimchi metabolites that enable it to prevent the transfer of necrosignals using chromatography, precipitation, or microscopic analysis. Future research can isolate the specific substances of kimchi LAB metabolites and offer new insights on how these substances can be used to develop effective treatment against superbugs formed through necrosignaling.

Acknowledgment

I wish to thank my parents who provided me the opportunity to conduct this research. Also, I would like to thank my mentor and research director, Sunny S. Kim, for giving me necessary training and guidance.

References

1. Centers for Disease Control and Prevention. 2021. How do germs become resistant? [online] Available at: https://www.cdc.gov/drugresistance/about/how-resistance-happens.html
2. B. Baral, M. R. Mozafari, "Strategic Moves of "Superbugs" Against Available Chemical Scaffolds: Signaling, Regulation, and Challenges", *ACS pharmacology & translational* science, vol. 3, April. 2020, pp. 373–400

3. S. Bhattacharyya, D. M. Walker, R. M. Harshey, “Dead cells release a ‘necrosignal’ that activates antibiotic survival pathways in bacterial swarms”. *Nat Commun*, vol. 11, Aug. 2020, pp. 4157
4. Lee, Ji-Eun et al. “Antimicrobial and anti-biofilm effects of probiotic *Lactobacillus plantarum* KU200656 isolated from kimchi.” *Food science and biotechnology* vol. 30,1 97-106. 23 Nov. 2020, doi:10.1007/s10068-020-00837-0
5. Khani, Nader et al. “Postbiotics as candidates in biofilm inhibition in food industries.” Letters in applied microbiology, ovad069. 12 Jun. 2023, doi:10.1093/lambio/ovad069
6. Lee, Se-Jin et al. “Some Important Metabolites Produced by Lactic Acid Bacteria Originated from Kimchi.” Foods (Basel, Switzerland) vol. 10,9 2148. 10 Sep. 2021, doi:10.3390/foods10092148
7. Inatsu, Y et al. “Survival of Escherichia coli O157:H7, Salmonella enteritidis, Staphylococcus aureus, and Listeria monocytogenes in Kimchi.” Journal of food protection vol. 67,7 (2004): 1497-500. doi:10.4315/0362-028x-67.7.1497
8. Inatsu, Y., Bari, M. L., Kawasaki, S., & Isshiki, K. (2004). Survival of Escherichia coli O157:H7, Salmonella enteritidis, Staphylococcus aureus, and Listeria monocytogenes in kimchi. *Journal of food protection*, 67(7), 1497–1500. https://doi.org/10.4315/0362-028x-67.7.1497

Improving Solar Flare Prediction using Deep Learning: Solar Flare Anticipation Algorithm (SOFAA)

Aaron Lee[1]

***Abstract*— High-energy solar superstorms can disrupt commercial, telecommunications, and energy infrastructure, posing a considerable risk to electronics in everyday life. Scientists have created deep-learning algorithms that can predict future solar superstorms, but these methods fail to incorporate numerical and visual data simultaneously. To increase the accuracy of deep-learning algorithms predicting solar flares, this paper proposes a deep-learning algorithm, SOFAA (Solar Flare Anticipation Algorithm), combining numerical telemetry and photos taken of the sun from the SDO (Solar Dynamics Observatory) and SOHO (Solar & Heliospheric Observatory) satellites. The SOFAA used data from the SOHO's total solar irradiance (TSI) measurements, measurements of energy from helium and hydrogen ions and electrons, and the SDO's solar images in the Fe IX ion spectrum. All data was taken in 2017, from January 1 to December 31. By utilizing GoogLeNet and multilayer perceptron models, the SOFAA achieved a loss value of 0.1255, demonstrating the ability to predict TSI values indicative of a solar flare a day in advance. In short, the incorporation of both numerical and visual data can give more accurate predictions of solar flare activity.**

I. Introduction

As the world becomes more reliant on electronic devices, the threat of solar superstorms grows increasingly relevant. High-energy solar superstorms—large ejections of charged particles and electromagnetic radiation [1]—exhibit a sporadic and hard-to-predict behavior that can threaten to shut down electrical grids; damage satellites, GPS systems, smartphones, solar cells, and telecommunication cables; disrupt avionics systems in airplanes; and disturb cellular, radio, and radar systems if proper measures are not taken to mitigate the effects [2, 3]. As such, scientists have made it an imperative to monitor the activity of the sun in order to predict the coming of a damaging superstorm. One of the ways scientists have analyzed data from tools like the Solar Dynamics Observatory (SDO) and the Solar & Heliospheric Observatory (SOHO) is by extracting patterns for predictions of storms through deep learning algorithms. Because these algorithms can detect hidden but noticeable patterns and relations between events, deep-learning programs are uniquely suited to solve the issue of solar flare and storm prediction [4]. However, previous models fail to make efficient use of all datasets available to them to make optimally accurate predictions.

Therefore, developing an accurate AI model for solar storm prediction with non-visual telemetry is vital to preventing the widespread destruction of the electrified global systems that support lives around the world. The Solar Flare Anticipation Algorithm, or SOFAA, was constructed in this study to respond to the rising awareness of the threat of high-energy solar storms on human transportation, communication, and commerce electronics. The aim of this paper is to improve prediction of solar storms by combining visual and non-visual data elements from the sun.

II. Materials and Methods

To create the training data set, this study used data from the SDO's AIA channel 171, recording the electromagnetic radiation from the ion Fe IX to provide visual data for the deep learning program's image processing [5]. The imaged wavelength provided simple gold-scale contrast for the program to derive patterns, specifically that of how the appearance of the sun prior to solar events changes from baseline solar appearance. The numerical data from the SOHO's COSTEP/EPHIN instruments were used to analyze how the energy of hydrogen ions emitted by the sun shifts as a solar event draws near and occurs, while the same from the SOHO's VIRGO was used as an indicator of solar flare presence, as average TSI peaks during solar flare events [6]. All data was derived from 1 January 2017 to 31 December 2017 because an X8.2 level solar flare occurred in 2017, serving as a good training dataset for the appearance of a large solar flare [7]. VIRGO instrument data was taken hourly; COSTEP/EPHIN instrument data was taken every five minutes; and AIA instrument data was taken about every three minutes. All data points from the COSTEP/EPHIN instrument and AIA instrument were averaged and associated with an hour of a day in accordance with the VIRGO instrument data to sync the data up with each other.

The perceptron, proposed by Frank Rosenblatt in 1957 and serving as the basic building block of deep-learning algorithms, is defined by a single equation, $Wx + b$, where W is weight and b is bias. The perceptron randomly sets a weight and bias value, inputs a training data input value for x, calculates the output, finds the difference between the predicted output and actual training data output, and performs those steps for each input value until the differences in all predicted outputs and actual outputs can be calculated into a loss value. The algorithm then resets the weight and bias values in a direction that reduces the loss value and repeats the previous steps again, effectively reducing the loss value to replicate a pattern in the data set. However, the line defined by the perceptron equation cannot predict all patterns as Rosenblatt thought, so a more complex structure of many perceptrons was needed.

[1]Aaron Lee is with the Meadow School, Las Vegas, NV 89128 USA (e-mail: aaronjlee0422@gmail.com).

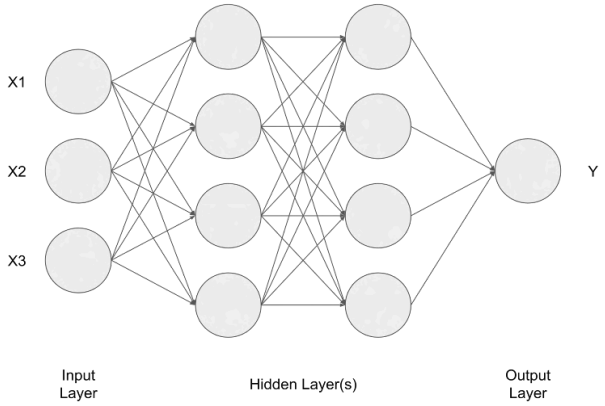

Figure 1. Multi-layer perceptron layer, input, and output structure

To resolve the shortcomings of the single-layer perceptron, the multilayer perceptron, or MLP, was invented. An MLP is composed of many perceptrons interconnected in webs with each other and one or more inputs and outputs. An MLP is organized into three "layers": an input layer that processes the raw input data, hidden layers that further process the input layer results, and an output layer that transforms the values from the hidden layer into meaningful output values. Due to the scalable nature of MLPs, they are able to derive complex patterns from any numerical data set.

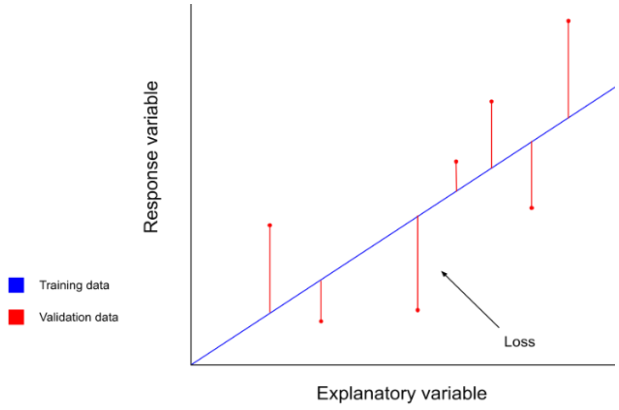

Figure 2. Deep-learning algorithm loss calculation method; blue line is training data set, red dots are predictions by the program, and red lines are the difference between the predicted data and the actual training data, also known as loss

Loss functions are mathematical functions that allow algorithms to calculate loss values measuring the deviation that the program predictions have from the training data presented. There are several types of loss functions, two of which are mean absolute error, MAE, and mean squared error, MSE. The following equation models MAE, given n is the sample size, y_i is the prediction value, and x_i is the actual value:

$$MAE = \frac{\sum_{i=1}^{n} |y_i - x_i|}{n}$$

The following equation models MSE, given the same variables above:

$$MSE = \frac{\sum_{i=1}^{n} (y_i - x_i)^2}{n}$$

The MAE loss function tends to adapt to large outliers less and gives greater corrective weight to small errors, while the MSE loss function amplifies and thus corrects to large outliers more due to squaring results. Regardless of the method, loss functions turn the comparisons between the outputs of the algorithm and those of the training data set into a score, the loss value, which the algorithm attempts to lower by adjusting the weight and bias values.

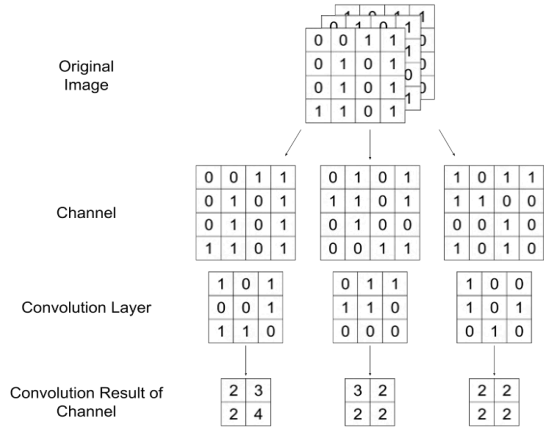

Figure 3. Convolutional layer processes; images are broken apart into three color channels, the convolution layer values are stacked and multiplied to every value underneath it at every possible position, and the resultant multiplied values are added up to create one value in the result matrix.

A convolutional neural network, or CNN, is an algorithm that replicates the way in which the human brain processes visual information. Like the actual brain, CNNs are used by computers to process images in a way understandable to itself. CNNs are made up of three parts: a convolutional layer, which breaks the image into RGB channels and runs the pixel values through filter matrices, a pooling layer, which removes outlier values skewing patterns from the final convolutional layer results, and a fully connected layer, an MLP that finds patterns in the numerical values of the final result matrix. It is through this algorithm that images can be processed by computers.

GoogLeNet is Google's rendition of a CNN that resolves previous issues with CNNs overfitting, where the algorithm finds patterns too specific to the training data set. GoogLeNet averts overfitting by diversifying the module architectures that make up the CNN's convolutional layer, removing repetitive and pointless actions in the CNN to ensure faster pattern retrieval. GoogLeNet is implemented into the Tensorflow-Keras AI program [8].

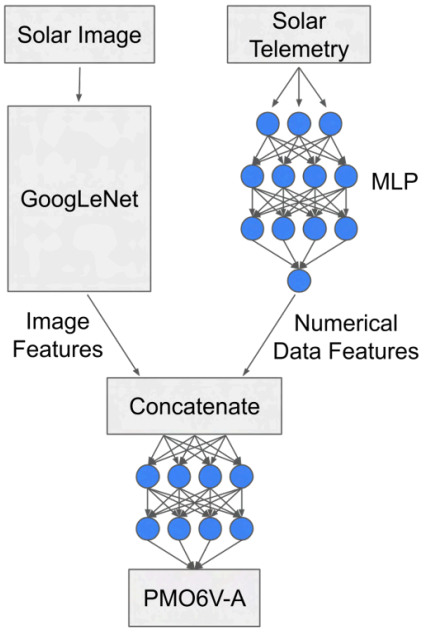

Figure 4. SOFAA deep-learning algorithm architecture

SOFAA is a combination of the GoogLeNet CNN and the individual MLP architectures. The SOFAA runs the SDO satellite's AIA solar images through the GoogLeNet CNN and the SOHO satellite's COSTEP proton energy level measurements through an MLP to get so-called "features," or patterns, from the input data. These features are concatenated, or combined, into a single feature set, which is then run through another MLP to get the final predicted TSI measurements to be compared with those of the SOHO satellite's VIRGO instrument. Three variables were changed to see their effects on the resultant loss value: loss function used, sample size, and dense layer arrangements and types. The loss values used to evaluate the effectiveness of variable changes were run through another MAE function to create comparable values. The training data TSI values were pushed forward one day to test for the SOFAA's ability to predict TSI values one day into the future.

III. Results

The loss values for all trials of the SOFAA model were less than 1, indicating high correlation between solar imaging patterns, charged proton intensity telemetry values, and TSI values from the sun. Differing dense layer sizes also did not affect the amount of loss experienced with the model. For the most part, an increase in sample size resulted in lower loss values, although by an arguably negligible amount. Loss remained consistent after slight variation in loss in the first epoch. This may indicate high correlation in the values of the three datasets, as finding patterns was of such ease that the ideal weight and bias values resulted after just one epoch. For sake of brevity, the number of epochs was reduced to 7.

TABLE I. SOFAA model experimentation results (7 epochs)

Trial #	Data point sample size	Dense layers	MAE/MSE	Loss Value
1	2000	100-300-100	MAE	0.3329
2	2000	100-300-100	MSE	0.1283
3	2000	100-300-900-500-100-100	MAE	0.3329
4	2000	100-300-900-500-100-100	MSE	0.1283
5	6000	100-300-100	MSE	0.1274
6	10000	100-300-100	MSE	0.1255

After verifying the ability of the program to find correlations between data taken at the same time, experiments displacing the TSI data by one day forward were performed. With 7 epochs, a 10000 data point sample size, 100-300-100 format dense layers, and an MSE loss calculation method, the SOFAA model was able to find synergy between solar imaging, proton intensity telemetry measurements, and TSI measurements a day into the future, as low loss indicates the ability of the program to find a pattern or correlation in the data input and output. The lowest loss value achieved was 0.1257.

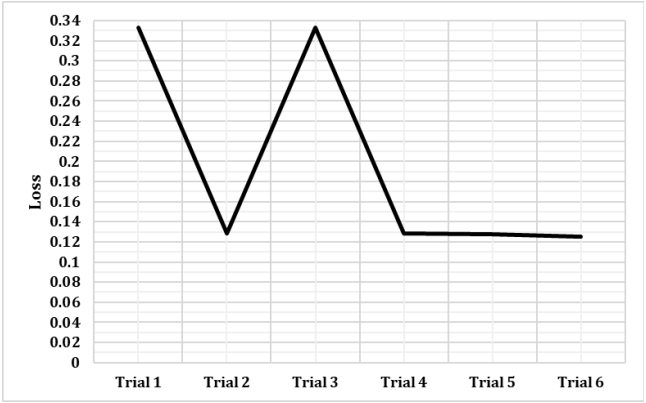

Figure 5. SOFAA model experimentation results chart

IV. Conclusion

In this study, the SOFAA model was created and refined with the goal of combining visual and numerical solar data to increase the accuracy of solar flare predictions. With the advancement of technology in the modern era, many more opportunities to ensure the security of human infrastructure have presented themselves. The SOFAA's results show promise in its ability to predict the value of TSI one day into the future when given solar imaging and proton energy intensity value data, predicting within a reasonable margin of error and loss of 0.1257. With the predicted TSI measurement, the determination of whether a solar flare will occur or not and of what intensity can be derived with a large amount of confidence, allowing for advance notice of solar flares.

V. Discussion

The SOFAA helps illuminate visual and numerical data concatenation as an important path to improving solar flare prediction moving forward. Most solar flare prediction model proposals still restrict themselves to the analysis of visual data and qualitative feature sets. Through the correlation found between the concatenated data set and the future TSI value of the sun here, the creation of a prediction

model for solar flares utilizing concatenated data sets is not far away.

However, despite the successes of the SOFAA model, there remains ample room to expand and further push the model to serve greater and more demanding purposes. In its current state, the prediction values for TSI from the sun must be analyzed manually to check for the probability of a solar flare or storm occurring. In most cases, this analysis would still require additional processing time. Another set of algorithms to further derive patterns in the TSI measurements to determine solar superstorm probability would solve this issue efficiently and quickly. Although the SOFAA model has low loss values in its predictions, there may still be concern about the verity of such results. However, due to the unknowable nature of the mechanisms in deep-learning algorithms, deriving an easy way to further analyze and interpret the resulting data is difficult. One way to increase certainty in the results besides directly analyzing the data is to cross-examine the results of the SOFAA model with other models of a similar nature, like that of the Deep Flare Net (DeFN) model, to check for similar results and rule out discrepancies manually as needed. Another way to improve the SOFAA model's verity would be to add more datasets into the pool of solar telemetry data used by SOFAA. By adding more solar telemetry data in the model, SOFAA would be able to further ensure that the patterns it does detect are noticeable and common across all analyzable elements of the sun. One more method to improve accuracy of SOFAA model result data would be to utilize the true skill statistics (TSS), a metric of discrimination performance, used to evaluate the DeFN model, as the TSS skill score considers many more factors, including loss, to help give an operational "skill score" of the TSS reflective of actual prediction performance in practical situations [9]. Overall, the SOFAA model demonstrates the great potential for solar flare prediction software improvement, which lies in the concatenation of different data set types by reinforcing trends present in both data sets and diminishing those only present in singular data sets.

VI. References

[1] J. Hu, V. S. Airapetian, G. Li, G. Zank, and M. Jin, "Extreme energetic particle events by superflare-associated CMEs from solar-like stars," *Science Advances*, vol. 8, no. 12, Mar. 2022.

[2] P. Cannon, M. Angling, L. Barclay, C. Curry, C. Dyer, R. Edwards, G. Greene, M. Hapgood, R. Horne, D. Jackson, C. Mitchell, J. Owen, A. Richards, C. Rogers, K. Ryden, S. Saunders, M. Sweeting, R. Tanner, A. Thomson, and C. Underwood, "Extreme space weather: impacts on engineered systems and infrastructure," *Royal Academy of Engineering*, Feb. 2013.

[3] Atmospheric and Environmental Research, "Solar Storm Risk to the North American Electric Grid," *Lloyd's*, 2013.

[4] E. Larsen, "Machine Learning Model Survey with the dataset for solar flare prediction," *PeopleTec, Inc.*, 2021.

[5] M. Lockheed. (n.d.). "Instrument. Atmospheric Imaging Assembly," https://aia.lmsal.com/public/instrument.htm

[6] M. Kretzschmar, T. D. d. Wit, W. Schmutz, S. Mekaoui, J. F. Hochedez, and S. Dewitte. "The effect of flares on total solar irradiance," *Nature Physics*, vol. 6, pp. 690-692, Aug. 2010.

[7] J. Zhao, W. Liu, and J. C. Vial, "White-light Continuum Observation of the Off-limb Loops of the SOL2017-09- 10 X8.2 Flare: Temporal and Spatial Variations," *The Astrophysical Journal Letters*, vol. 921, no. 2, Nov. 2021.

[8] C. Szegedy, W. Liu, Y. Jia, P. Sermanet, S. Reed, D. Anguelov, D. Erhan, V. Vanhoucke, and A. Rabinovich, "Going Deeper with Convolutions," *2015 IEEE Conference on Computer Vision and Pattern Recognition (CVPR)*, pp. 1-9, 2015.

[9] N. Nishizuka, Y. Kubo, K. Sugiura, M. Den, and M. Ishii, "Deep Flare Net (DeFN) Model for Solar Flare Prediction," *The Astrophysical Journal*, vol. 858, no. 113, May 2013.

The Use of iPSC-Derived Neural Organoids to Investigate Autism Spectrum Disorders

Alaina A. Shinde[1]

Abstract— **Autism spectrum disorders (ASD), characterized by impaired social communication, behavioral abnormalities, and restricted interests, affect an estimated 1 in 59 children worldwide. This review provides a comprehensive background on ASD, its historical context, genetic bases, and the influence of epigenetic and environmental factors. Neural organoids, 3D models that mimic human brain structure and functionality, are utilized with intrinsic organoid protocols and guided differentiation to gain insights into ASD modeling, risk gene identification, and environmental effects. Neural organoids also offer promise in drug screening and personalized treatment development for ASD. Despite limitations and ethical concerns, neural organoids stand as a transformative tool in understanding the molecular and cellular bases of ASD, ultimately paving the way for more effective interventions and support for affected individuals.**

I. Introduction

Autism spectrum disorders (ASD) are complex neurodevelopmental disorders characterized by impaired social communication, behavioral abnormalities, and restricted interests. Understanding the underlying molecular and cellular changes associated with ASD is crucial for advancing our knowledge of the disorders and developing effective interventions. In recent years, the development of neural organoids, three-dimensional models that mimic the structure and functionality of the human brain, has provided researchers with a powerful tool to study neurobehavioral disorders such as ASD.

A. Background on Autism Spectrum Disorders (ASD)

ASD, characterized by impacted communication, social interaction, and behavior, are a highly prevalent group of neurodevelopmental disorders, affecting an estimated 1 in 59 children [1]. Individuals with ASD may have difficulties with social interactions such as understanding nonverbal cues or engaging in conversation. They may also exhibit repetitive behaviors or restricted interests. ASD is considered a spectrum disorder due to the wide variation in severity of symptoms, ranging from mild to severe, with some symptom overlap across the spectrum, but also potential differences between mild and severe cases [2].

While individuals with mild ASD may have social difficulties, such as with initiating and maintaining conversations, understanding social cues, or interpreting emotions, they may still desire social interaction and have some capacity in adaptive functioning. People with mild ASD often have good language skills, although they may struggle with certain aspects of communication, such as understanding non-literal language. Intellectual functioning is often within the average or above-average range. They may excel in certain areas of interest or have specific talents. Individuals with mild ASD may exhibit repetitive behaviors that do not significantly interfere with their daily activities.

In severe ASD, social interaction may be extremely limited or absent. Communication difficulties are more pronounced, with limited or no verbal language. In severe ASD, intellectual disability may be present, and individuals may have significant cognitive impairments across multiple domains. Challenging behaviors can be more pronounced and disruptive, including self-injury, aggression, tantrums, or meltdowns.

1. History

ASD was first described by Kanner (1943) in a detailed report of 11 children with similar unusual behaviors, including improper language, indifference to other people, and obsessive tendencies [3]. As the 20th century progressed, the initial rarity of diagnoses of ASD became much more prevalent, with 1 in 59 individuals being diagnosed on the spectrum [4]. This increase can be partially attributed to the increasing awareness of mental health issues in the past century as well as scientific acknowledgement of a spectrum of neurodevelopmental disorders beyond the 1950s' automatic categorization of schizophrenia [4].

Current Diagnostic and Statistical Manual of Mental Disorders (DSM) criteria deems only two broad features as characteristic of an ASD diagnosis: deficits in social communication and social interaction across multiple contexts; and restricted, repetitive patterns of behavior, interests, or activities [5]. Due to the generality of these definitions, ASD often overlaps with other conditions, such as motor abnormalities, gastrointestinal issues, epilepsy, and intellectual disorder.

The causes of ASD are not fully understood, but it is believed to be caused by both genetic and environmental factors. About 10-20% of ASD cases can be attributed to a known genetic cause, and patients with similar mutations may be diagnosed on very different levels of the spectrum [1]. Considering the nature of its etiology, or the in-depth causation of a disease, ASD does not specifically "target" any particular demographic. ASD can affect individuals of any gender, race, ethnicity, or socioeconomic background. However, research has indicated that autism is diagnosed more frequently in males than females, with three times as many males diagnosed than females. This gender disparity may be due to a withstanding lack of diverse research, and research is ongoing in terms of possible sex-linked genes.

2. Genetics of ASD

High-throughput genotyping, or simultaneous genotyping for hundreds or thousands of markers in hundreds to thousands of individuals, of single-nucleotide polymorphisms (SNPs) using microarrays has enabled genome-wide association studies (GWAS) of ASD to detect any variants associated with the disorder. Several GWAS have investigated the link between common genetic variants and ASD diagnosis, identifying two

[1]Alaina Shinde is with Edison High School, Edison, NJ 08817 USA (corresponding author to e-mail: alaina.shinde@gmail.com).

*Research supported by Lumiere Education.

significant risk loci at chromosome 5p14.1 and within gene *MACROD2* [37]. However, replication of these loci has been challenging despite the high heritability and prevalence of the disease. Sample sizes in ASD GWAS are relatively small compared to studies on other common diseases, and larger sample sizes are needed to identify additional loci as ASD cohorts expand.

As said above, the effect size of individual polymorphisms in ASD is small based on GWAS: genetic linkage analysis has identified significant signals at specific loci, but common variants responsible for the linkage signals have not been identified. The search for rare deleterious variants that confer greater risk in ASD has thus been fueled by smaller-scale genetic models in families and the need to explain genetic heterogeneity. Strategies such as homozygosity mapping in families, identification of inherited variants on the X chromosome (often linked to fragile X mutations), and searching for rare knockout variants have yielded new leads in the search for inherited variation in ASD [7]. Similarly, many cases of autism appear to be caused by several abnormal genes acting in concert, indicating chromosomal aberration [6].

Rare *de novo* genetic variants, which arise from mutations in the parental germline or early somatic cells but are not present in either parent, are one genetic cause of ASD that is not accounted for in heritability estimates. *De novo* copy number variants (CNVs) and single-nucleotide variants (SNVs) have been found to play a role in ASD susceptibility. Recent advancements in sequencing technologies have enabled the study of *de novo* SNVs, revealing several new ASD susceptibility genes, such as *CHD8*, *DYRK1A*, *GRIN2B*, and *TBR1* [6].

ASD biomarkers are found in various pathways involved in growth regulation and protein synthesis. ASD has been connected to transcription factor families such as TCF; as well as related signaling pathways such as Wnt/β-catenin [6] (involved in embryonic development, tissue homeostasis, cell proliferation, gene expression, and cell fate decisions); mTOR [6] (involved in regulating protein degradation via the protein complex mTORC1, downstream from proteins coded by ASD risk genes); serotonin and oxytocin signaling; and neuron-glia signaling [6].

3. *Epigenetics and Environmental Factors of ASD*

Even in familial ASD cases that follow typical inheritance patterns, where a single gene mutation is responsible for the condition, the penetrance (i.e. the likelihood of expressing the disorder) is reported to be less than 50%. This suggests that environmental factors and epigenetic factors, which involve modifications to gene expression without altering the underlying DNA sequence, may play an important role in explaining some aspects of the etiology of ASD [8].

Epigenetic alterations refer to non-permanent changes in gene expression regulation that affect DNA shape and configuration, rather than the DNA sequence itself. These alterations can impact the transcription of specific genes by modifying the accessibility of chromatin threads, which carry genetic information. These alterations are seen in the form of DNA methylation, histone modifications, acetylation, phosphorylation, and noncoding RNA-related factors. DNA methylation, a mode of gene repression that involves the addition of methyl groups to DNA, is particularly prevalent in ASD [38]. For instance, DNA methylation of the brain-derived neurotrophic factor (*BDNF*) gene has been linked to autism and other neurological diseases [8].

Dysregulation of growth factors has been found in a number of adults with ASD. These growth factors are involved in neuronal growth, differentiation, proliferation, and survival in the course of neurodevelopment and can also modulate axonal and dendritic outgrowth [38].

Severe maternal viral infection in the first trimester of pregnancy and bacterial infection in the second trimester is also highly associated with a diagnosis of ASD. Maternal use of valproic acid during pregnancy could also affect the production of GABAergic neurons via the blocking of histone deacetylase. Gamma-aminobutyric acid (GABA) is an amino acid that functions as the primary inhibitory neurotransmitter for the CNS. It functions to reduce neuronal excitability by inhibiting nerve transmission. GABA is thought to play a major role in controlling nerve cell hyperactivity associated with anxiety, stress, and fear, and thus its dysregulation is associated with the symptoms of ASD [43].

Research on oxidative stress (imbalance between the production of reactive oxygen species (ROS) and the body's ability to neutralize them) in ASD has also revealed a potential role in the condition's neurobiology [9].

While ASD is mostly caused by the interaction between genes *and* the environment, many environmental factors alone play a role in its etiology. Various prenatal factors have been associated with an increased risk of ASD. As stated above, these include maternal exposure to certain medications (e.g., valproic acid and thalidomide) [10], maternal use of tobacco or alcohol during pregnancy, maternal infection (e.g., rubella, cytomegalovirus), and certain maternal health conditions (e.g., diabetes, obesity). Other examples include phenylketonuria, hypoxia during birth, and exposure to air pollution, pesticides, and heavy metals [11].

B. *Background on Neural Organoids*

Neural organoids, also called brain or cerebral organoids, are 3D models that mimic the structure and functionality of the human brain. They are derived from induced pluripotent stem cells (iPSCs) and can self-organize and differentiate into various cell types, superficially modeling the cellular diversity and complexity found in the real organ. Therefore, neural organoids provide a valuable tool for studying human development, disease modeling, drug screening, and personalized medicine.

1. *History*

Due to the complexity and inaccessibility of human brains, postmortem and surgical samples were often used in neural research. However, these methods were

typically inconsistent due to variability in genetic and environmental background and issues with tissue processing and preservation. Hence, animal model organisms, such as mice, have been extensively utilized to investigate brain development and function. However, there are notable differences in the developmental processes and structures of the human brain and that of mice (e.g. longer cell cycle times of neural progenitors and greater complexity of progenitor types in humans) [12].

The discovery of human pluripotent stem cells (hPSCs), which have the ability to differentiate into any cell type in the body, has provided exceptional prospects for investigating the intricacies of human brain development and understanding the underlying mechanisms of human disorders. The first extracted type of hPSC, embryonic stem cells (ESCs), discovered in 1998 [13], raise ethical concerns because their derivation requires the destruction of a human embryo. However, the 2007 discovery of iPSCs opened new doors into disease modeling and regenerative medicine [14]. iPSCs are generated from adult cells through reprogramming into an undifferentiated embryonic state.

Presently, there are *in vitro* protocols that allow for the differentiation of hPSCs into diverse human neural cell types, utilizing a 2D monolayer culture system, which offers several benefits, including uniform accessibility to growth/differentiation factors, feasibility, and scalability [39]. However, the 2D culture also presents various limitations, due to its lack of proper representation of very complex growth processes (cell-to-cell or cell-to-extracellular matrix interactions, spatial gradient of growth factors, cell polarity). Therefore, the necessity for a model that better represents the human brain development became even more dire.

The first neural organoid was created by Lancaster and Knoblich (2013) [15]. Their findings demonstrated the successful generation of 3D brain-like structures in the laboratory using iPSCs. These brain organoids exhibited the ability to self-organize and differentiate into various cell types found in the human brain, mimicking the early stages of brain development. The study provided valuable insights into the complex processes of human brain development and offered a novel experimental model for studying neurological disorders and diseases in a more accurate and ethical manner.

2. *Neural Organoid Protocols*

Generally, intrinsic organoid protocols artificially mimic the intrinsic patterning that guides cells into differentiation during embryonic development [16]. In intrinsic organoid protocols, specific conditions and factors are provided to the organoids that enable them to generate diverse brain regions. Exact protocols to achieve this self-organization may vary among research groups, and ongoing advancements in the field continually refine and improve the methods used to generate brain organoids. However, the creation of an organoid can be very broadly condensed into the following four steps:

1) Obtain hPSCs: hPSCs (iPSC or ESC) have the potential to differentiate into various cell types.

2) *Formation of embryoid bodies:* The pluripotent stem cells are aggregated in suspension and cultured to form 3D structures called embryoid bodies to initiate the differentiation process.

3) *Neural induction:* The embryoid bodies are exposed to specific signaling molecules or growth factors that promote the differentiation of stem cells into neural progenitor cells (NPCs), precursors of neurons and glial cells.

4) *Culture and maturation:* The NPCs are then cultured in conditions that support their growth and maturation, allowing them to organize and develop into more complex structures resembling brain tissue.

Oftentimes, scientists apply directed differentiation methods to guide the formation of specific brain regions within the organoids. By exposing the NPCs to precise combinations of signaling molecules (Steps 3 and 4 above), researchers can coax them to develop into ultra-specific brain cell types found in particular regions of the brain. Key signals used in neural induction include BMP inhibition, Wnt inhibition, Activin/Nodal and FGFs, SHH inhibition, Dual-SMAD inhibition, Notch signaling, and small molecule compounds. These signals are discussed further in Section II.

Besides the signaling molecules of neural induction, Matrigel or other extracellular matrix-like scaffolds can be used to support the self-organization and structural development of neural organoids. Co-culture with specific cell types is also seen: by introducing other cell types found in the brain, such as glial cells or neurons with specific genetic mutations associated with neurodevelopmental disorders like ASD, scientists can enhance the complexity and relevance of brain organoid models [17]. Finally, in some protocols, organoids are transferred to an air-liquid interface culture, where the upper portion is exposed to air, encouraging the development of neuronal connections and cellular maturation [17].

3. *General Application to Neurological Diseases*

Neural organoids have so far been used to study diseases such as microcephaly, ASD, Alzheimer's, and cancer. By generating organoids from individuals with neurobehavioral disorders or using genome editing techniques to introduce disease-related genetic mutations, researchers can observe and analyze the behavioral characteristics of the organoids. These characteristics include assessing neuronal activity, synaptic connections, and cellular interactions within the organoids. Furthermore, neural organoids can be combined with other techniques like single-cell RNA sequencing (scRNA-seq) or functional imaging to gain deeper insights into the molecular and cellular changes associated with neurobehavioral disorders. By comparing organoids derived from individuals with neurobehavioral disorders to those without, researchers can identify differences in gene expression patterns, neuronal connectivity, and functional activity that may contribute to the disorder.

II. Neural Organoids to Approach ASD

A. Modeling ASD

To develop brain organoids to model ASD, it is crucial to consider the choice of signaling factors and their timing of activation during the generation process [18]. Certain signaling pathways influence the formation of different brain regions and cell types (Table 1).

Signaling Pathway	Influence in Organoid
Wnt pathway	Neural induction and early patterning of the anterior-posterior patterning. Direct differentiation of iPSCs into NPCs and different brain regions, such as forebrain (activation), or midbrain and hindbrain (repression)
Bone Morphogenetic Protein (BMP) pathway	Dorsal-ventral patterning of the developing brain. Specify the locational identity of NPCs in an organoid, contributing to their specificity
Fibroblast Growth Factor (FGF) pathway	NPC proliferation and early brain regulation. Balance between neuronal subtypes (e.g. excitatory and inhibitory neurons). Anterior-posterior patterning during development
Sonic Hedgehog (SHH) and Notch pathways	Medial-lateral patterning and cell fate decisions during neurodevelopment. Differentiation of NPCs into cell types – neurons, glial cells, and differentiated neurons like motor neurons.
Retinoic acid signaling	Differentiation of NPCs into cortical neurons. Formation of cerebral cortex

Table 1. Signaling pathways in formation of neural organoid.

By manipulating these signals in a stepwise fashion, researchers can guide the development of brain organoids and generate specific brain regions or cell types that are relevant to ASD. Doing so has revealed various cellular phenotypes [19] associated with ASD.

B. Identification of Risk Genes

Many studies have employed regional brain organoids to identify risk genes and potential biomarkers for ASD. These studies have led to reports of the identified gene-related transcriptional pathways, neuronal networks, and other associated phenotypes [20]. Note that various types of brain organoids were used in the following discussed studies, each of which correspond to the modeling of different regions of the brain (forebrain, cerebral, telencephalic, cortical, etc.).

In a recent study, hundreds of brain organoids were analyzed, generated from iPSCs of individuals with ASD or CRISPR-edited cell lines, which presented haploinsufficiency of ASD risk genes including *SUV420H1* (also known as *KMT5B*), *ARID1B*, and *CHD8* [21]. *KMT5B* codes for a Histone-lysine N-methyltransferase involved in histone methylation and plays a role in DNA damage repair and gene silencing. *ARID1B* encodes a subunit of the BRG1/BRM-associated factor (BAF) chromatin complex and is essential for brain development and function. *CHD8* encodes the chromodomain-helicase-DNA-binding protein 8, which functions as a transcriptional regulator. *CHD8* is also involved in chromatin remodeling and is frequently associated with ASD due to mutations in this gene in patients with ASD.

CHD8 is one of the most strongly associated genes with ASD. A study focused on cerebral organoids generated from *CHD8* mutant and control hESCs to understand its impact on neurodevelopment related to ASD [22]. They observed changes in gene expression related to Wnt/β-catenin signaling and varying alterations in GABAergic neurons, indicating an imbalance between excitatory and inhibitory neurons. Another finding showed that *CHD8* haploinsufficiency in cerebral organoids disrupted the development of inhibitory and excitatory neurons, resembling the condition seen in patients with macrocephaly [23]. *CHD8* was also found to regulate the expression of ASD-related genes *TCF4* and *AUTS2* [22].

CNTNAP2 is another ASD-associated gene involved in neural processes. Studying forebrain organoids from ASD patients with a *CNTNAP2* mutation revealed increased expression in early-born excitatory neurons and larger organoid volume due to enhanced cell proliferation [24]. Mouse cortical organoids from *CNTNAP2* knockout mice also showed GABAergic neuron defects, possibly caused by downregulated expression of specific transcription factors in the ventricular zone.

Another major study used cerebral organoids from CRISPR-edited iPSCs (edited with ASD-associated 16p11.2 deletions and 15q11–13 duplications) [25]. RNA-seq was then performed on the samples and scRNA-seq data was integrated. The study found that *YPEL3*, *KCTD13*, and *INO80E* genes can be associated as driver genes linked with ASD. Other studies have also found that the neuronal hemizygous deletion of the ASD-related gene *SHANK3* exhibits intrinsic excitatory synaptic deficits [26]. *RAB39b* mutations are also known to result in over-proliferation and differentiation deficits of NPCs in cerebral organoid studies [27].

Organoids have been utilized to study mutations in the *MECP2* gene [28], which is essential for brain epigenetic regulation and gene expression. In addition to the loss of function mutations in *MECP2* that cause Rett Syndrome (RTT), a motor neurodegenerative disorder, duplication of *MECP2* causes a distinct disorder, indicating that the nervous system is very sensitive to *MECP2*, and any disruption in the function of the protein product, MeCP2, can lead to neurological and psychiatric problems. The many clinical features found in RTT and the various clinical problems that arise from disrupting MeCP2 function has led the concept that RTT is a “prototypical” neurological disorder to provide understanding and insight into a vast array of genetically defined and undefined clinical conditions such as idiopathic ASD. While RTT is primarily caused by *MECP2* loss-of-function mutations, the role of *MECP2* in ASD is more complex, with both loss-of-function and gain-of-function mutations reported [42]. The effects of *MECP2* dysfunction on brain development and neural circuits may contribute to the development of ASD.

Altogether, the studies reveal an imbalance between

excitatory and inhibitory pathways in ASD. Common pathways most often see molecular convergence with overexpression of transcription factor families and upregulated GABAergic neuron production.

C. Identification of Environmental/Epigenetic Effects

Considering the complexity of ASD, environmental factors are also known to play a role in its occurrence.

In one study [29], human forebrain organoids (hFOs) were used to investigate the relationship between valproic acid (VPA) [30], an anti-epileptic medication, and ASD risk. iPSCs from healthy individuals were used to create hFOs, which were exposed to a clinically relevant concentration of VPA for three days. Through various analyses, such as proteomics, genomics, electrophysiology, and scRNA-seq, the study identified specific genes (*AMK4*, *CLCN4*, *DPP10*, *GABRB3*, *KCNB1*, *PRKCB*, *SCN1A*, and *SLC24A2*) affected by VPA exposure. These genes overlapped significantly with pathways known to be dysregulated in the organoids of individuals with ASD. Furthermore, VPA exposure disrupted synaptic transmission in the hFOs.

Another study applied brain organoids carrying a heterozygote CRISPR-edited mutation in *CHD8* [31]. The organoids were then exposed to chlorpyrifos (CPF), a neurotoxic organophosphate pesticide, or its metabolite, chlorpyrifos oxon (CPO). The compounds caused detrimental effects on neurite outgrowth, increased oxidative stress, and disrupted neurotransmission after 24 hours of exposure. Overall, the study highlighted the adverse impacts of toxic agents on autistic patients with this gene mutation.

III. Limitations and Concerns

A. Identification of Risk Genes

While more effective than 2D cultures, neural organoids lack the full complexity and cellular diversity found in the actual brain. The intricate interactions between different cell types and regions in the brain are not fully replicated in organoids, which may limit their ability to fully capture the complexity of ASD [32]. One of the primary challenges is to induce the differentiation of specific non-neural cell types within the organoid without introducing additional heterogeneity.

To address this issue, scientists have been exploring various protocols and techniques to coax the organoid's neural stem cells to differentiate into different non-neural cell types intrinsically [40]. By manipulating the signaling pathways and environmental conditions, they hope to induce the generation of diverse cell populations within the organoid. An alternative approach is to artificially combine separately cultured cell types. This method involves separately differentiating various cell types outside the organoid and then assembling them together to create a more heterogeneous organoid. However, while this might be more feasible in the short term, it may not fully recapitulate the natural interactions and complexities of the developing brain [40].

Organoids also do not fully recapitulate the developmental maturity of a real brain. They are more representative of the early stages of human brain development, which may limit their relevance when studying the pathogenesis of ASD that typically manifests later in childhood. The human brain also interacts with a complex and dynamic environment, including the bloodstream, immune system, and other physiological factors. Organoids lack these external factors, which may influence the development and progression of ASD. And while organoids can be genetically engineered to carry specific mutations associated with ASD, the genetic complexity of ASD is vast and involves a combination of multiple genetic and environmental factors. Reproducing this complexity of circuit integration and plasticity accurately in organoids is challenging.

Due to organoids' poor maturity, several studies have delved into synapse formation and calcium signaling in neural organoids. Researchers have explored the presence and dynamics of synapses within organoids, aiming to understand how they form, stabilize, and mature over time. Additionally, calcium ion (Ca++) levels are indicative of neuronal activity and can influence processes like synaptic plasticity. Organoids so far have provided a platform to observe the initial stages of synapse formation and Ca++ signaling, but their simplified structure and lack of long-range connectivity could limit their ability to fully capture the complexity of these processes as they occur in the developing human brain [41].

B. Moral and Ethical Concerns

Obtaining informed consent from human cell donors is crucial, particularly when studying cells from children with ASD or their family members. Neural organoids offer an alternative to animal models [33], but the ethical implications of this choice require careful consideration [34]. Researchers must guard against potential misuse or unintended consequences, such as inappropriate enhancements or invasive experiments. Ethical considerations in ASD research extend beyond the laboratory, with implications for society's perception of the condition, stigmatization, and applications of research findings.

Transparent and inclusive discussions involving researchers, ethicists, individuals with ASD, and their families are essential to establish responsible guidelines and ethical frameworks for using brain organoids in ASD research. Balancing the potential benefits of organoids with upholding ethical standards and protecting the well-being and dignity of those affected by ASD is paramount.

Despite any physical limitations and moral concerns, neural organoids remain a promising tool for ASD research, allowing scientists to explore certain aspects of early brain development, study the effects of specific genetic mutations, and screen potential therapeutic interventions. However, they should be used in conjunction with other complementary approaches to gain a more comprehensive understanding of ASD.

IV. Conclusion and Perspective

Through the study of neural organoids, significant strides have been made in identifying ASD risk genes and

understanding the impact of environmental factors on neural development. The findings have shed light on key signaling pathways involved in the balance between excitatory and inhibitory signaling, providing valuable insights into potential therapeutic targets for ASD treatment. Furthermore, the application of personalized drug testing using patient-specific iPSC-derived organoids shows promise in tailoring unique treatments to individuals with ASD.

Looking to the future, neural organoids can be combined with other models, such as animal studies and patient-derived cell lines, to bridge the gap between cellular-level findings and whole-organism behavior. Animal models, while not perfect representations of human neurodevelopment, still offer valuable insights into the in vivo effects of genetic and environmental manipulations. By conducting parallel studies using both organoids and animal models, researchers can compare and validate their findings, thereby enhancing the translatability of research outcomes to humans.

Furthermore, patient-derived cell lines, obtained from individuals with ASD, can be incorporated into organoid research to investigate combined effects of specific genetic mutations and environmental factors on neural development. This personalized approach allows for a better understanding of the unique genetic underpinnings of each individual's ASD and can help identify potential personalized treatment strategies.

Moreover, brain imaging techniques, such as functional magnetic resonance imaging (fMRI) and positron emission tomography (PET), can also be employed to study brain activity in individuals with ASD and correlate these findings with the cellular-level changes observed in organoids [35]. Integrating these non-invasive imaging modalities with organoid research can provide a more holistic understanding of how alterations at the cellular level manifest as behavioral and functional changes at the macroscopic level.

Efforts to enhance the complexity and maturity of brain organoids are ongoing, through two main methods: vasculature and immune components, which can better replicate the dynamic interactions between neural cells and the surrounding microenvironment. The vascularization of organoids would introduce blood flow, nutrient delivery, and waste removal, more accurately mimicking in vivo conditions–essential for maintaining cell viability and supporting complex cellular interactions. Immune components within organoids can enable the study of neuroinflammation [36], which is implicated in various neurological disorders, including ASD.

Neural organoids have revolutionized the study of ASD, providing a more relevant and sophisticated model for exploring its complex pathogenesis. As this technology continues to advance, its integration with other models, validation of drug targets, and personalized medicine applications hold the potential for groundbreaking discoveries and transformative treatments for individuals and families affected by ASD. By addressing ethical concerns through establishment of global stipulations and refining organoid models, neural organoids are poised to play a central role in shaping the future of ASD research and improving the lives of those living with this challenging neurodevelopmental disorder.

V. Acknowledgements

I would like to express my thanks and gratitude to my mentor, Dr. Ryan Prestil from the University of Cambridge. Also, to Lumiere Education for their guidance and support in the development of this paper.

VI. References

[1] Rylaarsdam, L., & Gamboa, A. (2019, August 6). Genetic Causes and Modifiers of Autism Spectrum Disorder. *Frontiers*. Retrieved August 9, 2023, from frontiersin.org/articles/10.3389/Fncel.2019.00385/full

[2] Tsai, C.-H., Chen, K.-L., Li, H.-J., Chen, K.-H., Hsu, C.-W., Lu, C.-H., Hsieh, K.-Y., & Huang, C.-Y. (2020). The symptoms of autism including social communication deficits and repetitive and restricted behaviors are associated with different emotional and behavioral problems. *Nature News*. https://www.nature.com/articles/s41598-020-76292-y

[3] Kanner, L. (1943). Autistic Disturbances of Affective Contact. *Nervous Child*.

[4] Zeldovich, L. (2018, May 29). The evolution of "autism" as a diagnosis, explained. *Spectrum | Autism Research News*. https://www.spectrumnews.org/news/evolution-autism-diagnosis-explained/

[5] Hodges, H., Fealko, C., & Soares, N. (2020). Autism spectrum disorder: Definition, epidemiology, causes, and clinical evaluation. *Translational Pediatrics*, *9*(1), S55–S65. https://doi.org/10.21037/tp.2019.09.09

[6] Chen, J. A., Peñagarikano, O., Belgard, T. G., Swarup, V., & Geschwind, D.
H. (2015). The Emerging Picture of Autism Spectrum Disorder: Genetics and Pathology. *Annual Review of Pathology: Mechanisms of Disease*, *10*(1), 111–144. https://doi.org/10.1146/annurev-pathol-012414-040405

[7] Reddy, K. S. (2005). Cytogenetic abnormalities and fragile-x syndrome in Autism Spectrum Disorder. *BMC Medical Genetics*, *6*(1). https://doi.org/10.1186/1471-2350-6-3

[8] Forsberg, S. L., Ilieva, M., & Maria Michel, T. (2018). Epigenetics and cerebral organoids: promising directions in autism spectrum disorders. *Translational Psychiatry*, *8*(1), 1–11. https://doi.org/10.1038/s41398-017-0062-x

[9] Michel, T. M., Pulschen, D., & Thome, J. (n.d.). The Role of Oxidative Stress in Depressive Disorders. *Current Pharmaceutical Design*, *18*(36), 5890–5899. Retrieved August 21, 2023, from http://www.eurekaselect.com/article/46512

[10] Christensen, J., Grønborg, T. K., Sørensen, M. J., Schendel, D., Parner, E. T., Pedersen, L. H., & Vestergaard, M. (2013). Prenatal Valproate Exposure and Risk of Autism Spectrum Disorders and Childhood Autism. *JAMA*, *309*(16), 1696–1703. https://doi.org/10.1001/jama.2013.2270

[11] London, E. A. (2000). The environment as an etiologic factor in autism: a new direction for research. *Environmental Health Perspectives*, *108*(suppl 3), 401–404. https://doi.org/10.1289/ehp.00108s3401

[12] Koo, B., Choi, B., Park, H., & Yoon, K.-J. (2019). Past, Present, and Future of Brain Organoid Technology. *Molecules and Cells*, *42*(9), 617–627. https://doi.org/10.14348/molcells.2019.0162

[13] Thomson, J. A. (1998). Embryonic Stem Cell Lines Derived from Human Blastocysts. *Science*, *282*(5391), 1145–1147. https://doi.org/10.1126/science.282.5391.1145

[14] Takahashi, K., Tanabe, K., Ohnuki, M., Narita, M., Ichisaka, T., Tomoda, K., & Yamanaka, S. (2007). Induction of Pluripotent Stem Cells from Adult Human Fibroblasts by Defined Factors. *Cell*, *131*(5), 861–872.

[15] Lancaster, M. A., & Knoblich, J. A. (2014). Organogenesis in a dish: Modeling development and disease using organoid technologies. *Science*, *345*(6194), 1247125–1247125.

https://doi.org/10.1126/science.1247125

[16] Di Lullo, E., & Kriegstein, A. R. (2017). The use of brain organoids to investigate neural development and disease. *Nature Reviews Neuroscience*, *18*(10), 573–584. https://doi.org/10.1038/nrn.2017.107

[17] Mayhew, C. N., & Singhania, R. (2023). A review of protocols for brain organoids and applications for disease modeling. *STAR Protocols*, *4*(1), 101860. https://doi.org/10.1016/j.xpro.2022.101860

[18] Chan, W. K., Griffiths, R., Price, D. J., & Mason, J. O. (2020). Cerebral organoids as tools to identify the developmental roots of autism. *Molecular Autism*, *11*(1). https://doi.org/10.1186/s13229-020-00360-3

[19] Mariani, J., Coppola, G., Zhang, P., Abyzov, A., Provini, L., Tomasini, L., Amenduni, M., Szekely, A., Palejev, D., Wilson, M., Gerstein, M., Grigorenko, E. L., Chawarska, K., Pelphrey, K. A., Howe, J. R., & Vaccarino, F. M. (2015). FOXG1-Dependent Dysregulation of GABA/Glutamate Neuron Differentiation in Autism Spectrum Disorders. *Cell*, *162*(2), 375–390. https://doi.org/10.1016/j.cell.2015.06.034

[20] Lenon, J., Cecília Araújo, Araújo, C., Zaquer Suzana Munhoz Costa-Ferro, & Bruno. (2023). Modeling Autism Spectrum Disorders with Induced Pluripotent Stem Cell-Derived Brain Organoids. *Biomolecules*, *13*(2), 260–260. https://doi.org/10.3390/biom13020260

[21] Paulsen, B., Velasco, S., Kedaigle, A. J., Pigoni, M., Quadrato, G., Deo, A. J., Adiconis, X., Uzquiano, A., Sartore, R., Yang, S. M., Simmons, S. K., Symvoulidis, P., Kim, K., Tsafou, K., Podury, A., Abbate, C., Tucewicz, A., Smith, S. N., Albanese, A., & Barrett, L. (2022). Autism genes converge on asynchronous development of shared neuron classes. *Nature*, 1–6. https://doi.org/10.1038/s41586-021-04358-6

[22] Wang, P., Mokhtari, R., Pedrosa, E., Kirschenbaum, M., Bayrak, C., Zheng, D., & Lachman, H. M. (2017). CRISPR/Cas9-mediated heterozygous knockout of the autism gene CHD8 and characterization of its transcriptional networks in cerebral organoids derived from iPS cells. *Molecular Autism*, *8*(1). https://doi.org/10.1186/s13229-017-0124-1

[23] Villa, C. E., Cheroni, C., Dotter, C. P., López-Tóbon, A., Oliveira, B., Sacco, R., Yahya, A. Ç., Morandell, J., Gabriele, M., Tavakoli, M. R., Lyudchik, J., Sommer, C., Gabitto, M., Danzl, J. G., Testa, G., & Novarino, G. (2022). CHD8 haploinsufficiency links autism to transient alterations in excitatory and inhibitory trajectories. *Cell Reports*, *39*(1), 110615. https://doi.org/10.1016/j.celrep.2022.110615

[24] Tong, D., Chen, R., Lu, Y., Li, W., Zhang, Y., Lin, J., He, L., Dang, T., Shan, S., Xu, X.-H., Zhang, Y., Zhang, C., Du, Y.-S., Zhou, W.-H., Wang, X., & Qiu, Z. (2019). The critical role of ASD-related gene CNTNAP3 in regulating synaptic development and social behavior in mice. *Neurobiology of Disease*, *130*, 104486. https://doi.org/10.1016/j.nbd.2019.104486

[25] Lim, E. T., Chan, Y., Dawes, P., Guo, X., Erdin, S., Tai, D. J. C., Liu, S., Reichert, J. M., Burns, M. J., Chan, Y. K., Chiang, J. J., Meyer, K., Zhang, X., Walsh, C. A., Yankner, B. A., Raychaudhuri, S., Hirschhorn, J. N., Gusella, J. F., Talkowski, M. E., & Church, G. M. (2022). Orgo-Seq integrates single-cell and bulk transcriptomic data to identify cell type specific-driver genes associated with autism spectrum disorder. *Nature Communications*, *13*(1), 3243. https://doi.org/10.1038/s41467-022-30968-3

[26] Wang, Y., Chiola, S., Yang, G., Russell, C., Armstrong, C. J., Wu, Y., Spampanato, J., Tarboton, P., Ullah, H. M. A., Edgar, N. U., Chang, A. N., Harmin, D. A., Bocchi, V. D., Vezzoli, E., Besusso, D., Cui, J., Cattaneo, E., Kubanek, J., & Shcheglovitov, A. (2022). Modeling human telencephalic development and autism-associated SHANK3 deficiency using organoids generated from single neural rosettes. *Nature Communications*, *13*(1), 5688. https://doi.org/10.1038/s41467-022-33364-z

[27] Zhang, W., Ma, L., Yang, M., Shao, Q., Xu, J., Lu, Z., Zhao, Z., Chen, R., Chai, Y., & Chen, J.-F. (2020). Cerebral organoid and mouse models reveal a RAB39b–PI3K–mTOR pathway-dependent dysregulation of cortical development leading to macrocephaly/autism phenotypes. *Genes & Development*, *34*(7-8), 580–597. https://doi.org/10.1101/gad.332494.119

[28] Amir, R. E., Van den Veyver, I. B., Wan, M., Tran, C. Q., Francke, U., & Zoghbi, H. Y. (1999). Rett syndrome is caused by mutations in X-linked MECP2, encoding methyl-CpG-binding protein 2. *Nature Genetics*, *23*(2), 185–188. https://doi.org/10.1038/13810

[29] Meng, Q., Zhang, W., Wang, X., Jiao, C., Xu, S., Liu, C., Tang, B., & Chen, A (2022). Human forebrain organoids reveal connections between valproic acid exposure and autism risk. *Translational Psychiatry*, *12*(1). https://doi.org/10.1038/s41398-022-01898-x

[30] Wood, A. G., Nadebaum, C., Anderson, V., Reutens, D., Barton, S., O'Brien, T. J., & Vajda, F. (2015). Prospective assessment of autism traits in children exposed to antiepileptic drugs during pregnancy. *Epilepsia*, *56*(7), 1047–1055. https://doi.org/10.1111/epi.13007

[31] Modafferi, S., Zhong, X., Kleensang, A., Murata, Y., Fagiani, F., Pamies, D., Hogberg, H. T., Calabrese, V., Lachman, H., Hartung, T., & Smirnova, L. (2021). Gene–Environment Interactions in Developmental Neurotoxicity: a Case Study of Synergy between Chlorpyrifos and CHD8 Knockout in Human BrainSpheres. *Environmental Health Perspectives*, *129*(7), 077001. https://doi.org/10.1289/ehp8580

[32] Qian, X., Song, H., & Ming, G. (2019). Brain organoids: advances, applications and challenges. *Development*, *146*(8), dev166074. https://doi.org/10.1242/dev.166074

[33] Koplin, J. J., & Savulescu, J. (2019). Moral Limits of Brain Organoid Research. *The Journal of Law, Medicine & Ethics*, *47*(4), 760–767. https://doi.org/10.1177/1073110519897789

[34] Hyun, I., Scharf-Deering, J. C., & Lunshof, J. E. (2020). Ethical issues related to brain organoid research. *Brain Research*, *1732*, 146653. https://doi.org/10.1016/j.brainres.2020.146653

[35] Di Martino, A., Ross, K., Uddin, L. Q., Sklar, A. B., Castellanos, F. X., & Milham, M. P. (2009). Functional Brain Correlates of Social and Nonsocial Processes in Autism Spectrum Disorders: An Activation Likelihood Estimation Meta-Analysis. *Biological Psychiatry*, *65*(1), 63–74. https://doi.org/10.1016/j.biopsych.2008.09.022

[36] Rossignol, D. A., & Frye, R. E. (2011). A review of research trends in physiological abnormalities in autism spectrum disorders: immune dysregulation, inflammation, oxidative stress, mitochondrial dysfunction and environmental toxicant exposures. *Molecular Psychiatry*, *17*(4), 389–401. https://doi.org/10.1038/mp.2011.1

[37] Grove, J., Ripke, S., Als, T. D., Mattheisen, M., Walters, R. K., Won, H., Pallesen, J., Agerbo, E., Andreassen, O. A., Anney, R., Awashti, S., Belliveau, R., Bettella, F., Buxbaum, J. D., Bybjerg-Grauholm, J., Bækvad-Hansen, M., Cerrato, F., Chambert, K., Christensen, J. H., & Churchhouse, C. (2019). Identification of common genetic risk variants for autism spectrum disorder. *Nature Genetics*, 51(3), 431–444. https://doi.org/10.1038/s41588-019-0344-8

[38] Yoon, S. H., Choi, J., Lee, W. J., & Do, J. T. (2020). Genetic and Epigenetic Etiology Underlying Autism Spectrum Disorder. *Journal of Clinical Medicine*, 9(4), 966. https://doi.org/10.3390/jcm9040966

[39] Hong, Y. J., & Do, J. T. (2019). Neural Lineage Differentiation From Pluripotent Stem Cells to Mimic Human Brain Tissues. *Frontiers in Bioengineering and Biotechnology*, 7. https://doi.org/10.3389/fbioe.2019.00400

[40] Qian, X., Song, H., & Ming, G. (2019). Brain organoids: advances, applications and challenges. *Development*, 146(8), dev166074. https://doi.org/10.1242/dev.166074

[41] Revah, O., Gore, F., Kelley, K. W., Andersen, J., Sakai, N., Chen, X., Li, M.-Y., Birey, F., Yang, X., Saw, N. L., Baker, S. W., Amin, N. D., Kulkarni, S., Mudipalli, R., Cui, B., Nishino, S., Grant, G. A., Knowles, J. K., Shamloo, M., & Huguenard, J. R. (2022). Maturation and circuit integration of transplanted human cortical organoids. *Nature*, 610(7931), 319–326. https://doi.org/10.1038/s41586-022-05277-w

[42] Neul, J. L. (2012). The relationship of Rett syndrome and MECP2 disorders to autism. *Dialogues in Clinical Neuroscience*, 14(3), 253–262. https://www.ncbi.nlm.nih.gov/pmc/articles/PMC3513680/

[43] Allen, M. J., Sabir, S., & Sharma, S. (2022, February 17). *GABA receptor*. PubMed; StatPearls Publishing. https://www.ncbi.nlm.nih.gov/books/NBK526124/

Exploring the Genetic, Neurobiological, and Psychological Mechanisms Involved in the Connection Between Anxious Attachment and Problematic Internet Use

Clare Peng[1]

Abstract— **Internet addiction, a behavioral disorder characterized by excessive and pathological internet use, is a growing concern with profound implications for mental health in today's digital age. Anxious-ambivalent attachment, a subtype of insecure attachment rooted in adverse early life experiences, influences regulation of emotions and interpersonal relationships. Several studies have established a significant correlation between attachment anxiety and problematic internet use (PIU), as individuals exhibiting this attachment style are more prone to internet addiction tendencies. The potential mechanisms underlying the association between internet addiction and anxious-attachment style hold significant importance in the fields of psychology and addiction research. While the specific biological origins of this phenomenon are currently unknown, this review explores the intricate relationships between attachment styles, genetic factors such as monoamine neurotransmitters (dopamine and serotonin), the personality trait of neuroticism, and cortisol stress responses in the context of internet addiction. By establishing these connections, we will be able to better understand the factors contributing to PIU and develop targeted interventions and preventive strategies to combat this increasingly critical public health concern. In this review, we will address the gap in knowledge regarding possible mechanisms driving the association between internet addiction and anxious-ambivalent attachment style.**

I. Introduction

Internet addiction, also commonly referred to as problematic internet use (PIU), is the uncontrollable urge to access the internet. While not officially recognized as a mental disorder, PIU can lead to a decrease in appreciation for non-internet-based activities, jittery or hostile behavior when offline, and a disturbance in socialization [38]. Attachment theory is the effect of early life experiences on children's expectations of the responsiveness and trustworthiness of significant individuals [1]. These expectations play a crucial role in how people behave in relationships as well as their social and emotional development. The anxious-ambivalent attachment style is characterized by a heightened fear of rejection or abandonment [18].

Insecure attachment styles (such as avoidant or anxious-ambivalent) have a direct relationship with internet addiction disorder, problematic smartphone use, and a risk to develop gaming disorder [12, 13, 16]. Research has shown that a majority of individuals who exhibit trends of internet addiction have ambivalent attachments [12]. In one study, despite only a small percentage of subjects having anxious-ambivalent attachment, around 70% of the participants demonstrating internet addiction tendencies had attachment ambivalence [12]. Similarly, individuals with higher attachment anxiety and lower avoidant attachment are more likely to display depressive symptomatology caused by problematic use of social networking services [39]. In addition, these results seem to be consistent between both adolescents and adults, as avoidance towards the mother and anxiety towards the father have been directly linked to PIU, while other variations of insecure childhood attachments are also indirectly correlated with internet addiction [28]. However, while a significant correlation is present, it is still unknown how attachment styles physiologically contribute to the possible development of internet addiction. Therefore, in this review we will explore the potential biological mechanisms that drive the association between the anxious-ambivalent attachment style and problematic internet use.

II. Neurotransmitters And Hormones As Potential Mechanisms

Many studies have demonstrated a relationship between insecure attachment styles and various addictive disorders. In particular, anxious-ambivalent attachment has been associated with internet addiction. A recent study showed that while only 30% of all participants had attachment anxiety, 70% of subjects with PIU tendencies had an ambivalent attachment style [12]. The researchers found that people with an anxious-ambivalent attachment style were primarily motivated by anonymity and social support to access the internet, subsequently developing pathological use. These results suggest that these individuals' social compensation and escapism may serve as moderators for the association between problematic internet use and anxious-ambivalent attachment style [12].

Likewise, another study provided supportive evidence for a correlation between internet addiction and the anxious-ambivalent attachment style [32]. The research demonstrated that the 30 patients clinically diagnosed with internet addiction scored higher on attachment anxiety compared to the healthy controls. While taking into account influences from social or environmental factors, the association between anxious-ambivalent attachment style and internet addiction highlights the potential value of attachment anxiety in predicting the risk of developing internet addiction. These findings suggest that although anonymity and social support play a pivotal role in internet addiction tendencies for those with an anxious-ambivalent attachment style, external factors cannot solely account for such an elaborate phenomenon.

A. Dopamine and genetic correlations between attachment styles and internet addiction

Although anxious-ambivalent attachment style and internet addiction have not yet been physiologically linked,

[1] C.P. is with Watchung Hills Regional High School, Warren, NJ 07059 USA (e-mail: clarepeng100@gmail.com).

several studies suggest that monoamine transmitters such as dopamine may play a role [6, 10]. Dopamine pathways to certain parts of the brain, such as the striatum, influence numerous psychological and physiological functions, including motivational and reward-related behaviors [3]. Furthermore, dopamine is crucial in reward prediction error, or the distinction between anticipated rewards and actual ones [25].

The brain's reward pathways have been extensively correlated with the dopaminergic system, particularly the dopamine D2 receptor (D2R) [5]. Abnormal functioning of D2R can result in various addictive behaviors, including substance abuse and compulsive gambling [5]. The gene that codes for the dopamine D2 receptor (*DRD2*), specifically with the *TaqI A1* allele, has potential involvement in both attachment styles and internet addiction tendencies [14, 17]. For example, ambivalent attachment has been linked with the *DRD2*A1 TaqI* polymorphism, which is associated with a reduced density of dopamine D2 receptors [14]. Similarly, there is a correlation between reduced striatal levels of D2R and problematic internet use [22]. One study hypothesized that specific polymorphisms such as *DRD2*A1 TaqI* in the dopaminergic system may be associated with adult attachment insecurities [14]. These findings indicate that anxious-ambivalent attachment style is linked to multiple *A1 DRD2* alleles, where participants with two alleles scored higher on attachment anxiety than those with fewer [14].

These results suggest that, alongside social experiences, certain genetic polymorphisms in the neurotransmitter dopamine are plausible predictors for insecure attachment. In addition, as multiple studies have concluded that the *A1* allele of *DRD2* is correlated with reduced binding and lower levels of striatal dopamine D2 receptors, anxious-ambivalent attachment style is likely to also be linked with these effects [19, 30]. Moreover, decreased levels of D2R correspond with reduced maternal responsiveness, and inconsistent responses from maternal figures are also associated with insecure attachment styles [2, 8]. Collectively, these findings suggest that anxious attachment may be correlated with a reduction in striatal dopamine D2 receptors through the TaqI A1 polymorphism as well as having a mutual association with poor responsiveness from maternal sources.

Similarly, the *DRD2*A1 TaqI* allele has been implicated in excessive internet video game play, a subtype of internet addiction [17]. The study found that the participants with internet addiction had a higher occurrence of the *DRD2*A1* allele compared to controls. This suggests that genetic polymorphisms in dopamine, particularly the *DRD2*A1 TaqI* allele, are associated with reward dependence and contribute to internet addiction [17]. Likewise, another study investigating possible neurobiological mechanisms underlying internet addiction demonstrated that individuals with PIU exhibited reduced levels of D2R in the striatum, particularly the bilateral dorsal caudate and right putamen [22]. These findings demonstrated that internet addiction may have physiological similarities to other addictive disorders involving substance abuse [22]. Consequently, these studies hint at possible workings of the association between anxious-ambivalent attachment style and problematic internet use by highlighting the significance of the dopamine D2 receptor gene in provoking addictive behaviors. Taken together, the association between two *A1* alleles of *DRD2*, reduced availability of striatal dopamine D2 receptors, and anxious-ambivalent attachment style may serve as a predictor for the development of internet addiction disorder. Therefore, further research is needed to investigate the potential overlap between anxious attachment, reduced striatal dopamine D2 receptors due to the *DRD2*A1 TaqI* polymorphism, and internet addiction.

B. The serotonin 5-HTTLPR polymorphism and implications with neuroticism, attachment anxiety, and problematic internet use

The monoamine transmitter serotonin, particularly its transporter (5-HT), may be associated with the correlation between anxious-ambivalent attachment style and internet addiction. Serotonin modulates various behavioral and neurological processes including mood, perception, reward, aggression, memory, and attention [4]. Beyond its extensive involvement in neurobiology, 5-HT is also involved in numerous disorders in the central nervous system such as depression, anxiety, schizophrenia, obsessive-compulsive disorder, addiction, and Parkinson's disease [9]. A specific polymorphism in the promoter region of the serotonin transporter gene (*5-HTTLPR*) has potential implications for attachment anxiety [35]. For example, attachment insecurities have been significantly associated with the short allele variant of *5-HTTLPR*, which is likely due to its genotype influencing components that trigger attachment behaviors, such as emotional responsiveness or reactivity to threatening stimuli [35].

Consequently, the researchers in one study hypothesized that polymorphisms in the serotonin transporter impact sensitivity to parental behaviors or cause biases when taking in information, leading to negative interpretations of childhood experiences [35]. These conclusions suggest that the short allele of the *5-HTTLPR* polymorphism may be implicated in brain development and the effect of adverse childhood experiences on attachment style, which could potentially explain why individuals with anxious-ambivalent attachment style seem to be susceptible to internet addiction [32]. Moreover, *5-HTTLPR* is also correlated with problematic internet use, particularly the variant with homozygous short alleles [24, 34]. One study showed that the participants with homozygous short alleles in *5-HTTLPR* demonstrated significantly higher scores of internet addiction compared to those with long alleles [34]. The researchers suggested that the association between *5-HTTLPR* short alleles and a decreased risk of inattentiveness contributes to Internet overuse, the collective phenomenon of internet addiction [34].

Likewise, another study substantiated these results by demonstrating that individuals with PIU exhibited a higher frequency of the *5-HTTLPR* homozygous short allelic variant compared to healthy controls [24]. Collectively, this evidence suggests that anxious-ambivalent attachment style

and PIU may be linked by changes in *5-HTTLPR*. Consequently, these studies provide a plausible mechanism for the correlation between anxious-ambivalent attachment style and problematic internet use, emphasizing the role of the short allele of the *5-HTTLPR* in provoking risk for internet addiction. The convergence of these results reveals a potentially compelling channel for linking anxious-ambivalent attachment style to the development of problematic internet use. Further research is needed to investigate the physiological overlap between anxious-ambivalent attachment, *5-HTTLPR* influencing brain development, and its association with high attentiveness playing a role in developing internet addiction.

In addition, the *5-HTTLPR* polymorphism and attachment anxiety have both been linked to issues with coping, a heightened sensitivity to criticism, and neuroticism, the tendency to experience negative emotions [27]. Compared to individuals with other allelic variants, subjects with homozygous short-alleles of *5-HTTLPR* had significantly elevated neuroticism scores [23]. Furthermore, several other studies have supported the correlation of *5-HTTLPR*, specifically with the short allele, to the presence of neurotic symptoms [15, 33]. Comparably, anxious-ambivalent attachment style has a significant and well-documented relationship with neuroticism [14, 29].

Both attachment anxiety and neurotic personality are conceptually similar and are characterized by facets of insecurity, depression, vulnerability, and anxiety [29]. Similarly, one study found a correlation between neuroticism and the likeliness of developing internet addiction, which was mediated by anxious feelings toward online interactions [7]. According to the researchers, people with neuroticism used the internet to develop a sense of social belonging in order to increase self-esteem [7]. Correspondingly, heightened fear of rejection or abandonment is a characteristic of attachment anxiety [18]. Therefore, as the association between internet addiction and neurotic personality is mediated by anxious feelings, it could be possible that the heightened fear of abandonment from attachment anxiety could drive individuals to become more dependent on the internet, causing pathological internet use.

These studies all suggest a correlation between attachment anxiety, the short allele of *5-HTTLPR*, and problematic internet use in regard to a correlative association with neuroticism. In addition, the influence of serotonin on cognitive and emotional processes and its possible involvement in psychiatric disorders highlights the complex interactions of *5-HTTLPR*, anxious-ambivalent attachment style, and internet addiction, thus underlining the need for a deeper understanding of the factors contributing to problematic internet use. Further research is needed to pinpoint how *5-HTTLPR* can impact brain development and how neuroticism may provide an explanation for the relationship between anxious-ambivalent attachment style and problematic internet use.

C. Blunted cortisol responses to stress as a neurobiological correlation between anxious attachment and internet addiction

Similarly to serotonin and dopamine, the steroid hormone cortisol, particularly its involvement in stress response, has a demonstrated involvement in the correlation between anxious-ambivalent attachment and internet addiction. When stress is experienced, cortisol is released from the adrenal glands to regulate the magnitude and duration of inflammatory responses [31]. The hypothalamus controls the secretion of cortisol, which is acutely sensitive during times of stress [31]. Several types of addiction, such as substance and alcohol abuse, have been linked with dysregulated cortisol stress responses [26]. In fact, one study demonstrated that, compared to healthy controls, subjects with internet addiction had blunted cortisol responses to psychosocial stressors [36]. Another study had similar results, where patients with internet addiction exhibited attenuated cortisol response to acute stress (as opposed to the healthy participants) [21]. When integrated, these studies indicate a strong correlation between internet addiction and dysregulated cortisol levels in response to stress. The association between dysregulated cortisol responses and addiction processes is significant in understanding how the risk for internet addiction may develop.

In addition, the interactions between anxious-ambivalent attachment and adverse childhood experiences have been found to be moderated by blunted cortisol reactivity in response to a stressor [11]. This suggests attachment anxiety may share similar stress responses to those with internet addiction; both anxious attachment and PIU are associated with lower cortisol levels in response to an acute stressor. Additional studies are required to delve deeper into the precise nature of this elaborate relationship and the broader implications it may hold for understanding the ties between internet addiction, anxious-ambivalent attachment, and cortisol.

III. DISCUSSION

The present review explored the potential mechanisms underlying the association between anxious-ambivalent attachment style and problematic internet use, highlighting the various complexities of behavioral addiction. For example, the research indicated that individuals with anxious-ambivalent attachment are more likely to develop internet addiction tendencies, driven motivationally by anonymity and social support [12]. The presence of two *A1* alleles in *DRD2* and the short allele of *5-HTTLPR* were correlated with both attachment anxiety and problematic internet use [24, 34]. Both anxious-ambivalent attachment and internet addiction were also linked to elevated levels of neuroticism, hinting at a shared psychological predisposition [7, 14, 29]. Furthermore, dysregulated cortisol stress responses were implicated in the correlation between anxious-ambivalent attachment and internet addiction due to blunted cortisol reactivity being mutually associated [11, 21, 36]. Collectively, these workings demonstrate the multifaceted interactions between genetic, neurobiological,

and psychological factors in the link between anxious attachment and problematic internet use. Further research is crucial to comprehend the intricate nature of this relationship and its implications for addiction development.

However, there are several limitations to this review. Firstly, the studies cited are predominantly cross-sectional, which allow for correlational but not causal studies. Therefore, longitudinal studies are necessary to establish a definitive and causal relationship between anxious attachment style and internet addiction. In addition, many researchers primarily used methods of self-reporting to determine the attachment styles of subjects, making the findings potentially susceptible to personal bias and desire for social conformity [12, 39]. Therefore, future studies should include standardized and validated behavioral or physiological assessments to more accurately pinpoint other aspects of attachment, as opposed to reports from the participants themselves.

Next, the majority of the studies focused on relatively similar cultural backgrounds as well as specific age groups, where the participants were solely adolescents or young adults. Given that attachment styles and internet use tendencies may vary across a wide range of age and culture, the results may not be consistent when testing broader populations. Samples with more diversity are needed to validate these associations.

Furthermore, the biological mechanisms proposed in the reviewed studies are mainly correlational. While there is evidence linking specific genetic polymorphisms, such as *DRD2 TaqIA* and *5-HTTLPR*, to attachment styles and internet addiction, the precise biological underpinnings have not been fully explored. Future research should focus on identifying specific neurobiological pathways and genetic factors that may interact with insecure attachment to contribute to the risk of developing problematic internet use.

Likewise, although attachment and genetic factors were found to be significant in driving PIU, internet addiction is a complex phenomenon with influences from a variety of individual, social, and environmental factors, which should be considered when analyzing the relationship between internet addiction and anxious attachment style [20]. Therefore, these limitations highlight the need for more accurate methods of determining attachment, diversity in samples, and a consideration of other factors contributing to problematic internet use. Addressing these limitations will ultimately be crucial in strengthening our knowledge of the link between insecure attachment and PIU.

Additionally, as adverse early life experiences shape attachment style , the role of traumatic events during childhood can be another avenue for exploration in order to understand the development of these problematic behaviors [37]. Further research can aim to uncover whether insecure attachment styles serve as risk factors for addictive behaviors as well as the dynamic between attachment and internet addiction through neurotransmitters and stress response, which will help in producing therapeutic interventions. For example, as the association between problematic internet use and insecure attachment becomes clearer, developing therapy for internet addiction such as attachment-specific drug treatments can focus on polymorphisms in monoamine neurotransmitters or stress hormones.

IV. Conclusion

This review sheds light on the association between the anxious-ambivalent attachment style and problematic internet use by proposing several prospective mechanisms that may sustain this connection. The evidence presented in this review suggests that individuals with an anxious-ambivalent attachment style are more prone to problematic internet use tendencies than others, with genetic polymorphisms in dopamine and serotonin, heightened levels of neuroticism, and altered cortisol stress responses as potential contributing factors. While these findings introduce possible moderators for this association, the precise channels linking attachment style to internet addiction are highly intricate and warrant further exploration. Overall, these findings demonstrate the elaborate interactions between genetic and psychophysiological factors, offering valuable insights into the complexities of behavioral disorders and insecure attachment.

References

[1] Ainsworth, M. D. S., Blehar, M. C., Waters, E., & Wall, S. (2014). *Patterns of Attachment* (1st Edition). Psychology Press.

[2] Alhusen, J. L., Hayat, M. J., & Gross, D. (2013). A longitudinal study of maternal attachment and infant developmental outcomes. *Archives of Women's Mental Health*, *16*(6). https://doi.org/10.1007/s00737-013-0357-8

[3] Baik, J.-H. (2013). Dopamine Signaling in reward-related behaviors. *Frontiers in Neural Circuits*, *7*, 61390.

[4] Berger, M., Gray, J. A., & Roth, B. L. (2009). The expanded biology of serotonin. *Annual Review of Medicine*, *60*. https://doi.org/10.1146/annurev.med.60.042307.110802

[5] Blum, K., Sheridan, P. J., Wood, R. C., Braverman, E. R., Chen, T. J., Cull, J. G., & Comings, D. E. (1996). The D2 dopamine receptor gene as a determinant of reward deficiency syndrome. *Journal of the Royal Society of Medicine*, *89*(7), 396.

[6] Burkett, J. P., & Young, L. J. (2012). The behavioral, anatomical and pharmacological parallels between social attachment, love and addiction. *Psychopharmacology*, *224*(1), 1.

[7] Chang, Y.-H., Lee, Y.-T., & Hsieh, S. (2019). Internet Interpersonal Connection Mediates the Association between Personality and Internet Addiction. *International Journal of Environmental Research and Public Health*, *16*(19). https://doi.org/10.3390/ijerph16193537

[8] Curry, T., Egeto, P., Wang, H., Podnos, A., Wasserman, D., & Yeomans, J. (2013). Dopamine receptor D2 deficiency reduces mouse pup ultrasonic vocalizations and maternal responsiveness. *Genes, Brain, and Behavior*, *12*(4). https://doi.org/10.1111/gbb.12037

[9] De Deurwaerdère, P., & Di Giovanni, G. (2020). Serotonin in Health and Disease. *International Journal of Molecular Sciences*, *21*(10). https://doi.org/10.3390/ijms21103500

[10] De Nardi, L., Carpentieri, V., Pascale, E., Pucci, M., D'Addario, C., Cerniglia, L., Adriani, W., & Cimino, S. (2020). Involvement of DAT1 Gene on Internet Addiction: Cross-Correlations of Methylation Levels in 5'-UTR and 3'-UTR Genotypes, Interact with Impulsivity and Attachment-Driven Quality of Relationships. *International Journal of Environmental Research and Public Health*, *17*(21). https://doi.org/10.3390/ijerph17217956

[11] Ehrenthal, J. C., Levy, K. N., Scott, L. N., & Granger, D. A. (2018). Attachment-Related Regulatory Processes Moderate the Impact of Adverse Childhood Experiences on Stress Reaction in Borderline Personality Disorder. *Journal of Personality Disorders*, *32*(Suppl). https://doi.org/10.1521/pedi.2018.32.supp.93

[12] Eichenberg, C., Schott, M., Decker, O., & Sindelar, B. (2017).

Attachment Style and Internet Addiction: An Online Survey. *Journal of Medical Internet Research*, *19*(5), e6694.

[13] Eichenberg, C., Schott, M., & Schroiff, A. (2019). Comparison of Students With and Without Problematic Smartphone Use in Light of Attachment Style. *Frontiers in Psychiatry / Frontiers Research Foundation*, *10*, 681.

[14] Gillath, O., Shaver, P. R., Baek, J.-M., & Chun, D. S. (2008). Genetic Correlates of Adult Attachment Style. *Personality & Social Psychology Bulletin*. https://doi.org/10.1177/0146167208321484

[15] Gonda, X., Fountoulakis, K. N., Juhasz, G., Rihmer, Z., Lazary, J., Laszik, A., Akiskal, H. S., & Bagdy, G. (2009). Association of the s allele of the 5-HTTLPR with neuroticism-related traits and temperaments in a psychiatrically healthy population. *European Archives of Psychiatry and Clinical Neuroscience*, *259*(2). https://doi.org/10.1007/s00406-008-0842-7

[16] Grajewski, P., & Dragan, M. (2020). Adverse childhood experiences, dissociation, and anxious attachment style as risk factors of gaming disorder. *Addictive Behaviors Reports*, *11*. https://doi.org/10.1016/j.abrep.2020.100269

[17] Han, D. H., Lee, Y. S., Yang, K. C., Kim, E. Y., Lyoo, I. K., & Renshaw, P. F. (2007). Dopamine Genes and Reward Dependence in Adolescents with Excessive Internet Video Game Play. *Journal of Addiction Medicine*, *1*(3), 133.

[18] Hazan, C., & Shaver, P. (1987). Romantic love conceptualized as an attachment process. *Journal of Personality and Social Psychology*, *52*(3). https://doi.org/10.1037//0022-3514.52.3.511

[19] Jönsson, E. G., Nöthen, M. M., Grünhage, F., Farde, L., Nakashima, Y., Propping, P., & Sedvall, G. C. (1999). Polymorphisms in the dopamine D2 receptor gene and their relationships to striatal dopamine receptor density of healthy volunteers. *Molecular Psychiatry*, *4*(3). https://doi.org/10.1038/sj.mp.4000532

[20] Juthamanee, S., & Gunawan, J. (2021). Factors related to Internet and game addiction among adolescents: A scoping review. *Belitung Nursing Journal*, *7*(2). https://doi.org/10.33546/bnj.1192

[21] Kaess, M., Parzer, P., Mehl, L., Weil, L., Strittmatter, E., Resch, F., & Koenig, J. (2017). Stress vulnerability in male youth with Internet Gaming Disorder. *Psychoneuroendocrinology*, *77*. https://doi.org/10.1016/j.psyneuen.2017.01.008

[22] Kim, S. H., Baik, S.-H., Park, C. S., Kim, S. J., Choi, S. W., & Kim, S. E. (2011). Reduced striatal dopamine D2 receptors in people with Internet addiction. *Neuroreport*, *22*(8), 407–411.

[23] Kruschwitz, J. D., Walter, M., Varikuti, D., Jensen, J., Plichta, M. M., Haddad, L., Grimm, O., Mohnke, S., Pöhland, L., Schott, B., Wold, A., Mühleisen, T. W., Heinz, A., Erk, S., Romanczuk-Seiferth, N., Witt, S. H., Nöthen, M. M., Rietschel, M., Meyer-Lindenberg, A., & Walter, H. (2015). 5-HTTLPR/rs25531 polymorphism and neuroticism are linked by resting state functional connectivity of amygdala and fusiform gyrus. *Brain Structure & Function*, *220*(4). https://doi.org/10.1007/s00429-014-0782-0

[24] Lee, Y. S., Han, D. H., Yang, K. C., Daniels, M. A., Na, C., Kee, B. S., & Renshaw, P. F. (2008). Depression like characteristics of 5HTTLPR polymorphism and temperament in excessive internet users. *Journal of Affective Disorders*, *109*(1-2). https://doi.org/10.1016/j.jad.2007.10.020

[25] Lerner, T. N., Holloway, A. L., & Seiler, J. L. (2021). Dopamine, Updated: Reward Prediction Error and Beyond. *Current Opinion in Neurobiology*, *67*, 123.

[26] Lovallo, W. R. (2006). Cortisol secretion patterns in addiction and addiction risk. *International Journal of Psychophysiology: Official Journal of the International Organization of Psychophysiology*, *59*(3), 195.

[27] Marciano, L., Camerini, A.-L., & Schulz, P. J. (2022). Neuroticism and internet addiction: What is next? A systematic conceptual review. *Personality and Individual Differences*, *185*, 111260.

[28] Marci, T., Marino, C., Sacchi, C., Lan, X., & Spada, M. M. (2021). Problematic Internet Use in early adolescence: The role of attachment and negative beliefs about worry. *Journal of Behavioral Addictions*, *10*(1), 194–200.

[29] Noftle, E. E., & Shaver, P. R. (2006). Attachment dimensions and the big five personality traits: Associations and comparative ability to predict relationship quality. *Journal of Research in Personality*, *40*(2), 179–208.

[30] Pohjalainen, T., Rinne, J. O., Någren, K., Lehikoinen, P., Anttila, K., Syvälahti, E. K., & Hietala, J. (1998). The A1 allele of the human D2 dopamine receptor gene predicts low D2 receptor availability in healthy volunteers. *Molecular Psychiatry*, *3*(3). https://doi.org/10.1038/sj.mp.4000350

[31] Sapolsky, R. M., Zola-Morgan, S., & Squire, L. R. (1991). Inhibition of glucocorticoid secretion by the hippocampal formation in the primate. *The Journal of Neuroscience: The Official Journal of the Society for Neuroscience*, *11*(12), 3695.

[32] Şenormancı, Ö., Şenormancı, G., Güçlü, O., & Konkan, R. (2014). Attachment and family functioning in patients with internet addiction. *General Hospital Psychiatry*, *36*(2), 203–207.

[33] Sen, S., Burmeister, M., & Ghosh, D. (2004). Meta-analysis of the association between a serotonin transporter promoter polymorphism (5-HTTLPR) and anxiety-related personality traits. *American Journal of Medical Genetics. Part B, Neuropsychiatric Genetics: The Official Publication of the International Society of Psychiatric Genetics*, *127B*(1). https://doi.org/10.1002/ajmg.b.20158

[34] Sun, C., Spathis, R., Chan, C. W., Sankaranarayanan, K., & Koji Lum, J. (2016). Genetic-linked inattentiveness protects individuals from internet overuse: A genetic study of internet overuse evaluating hypotheses based on addiction, inattention, novelty-seeking and harm-avoidance. *Informing Science: The International Journal of an Emerging Transdiscipline*, *19*, 173–201.

[35] Troisi, A., Carola, V., & Gross, C. (2017). Genetic variation in the serotonin transporter gene influences adult attachment style. *Neuropsychiatry, 14*(4), 241246.

[36] Tsumura, H., Fukuda, M., & Kanda, H. (2022). Blunted cortisol and normal sympathetic nervous system responses to an acute psychosocial stressor in internet addiction. *Heliyon*, *8*(12). https://doi.org/10.1016/j.heliyon.2022.e12142

[37] Yan, M., Hodgdon, E. A., Yang, R., Yu, Q., Inagaki, T. K., & Wiggins, J. L. (2022). Neural correlates of attachment in adolescents with trauma: a preliminary study on frustrative non-reward. *Social Cognitive and Affective Neuroscience*, *17*(12). https://doi.org/10.1093/scan/nsac038

[38] Young, K. S. (2004). Internet Addiction: A New Clinical Phenomenon and Its Consequences. *American Behavioral Scientist*, *48*(4). https://doi.org/10.1177/0002764204270278

[39] Young, L., Kolubinski, D. C., & Frings, D. (2020). Attachment style moderates the relationship between social media use and user mental health and wellbeing. *Heliyon*, *6*(6). https://doi.org/10.1016/j.heliyon.2020.e04056

Columbia Undergraduate Science Journal

The *Columbia Junior Science Journal* (*CJSJ*) is an extension of the *Columbia Undergraduate Science Journal* (*CUSJ*), an open-access science journal that is committed to publishing undergraduate manuscripts of the highest scholarship resulting from significant scientific research or outstanding scientific analysis. The *CJSJ* provides high school students with a platform to publish manuscripts in the fields of natural sciences, physical sciences, engineering, and social sciences.